Transition metal compounds with S/N-functionalized NHC ligands: structures, redox properties and electrocatalytic activity

Luo, S.; Luo S.

Transition metal compounds with S/N-functionalized NHC ligands: structures, redox properties and electrocatalytic activity

PROEFSCHRIFT

ter verkrijging van
de graad van Doctor aan de Universiteit Leiden,
op gezag van Rector Magnifcus Prof. mr. C. J. J. M. Stolker,
volgens besluit van het College voor Promoties,
te verdedigen op dinsdag 17 oktober 2017
klokke 13.45 uur

door

Siyuan Luo

geboren te Wuhan, P.R.China in 1989

Samenstelling Promotiecommissie

Promotor	Prof. Dr. E. Bouwman
Co-promotor	Dr. D.G.H. Hetterscheid
Overige leden	Prof. Dr. H.S. Overkleeft
	Prof. Dr. M.T.M. Koper
	Prof. Dr. B. de Bruin (Universiteit van Amsterdam)
	Dr. M.-E. Moret (Universiteit Utrecht)

ISBN: 978-94-6295-720-6

Printed by www.proefschriftmaken.nl

To my parents

and my sister

Table of Contents

List of abbreviations

CPC	controlled-potential coulometry
CPE	controlled-potential electrolysis
CV	cyclic voltammetry
Cys	cysteine
DCM	dichloromethane
DMF	dimethylformamide
DMSO	dimethylsulfoxide
dme	dimethoxyethane
dd (NMR)	doublet of doublets
Eq	equation
ESI	electrospray ionization
GC	gas chromatography
HER	hydrogen evolution reaction
IR	infrared
J	coupling constant (Hz)
m (NMR)	multiplet
MS	mass spectrometry
MeCN	acetonitrile
MeOH	methanol
NMR	nuclear magnetic resonance
NHC	N-Heterocyclic Carbene
OAc	acetate
PE	petroleum ether 40-65
ppm	parts per million
p (NMR)	pentet
PCET	proton-coupled electron transfer
q (NMR)	quintet
s (NMR)	singlet
t (NMR)	triplet
TBAB	tetrabutylammonium bromide
TBAP	tetrabutylammonium hexafluoridophosphate
THF	tetrahydrofuran
TMS	tetramethylsilane
UV	ultraviolet

CHAPTER 1

Introduction

The active sites of hydrogenases are briefly discussed. A brief overview of structural models and functional models of hydrogenases as catalysts for the hydrogen evolution reaction (HER) is provided. Recently reported electrocatalysts for HER are described in more detail. Furthermore, a brief introduction to Metal-NHC (NHC = N-heterocyclic carbene) complexes is provided and related electrochemical research is described. At the end of this Chapter a short overview of the aim and contents of the research described in this thesis is given.

1.1 Hydrogen evolution reaction (HER) and hydrogenases

Hydrogen gas is considered as one of the most attractive clean fuels, which produces only water when it is combusted with pure dioxygen.[1] Nowadays, the largest fraction of dihydrogen gas is produced from fossil fuels by steam reforming and coal gasification; only a small quantity is produced by other renewable methods such as electrolysis of water.[2]

The hydrogen evolution reaction (HER) is a chemical reaction taking place at the cathodic electrode during electrolysis of water. It is one of the most intensively studied reactions, in which with the use of electrical energy two protons are reduced to dihydrogen (Eq. 1).

$$2H^+ + 2e^- \rightarrow H_2 \qquad \text{Eq. 1}$$

Catalysts for the hydrogen evolution reaction generally can be divided into two categories: heterogeneous catalyst and molecular catalyst.

The most typical heterogeneous catalyst for HER is platinum metal; using platinum as the cathode material, H_2 can be produced efficiently.[3] However the downside is evident: platinum is a scarce noble metal with relatively high price and limited reserves.

In nature, hydrogenases efficiently catalyze the transformation between protons and dihydrogen.[4] The hydrogenases are classified in three groups, the [FeFe], [NiFe] and [Fe] hydrogenases, which are encountered in different microorganisms and differ in the structure of the active site (Figure 1.1 and Figure 1.2).

[FeFe] hydrogenases, which have been found in bacteria and lower eukaryotes, are generally recognized as the fastest and most evolved of the hydrogenases.[5] The active site in the [FeFe] hydrogenase contains a dithiolate-bridged dinuclear ion center (Figure 1.1). The ion center connects with a bridging cysteine thiolate to a [4Fe-4S] cluster, which is important for the electron transfer. The bridging cofactor contains a secondary amine that is involved in proton transfer.

[NiFe]-hydrogenases are commonly found in a wide variety of bacteria, archaea and cyanobacteria, but are not found to be associated with any lower eukaryotes.[6] In the active site of the heterodimeric [NiFe]-hydrogenases, four cysteine thiolates are coordinated to the nickel center, two of which bridge to connect the iron center. Several mechanisms have been proposed for the uptake of dihydrogen by these enzymes but no consensus has been reached yet.[7] The formation of a bridging hydride between the two metal centers during the catalytic cycle is one of the general considerations.

In the active site of both the [FeFe] and the [NiFe] hydrogenases the iron center is bound to carbon monoxide and cyanide. In nature, [FeFe] hydrogenase enzymes catalyze the formation of H_2 from water, with reported rate constants as high as 9000 s^{-1} which is more

active than [NiFe] hydrogenases (700 s^{-1}).[5, 8] However, [NiFe] hydrogenases are less sensitive to inhibition by oxygen and carbon monoxide than [FeFe] hydrogenase.[8]

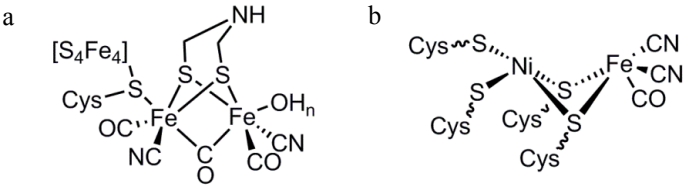

Figure 1.1. Schematic representation of the active site in (a) [FeFe] hydrogenase and (b) [NiFe] hydrogenase.

The [Fe]-hydrogenase, also known as Hmd (hydrogen-forming methylenetetrahydro methanopterin dehydrogenase), is not a redox enzyme and thus does not feature an Fe-S cluster.[5] It only can be observed in some hydrogenotrophic methanogenic archaea. Different from the two other classes of hydrogenase enzymes, it requires the presence of a hydride acceptor/donor substrate to react with or produce H_2.[4] The active site contains an $Fe(CO)_2(SCys)$ fragment bound to a unique guanylylpyridinol/pyridonate ligand through its acyl and pyridyl donor groups (Figure 1.2).

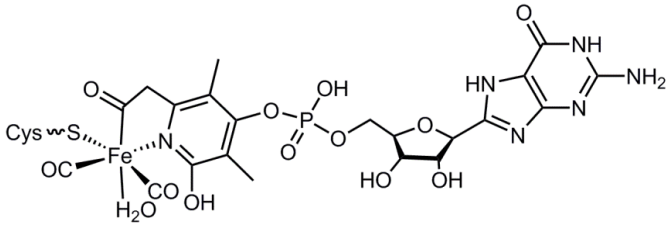

Figure 1.2. Schematic representation of [Fe] hydrogenase active site.[4]

Unfortunately, most of these natural enzymes are extremely air sensitive, restricting their industrial application. However, inspired by the structures of their active sites, chemists are active in the design of molecular electrocatalysts for HER, either by development of structural mimics for the hydrogenase active site or by mimicking the activity of hydrogenases through understanding of their catalytic mechanism. In the next two sections, the structural models as well as functional models for hydrogenases are discussed.

1.2 Structural models for the active sites in hydrogenases

Structural mimics for the active sites of all three classes of hydrogenases have been reported. Compared to the [FeFe] and [NiFe] hydrogenases, relatively few studies have been focused on the design of molecular mimics of the active site in [Fe] hydrogenases.

In the design of structural models for the active site of [FeFe] hydrogenases, the dithiolate ligand bridging the two iron centers is the most important part of the biomimetic

approach.[9] Group of Sun has reported that the nature of this bridge influences the redox properties of the diiron dithiolate model compounds: the use of a rigid and conjugated bridge results in a decrease of the potentials for the $Fe^{I}Fe^{I}$ to $Fe^{I}Fe^{0}$ reduction process.[10] In several cases, an N-heterocyclic carbene (NHC) ligand was used as a ligand for structural mimics, because of its strong σ-donation with negligible π-accepting ability (Figure 1.3a).[11-13] These few NHC-related structural models for [FeFe] hydrogenases indeed present electrocatalytic activities on proton reduction, but the activities are relatively low.

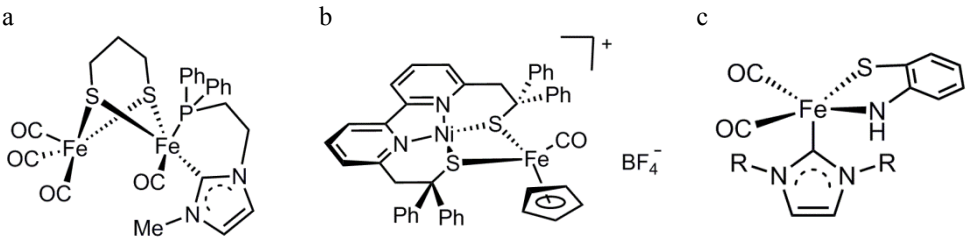

Figure 1.3. Schematic drawing of (a) a NHC-containing structural model for the active site in [FeFe]-hydrogenase;[13] (b) a structural model for the active site in [NiFe] hydrogenase;[14] (c) a NHC-containing structural model for the active site in [Fe] hydrogenase.[15]

As described in Section 1.1 the active site in the [NiFe] hydrogenase comprises a nickel center coordinated to four cysteine thiolates. A general approach to the development of model systems for [NiFe] hydrogenases thus includes tuning of the sulfur-containing ligand with various substituents to directly influence the electron density on the nickel center.[14, 16, 17] Alternatively, inspired by the active site of [FeFe] hydrogenases, an extra functional group on the sulfur bridge can be employeed, which also might affect the efficiency of the molecular catalyst.[18]

Unfortunately, for most of the functional mimics for the active site in [NiFe] hydrogenases it was found that the iron center acted as the catalytic proton reduction center, whereas in the enzyme the iron center does not have a role in catalysis. Recently a new [NiFe] compound was reported in which proton reduction appeared to be nickel centered (Figure 1.3b).[14] Instead of a $[NiS_4]$ coordination sphere, the compound featured an $[NiN_2S_2]$ chromophore.

There are many other strategies to design a functional mimic of [NiFe] hydrogenases. For instance, the synthesis of structural and functional models for the [NiFeSe] hydrogenases – a subclass of the [NiFe] hydrogenases containing a selenocysteine bound to the nickel center in the active site. Novel ligands were developed in which selenium was used instead of sulfur.[19, 20] Apart from nickel and iron, other metal ions have been used in the design and synthesis of structural and functional models for the hydrogenases. Ruthenium has been used to replace the iron center, as ruthenium is known to form more stable coordination compounds.[21-25]

The design and synthesis of structural models of the active site in [Fe] hydrogenase have received relatively less attention.[26, 27] Jiang and coworkers used a strongly electron-donating NHC ligand and the dianionic ligand 2-amidothiophenolate bound to an iron center to mimic the [Fe] hydrogenase active site (Figure 1.3c).[15] Two of the models reported by Jiang *et al*. showed reversible protonation and deprotonation properties.

Apart from the attempts of combining the structural features in an enzyme mimic with functional activity of the enzyme, functional models of the hydrogenases are prepared in which the coordination environment of the metal centers in the synthetic molecules is no longer similar with that of the active site in the natural enzyme. Instead, scientists extracted the core essence of the active site structure and design the catalysts with functional groups or metal centers purely to facilitate the catalysis of H_2 evolution. Examples of this approach are described in the next section.

1.3 Bio-inspired molecular electrocatalysts for hydrogen evolution

1.3.1 Nickel bisdiphosphane complexes

Inspired by the structure of the active site in [FeFe] hydrogenases, two of its critical features were used in the rational design of efficient molecular electrocatalysts for proton reduction: the use of first-row transition metals and the incorporation of a pendant amine as a proton relay.[28] New mononuclear compounds were developed containing a square-planar nickel(II) ion coordinated with four phosphane donor atoms in the first coordination sphere, and including several amine groups in the second coordination sphere. With the aim to understand the role of the pendant amine in the active site of [FeFe] hydrogenases both a computational[29] and an experimental study[30] were undertaken. DuBois *et al*. have discussed the role of the amine pendant group in Co-diphosphane electrocatalysts for hydrogen evolution in an experimental way.[30] Comparison of $[Co(P^{Ph}_2N^{Ph}_2)(CH_3CN)_3](BF_4)_2$ ($P^{Ph}_2N^{Ph}_2$ = 1,3,5,7-tetraphenyl-1,5-diaza-3,7-diphosphacyclooctane) comprising a pendant amine, with the compound $[Co(dppp)(CH_3CN)_3](BF_4)_2$ (dppp = 1,3-bis(diphenylphosphanyl)propane) showed that, although the two compounds are equipped with similar diphosphane ligands, only the former one presented proton reduction activity. Similar compounds containing a nickel center were also developed, and these nickel-based bisdiphosphane complexes have been intensively studied for their electrocatlytic activity in the last decade.[31-37] The activity of the nickel-based catalyst was shown to depend on the exact orientation of the pendant amines with respect to each other and the metal center: the formation of undesired endo-exo and exo-exo isomers appeared to be unfavorable for high activity in proton reduction (Figure 1.4).[1] Helm *et al*. developed a new complex $[Ni(P^{Ph}_2N^{Ph})_2](BF_4)_2$ ($P^{Ph}_2N^{Ph}$ = 1,3,6-triphenyl-1-aza-3,6-diphosphacycloheptane). The ligand $P^{Ph}_2N^{Ph}$ has only one pendant amine, which precluded the possibility of forming the unfavorable orientation. Turnover frequencies of 33,000 s^{-1} of $[Ni(P^{Ph}_2N^{Ph})_2](BF_4)_2$ as HER catalyst in acetonitrile can be calculated.[38] Unfortunately, the stability of this kind of catalyst is not yet ideal: some of

the catalysts decompose with a loss of activity of approximately 10% within 1 hour in an acidic environment.[35]

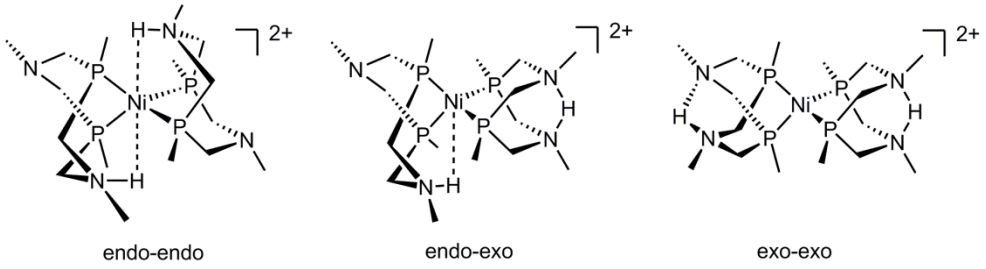

Figure 1.4. Nickel-diphosphane electrocatalysts for proton reduction; different orientations of pendant amines and interactions with protons.[38]

1.3.2 Cobaloxime and cobalt diimine-dioxime complexes

A family of cobalt-based hydrogen evolving catalysts has been reported comprising either two dimethylglyoxime ligands (Figure 1.5a), or a stable tetradentate ligand providing a diimine-dioxime coordination sphere (Figure 1.5b).[39] During the catalytic cycle of proton reduction, the oxime proton from the ligand assists with the proton delivery and is involved in the rate-determining step. The catalytic activity in electrocatalytic proton reduction of the cobalt(III) diimine-dioxime complexes, showing a similar coordination sphere as the cobal(II) dimethylglyoxime compound (also known as cobaloxime) (Figure 1.5), has been studied after that of the cobaloxime.[40-42] It has been suggested that the tetradentate nature of the diimine−dioxime ligand warrants stability of cobal(II) dimethylglyoxime compound against hydrolysis, which is a merit comparing to cobaloxime complexes.[39, 43]

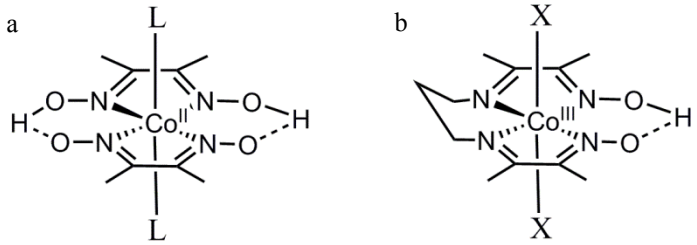

Figure 1.5. General structures of (a) cobalt(II)-dimethylglyoxime compound (cobaloxime compound), L = solvent (H_2O, CH_3CN, DMF) and (b) cobalt(III) diimine-dioxime complex (X = e.g. Br, Cl).[39]

1.3.3 Other molecular catalysts

New classes of molecular catalysts for HER are still being developed and reported over the years (Figure 1.6). Recently, group of Masuda reported a nickel(II) complex with two bidentate phosphanylpyridyl ligand (Figure 1.8a).[44] Catalytic dihydrogen generation was observed even in the absence of proton sources, indicating that the proton transfer is facilitated through the basic site of the amines.

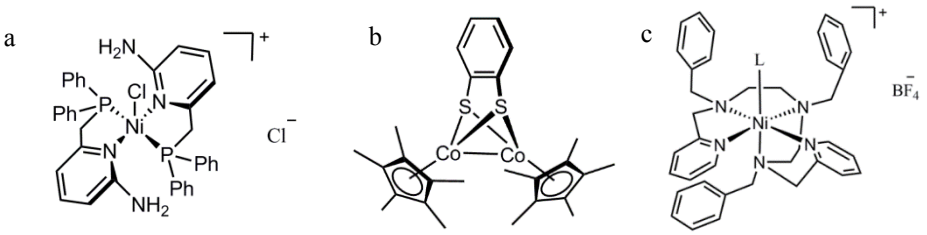

Figure 1.6. Other new classes of molecular catalysts for HER. Schematic drawing of molecular catalysts for proton reduction: a) reported by Tatematsu;[44] b) reported by Tong;[45] c) reported by Zhang.[46]

Additionally, a new type of proton reduction catalytsts based on dinuclear cobalt or CoFe complexes have been reported, although the catalytic activity need to be improved (second-ordered rate constant ca. 4.67 $M^{-2} s^{-1}$) (Figure 1.6b).[45] Noteworthy are the transition metal complexes bearing the pyridine-based pentadentate ligand reported by Sun's group. Complexes with different metal centers and different amine-to-pyridine ratios showed significantly different catalytic activities.[46] The fastest catalyst they investigated is a nickel complexes with a 2 to 3 amine-to-pyridine ratios (see Figure 1.6c). The calculated turnover frequency of this catalyst reaches 1650 mol H_2 $(mol\ cat)^{-1}h^{-1}cm^{-2}$ in neutral aqueous solutions, which is more than one-fold higher than that displayed by the analogous cobalt catalysts at the same applied potential.

In comparison with the intensively studied nickel bisdiphosphane and cobaloxime systems, these new types of electrocatalysts still require more investigations to unravel their exact catalytic mechanism and to optimize their structures in order to achieve more efficient electrocatalysis.

1.4 Electrochemical properties of metal-NHC complexes

1.4.1 N-Heterocyclic carbenes

N-Heterocyclic carbenes (NHCs) are cyclic molecules in which the carbene center is found in the α-position of at least one nitrogen atom.[47] Diez-Gonzalez defined N-Heterocyclic carbenes as "cyclic carbenes, bearing at least one R-amino substituent".[48] Nowadays, NHCs are regarded as "broadly catalytically useful ligands comparable with cyclopentadienyls and phosphines", because of their strong σ electron donating properties and redox innocence.[49, 50] In addition, in some cases metal-to-carbene π-back donation further stabilizes the interaction between the metal center and the carbene. Furthermore, NHC ligands are less sensitive to oxidation than alkyl phosphane ligands.[51] The most common subclasses of NHCs are represented in Figure 1.7. The carbene ligands are recognized as an alternative to phosphane ligands in the field of organometallic chemistry and homogeneous catalysis.[52]

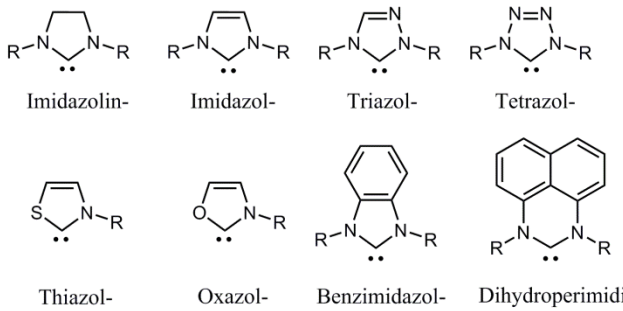

Figure 1.7. Common structures of N-Heterocyclic carbenes. The suffix "ylidene" should be added to obtain the generic name of each NHC subclass.

In some cases binding of the carbene with metal centers may occur through the C4 atom ('abnormal' carbene, Figure 1.8). It is still difficult to achieve selective binding of the NHC through the C4 atom, and a mixture of normal NHC and abnormal NHC complexes is generally obtained.[53, 54] However, methylation of the C2 position of the ligand precursors is a viable method for formation of abnormal NHC complexes.[55]

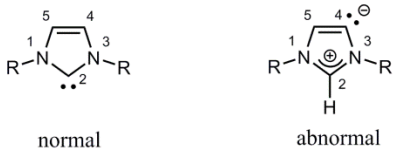

Figure 1.8. Binding sites of normal and abnormal NHC ligands.

1.4.2 N-Heterocyclic carbene complexes and their application

Since Herrmann published an article entitled "Metal Complexes of N-Heterocyclic Carbenes—A New Structural Principle for Catalysts in Homogeneous Catalysis",[56] metal-NHC complexes have received intensive attention in the field of organometallic chemistry and catalysis.[57-60] Various metal-NHC complexes have been synthesized and used as efficient homogenous catalysts for different reactions, such as dehydrogenation,[61, 62], hydrosilylation,[63] C−C coupling reactions,[64-68] hydroamination,[69] and C−H activation.[70] The NHC ligands employed in these homogenous catalysts generally comprise sterically hindered substrates. These bulky auxiliary NHC ligand can help with improving the stability and catalytic performance of the catalysts in homogenous catalytic reactions.[51, 71, 72]

On the other hand, various metal-NHC complexes with a dangling functionality have been designed and synthesized. The hemilabile systems usually comprise a carbene-metal bond in combination with at least one pyridine,[73] phosphane,[74-76] alcohol,[77] or thioether[69, 78] donor atom that during catalysis may dissociate from the metal center. It has been suggested that metal compounds comprising chelating hemilabile NHC ligand systems may display better catalytic activity in comparison to compounds containing a rigid chelating ligand.[77, 79]

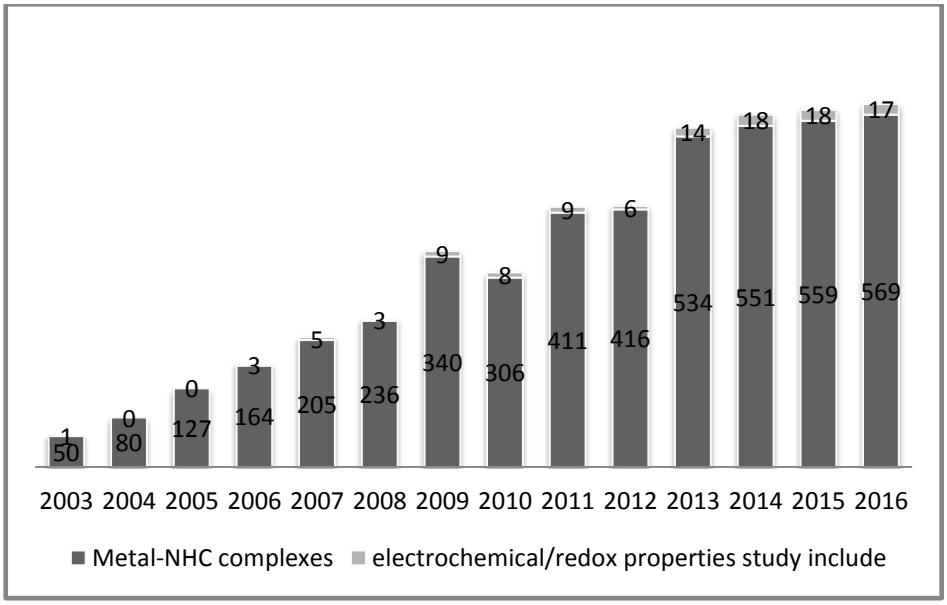

Figure 1.9. Number of publications related to metal-NHC compounds.(until December 2016, using web of science engine)

As carbene ligands are generally regarded as stable auxiliary moieties, research is mainly focused on the synthesis of new metal-NHC compounds and the determination of their catalytic properties. So far, the redox properties of metal-NHC complexes, especially the ones of NHC complexes with functionalized group, have been largely neglected. A search in the Web of Science shows that the electrochemical properties of metal-NHC complexes have been receiving more attention in last four years (Figure 1.9), although such studies still are quite limited in number. Among these studies related to the electrochemical properties of the metal-NHC compounds, reports on metal-NHC compounds as potential electrocatalysts for HER are scarce.[80, 81] Recently reported metal-NHC complexes as catalysts for proton reduction comprise mononuclear cobalt-based compounds with pyridine-functionalized NHC ligands (Figure 1.10).[80, 81]

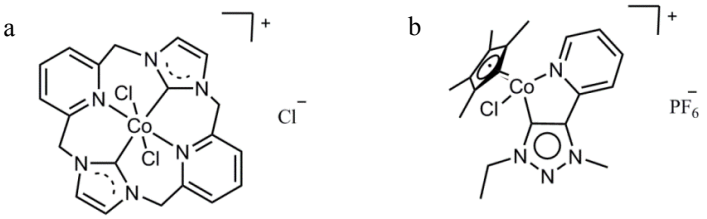

Figure 1.10. Cobalt-NHC complexes that have been studied for their use in HER electrocatalysis from: (a) group of Sakai;[80] (b) group of Sarkar.[81]

1.4.3 Synthesis of metal-NHC complexes

Several methods have been reported for the synthesis of NHC-bearing transition metal complexes. The most accessible synthesis route avoids the use of exotic or unstable reagents and can be handled by 'beginners' in organometallic synthesis.[82] In general, the methods for the preparation of metal-NHC compounds follow a similar recipe: a ligand precursor (azolium salt), metal precursor, and mild base (if necessary) are dissolved in a solvent, and the mixture is stirred with heating if necessary. Such recipes avoid the preparation of the unstable, free carbene.

In recent years the following three synthesis routes have been the most common: 1) the reaction of nickel acetate with the azolium salt under vacuum with the loss of acetic acid;[64, 65, 78, 83] 2) the reaction of a nickel precursor with the azolium salt in presence of a mild base in an atmosphere of an inert gas;[54, 84-87] 3) via the synthesis of a silver-NHC complex by the deprotonation of the azolium salt with Ag_2O, after which the NHC is transferred from the silver ion to a transition metal.[69, 88]

The compounds reported in Chapters 2, 3, 4 of this Thesis were obtained using the first synthesis method whereas the compounds reported in Chapters 5 and 6 were obtained using the second method.

1.5 General mechanism of electrocatalytic proton reduction with molecular catalysts

The mechanism of the hydrogen evolution reaction based on metal-based homogenous electrocatalysts can be simplified to three basic steps (Figure 1.11). The metal center of the molecular catalyst will be reduced first by an electron (step (A)), which is followed by a proton-transfer (step (B)) leading to the formation of a metal hydride. Finally, with the addition of a second electron and a proton dihydrogen is formed and the catalyst is regenerated (step (C)).

Under this mechanism, an anti-correlation was found between step (A) and step (B). When the metal bears more election-withdrawing ligand, the electron density at the metal center will be lower, which makes the metal center easier to be reduced. However, on the other hand the lower electron density at the metal center will make formation of the metal hydride more difficult. Overall, this means that a lower energy cost in step (A) generally results in a larger kinetic barrier in step (B). This anti-correlation between the reduction potential of the metal center and the kinetics of metal-hydride formation is a major challenge to be overcome in the design of catalyst for HER with both low overpotentials and high catalytic rates.[89]

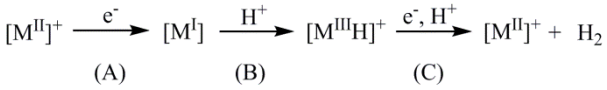

Figure 1.11. Simplified mechanism of the hydrogen evolution reaction. (A): reduction of the metal center; (B): formation of the metal hydride; (C): dihydrogen generation.

The mechanistic pathway shown in Figure 1.11 is only applicable when the metal center of the electrocatalyst takes part in catalytic cycle, and two electron transfer process have been simplified into one-step speed controlled progress.[90, 91]

Inspired by nature, the concept of "proton relay" was introduced in electrocatalytic proton reduction, as discussed in Section 1.3. The proton relay built into molecular catalysts can be an amine,[28, 44] a pyridine[89, 92, 93]. The ligand that is modified with a functional group acting as a proton relay becomes less innocent and takes part in the catalytic cycle (Figure 1.12). First the ligand can be protonated, after which the metal center is reduced. Two different proton transfer pathways may be operative. Either the proton is directly transferred from ligand to the reduced metal center to form a metal hydride, which is followed by the second electron and proton transfer (pathway I in Figure 1.12);[29, 35] or the reduced metal center accepts the second proton and a second electron to form a metal-hydride which then reacts with the proton carried by the ligand to generate dihydrogen (pathway II in Figure 1.12).[93] The intramolecular proton transfer would break the anti-correlation between reduction potential of the metal center and the kinetics of metal-hydride formation. Thus the incorporation of a proton relay is a promising design principle to improve the efficiency of electrocatalysts for proton reduction.

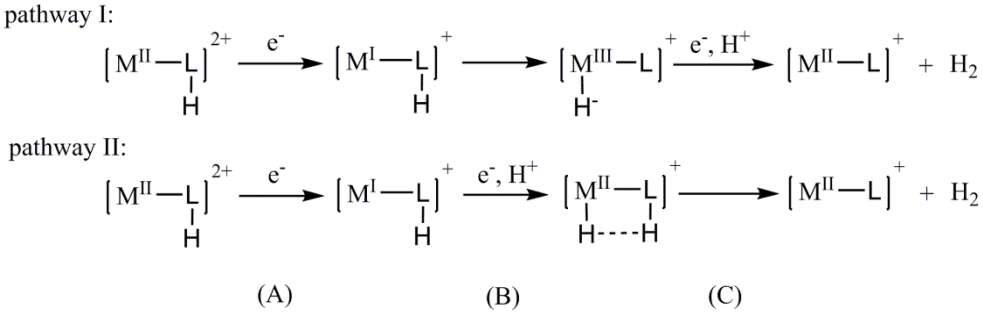

Figure 1.12. Proposed pathways I and II for dihydrogen evolution by a molecular catalyst involving a proton relay. (A): reduction of the metal center; (B): formation of metal hydride; (C): hydrogen generation.

1.6 Aim and outline of this thesis

The research described in this thesis focused on the preparation of S/N functionalized carbene ligands and their transition metal complexes, and the exploration of their application as electrocatalysts for proton reduction. In Chapter 1, an overview is given of

homogenous molecular electrocatalysts that are inspired by natural systems and general mechanisms for the electrocatalytic hydrogen evolution reaction (HER) have been addressed. It was found that the use of transition metal carbene complexes as electrocatalysts for HER is still an unexplored field of research.

In Chapter 2, two sulfur-functionalized carbene ligands and their dinuclear nickel-NHC complexes are described. In addition two carbene ligands functionalized with both a thiolate donor and a pyridyl group and their dinuclear nickel compounds are described. Electrochemical investigations revealed that the nickel-NHC complexes with the additional pyridine proton relays show better electrocatalytic activity in HER.

Four mononuclear nickel compounds with chelating biscarbene ligands comprising pendant pyridyl arms are reported in Chapter 3. The redox properties and catalytic activity in proton reduction of the complexes is influenced by the nature of the NHC carbene group in the chelating ligands as well as the counter ions present in the nickel compounds.

In Chapter 4, the synthesis and characterization is reported of two new mononuclear nickel complexes bearing two pyridine-functionalized carbene ligands. The ligands described in this Chapter are a potentially bidentate NHC ligand with one pyridyl and one benzyl pendant arm, whereas the other ligand is potentially tridentate with two pyridyl pendant arms. Mononuclear nickel compounds are formed bound to two ligands coordinating in a bidentate mode; as a result the nickel compound of the potentially tridentate ligand has two unbound pyridyl groups that can act as a nearby proton binding site for electrocatalysis. This results not only in a higher activity in electrocatalytic proton reduction, but also in a smaller overpotential for proton reduction.

In Chapter 5 the synthesis is described of two new pyridine-amide functionalized (benz)imidazolium salts. Using these (benz)imidazolium salts as ligand precursors two new square-planar nickel-NHC compounds were obtained, whose redox potentials and electrocatalytic behavior are reported. The catalytic activity of the two compounds in HER has been studied in organic solvent using acetic acid as the proton source. Although the nickel compound of the imidazole-based carbene is water soluble, its poor stability in acidic environments restricts further exploration of its application.

With the aim to understand how different metal centers affect the redox behavior and catalytic activity in HER, two cobalt compounds bearing pyridine-amide NHC ligands have been prepared and are reported in Chapter 6. Two different ligands are used in the compounds described in this Chapter: a potentially tridentate NHC ligand with one pyridine-amidate arm and one benzyl pendant arm, whereas the other ligand is potentially tetradentate with two pyridyl pendant arms. The cobalt(III) centers in the obtained compounds are in octahedral geometries bound by two tridentate ligands. Due to the large ligand-field splitting and the coordination geometry, the cobalt ions are reduced only at quite negative potentials. Both of the Co(III) complexes exhibit electrocatalytic activity in

HER, but the compound with the additional free unbound pyridyl groups revealed twice higher catalytic activity compared to the benzyl-substituted analogue.

This thesis is concluded with a general summary and outlook in Chapter 7.

Parts of this thesis have been published (Chapter 3),[94] have been submitted for publication or are in preparation for publication.

1.7 References

[1] P.D. Tran, J. Barber, *Phys. Chem. Chem. Phys.* 2012, 14, 13772-13784.
[2] C.L. Muhich, B.D. Ehrhart, I. Al-Shankiti, B.J. Ward, C.B. Musgrave, A.W. Weimer, *Wires Energy Environ.* 2016, 5, 261-287.
[3] A. Dey, *Inorg. Chem.* 2016, 55, 10831-10834.
[4] T.R. Simmons, G. Berggren, M. Bacchi, M. Fontecave, V. Artero, *Coord. Chem. Rev.* 2014, 270, 127-150.
[5] D. Schilter, J.M. Camara, M.T. Huynh, S. Hammes-Schiffer, T.B. Rauchfuss, *Chem. Rev.* 2016, 116, 8693-8749.
[6] S.E. McGlynn, D.W. Mulder, E.M. Shepard, J.B. Broderick, J.W. Peters, *Dalton Trans.* 2009, 4274-4285.
[7] S. Canaguier, V. Artero, M. Fontecave, *Dalton Trans.* 2008, 315-325.
[8] M. Frey, *Chembiochem* 2002, 3, 153-160.
[9] L.-C. Song, Q.-S. Li, Z.-Y. Yang, Y.-J. Hua, H.-Z. Bian, Q.-M. Hu, *Eur. J. Inorg. Chem.* 2010, 1119-1128.
[10] P. Li, M. Wang, J. Pan, L. Chen, N. Wang, L. Sun, *J. Inorg. Biochem.* 2008, 102, 952-959.
[11] L.-C. Song, X. Luo, Y.-Z. Wang, B. Gai, Q.-M. Hu, *J. Organomet. Chem.* 2009, 694, 103-112.
[12] D. Morvan, J.-F. Capon, F. Gloaguen, A. Le Goff, M. Marchivie, F. Michaud, P. Schollhammer, J. Talarmin, J.-J. Yaouanc, R. Pichon, N. Kervarec, *Organometallics* 2007, 26, 2042-2052.
[13] D. Morvan, J.-F. Capon, F. Gloaguen, F.Y. Pétillon, P. Schollhammer, J. Talarmin, J.-J. Yaouanc, F. Michaud, N. Kervarec, *J. Organomet. Chem.* 2009, 694, 2801-2807.
[14] D. Brazzolotto, M. Gennari, N. Queyriaux, T.R. Simmons, J. Pecaut, S. Demeshko, F. Meyer, M. Orio, V. Artero, C. Duboc, *Nat. Chem.* 2016, 8, 1054-1060.
[15] S. Jiang, T. Zhang, X. Zhang, G. Zhang, L. Hai, B. Li, *RSC Advances* 2016, 6, 84139-84148.
[16] S. Canaguier, M. Field, Y. Oudart, J. Pecaut, M. Fontecave, V. Artero, *Chem. Commun.* 2010, 46, 5876-5878.
[17] L.-C. Song, J.-P. Li, Z.-J. Xie, H.-B. Song, *Inorg. Chem.* 2013, 52, 11618-11626.
[18] P. Sun, D. Yang, Y. Li, Y. Zhang, L. Su, B. Wang, J. Qu, *Organometallics* 2016, 35, 751-757.
[19] C. Wombwell, E. Reisner, *Chem. Eur. J.* 2015, 21, 8096-8104.
[20] C. Wombwell, C.A. Caputo, E. Reisner, *Acc. Chem. Res.* 2015, 48, 2858-2865.
[21] G.M. Chambers, R. Angamuthu, D.L. Gray, T.B. Rauchfuss, *Organometallics* 2013, 32, 6324-6329.

[22] G.M. Chambers, J. Mitra, T.B. Rauchfuss, M. Stein, *Inorg. Chem.* 2014, 53, 4243-4249.
[23] Y. Oudart, V. Artero, J. Pécaut, M. Fontecave, *Inorg. Chem.* 2006, 45, 4334-4336.
[24] S. Canaguier, V. Fourmond, C.U. Perotto, J. Fize, J. Pecaut, M. Fontecave, M.J. Field, V. Artero, *Chem. Commun.* 2013, 49, 5004-5006.
[25] S. Canaguier, L. Vaccaro, V. Artero, R. Ostermann, J. Pécaut, M.J. Field, M. Fontecave, *Chem. Eur. J.* 2009, 15, 9350-9364.
[26] B. Hu, D. Chen, X. Hu, *Chem. Eur. J.* 2014, 20, 1677-1682.
[27] B.V. Obrist, D. Chen, A. Ahrens, V. Schünemann, R. Scopelliti, X. Hu, *Inorg. Chem.* 2009, 48, 3514-3516.
[28] D.L. DuBois, R.M. Bullock, *Eur. J. Inorg. Chem.* 2011, 1017-1027.
[29] A. Kochem, M. O'Hagan, E.S. Wiedner, M. van Gastel, *Chem. Eur. J.* 2015, 21, 10338-10347.
[30] G.M. Jacobsen, J.Y. Yang, B. Twamley, A.D. Wilson, R.M. Bullock, M.R. DuBois, D.L. DuBois, *Energy Environ Sci.* 2008, 1, 167-174.
[31] J.A. Gillespie, D.L. Dodds, P.C.J. Kamer, *Dalton Trans.* 2010, 39, 2751-2764.
[32] M.A. Gross, C.E. Creissen, K.L. Orchard, E. Reisner, *Chem. Sci.* 2016, 7, 5537-5546.
[33] M.A. Gross, A. Reynal, J.R. Durrant, E. Reisner, *J. Am. Chem. Soc.* 2014, 136, 356-366.
[34] L.-C. Song, H. Tan, F.-X. Luo, Y.-X. Wang, Z. Ma, Z. Niu, *Organometallics* 2014, 33, 5246-5253.
[35] M.P. Stewart, M.-H. Ho, S. Wiese, M.L. Lindstrom, C.E. Thogerson, S. Raugei, R.M. Bullock, M.L. Helm, *J. Am. Chem. Soc.* 2013, 135, 6033-6046.
[36] R.M. Stolley, J.M. Darmon, M.L. Helm, *Chem. Commun.* 2014, 50, 3681-3684.
[37] A.D. Wilson, K. Fraze, B. Twamley, S.M. Miller, D.L. DuBois, M.R. DuBois, *J. Am. Chem. Soc.* 2008, 130, 1061-1068.
[38] M.L. Helm, M.P. Stewart, R.M. Bullock, M.R. DuBois, D.L. DuBois, *Science* 2011, 333, 863-866.
[39] P.A. Jacques, V. Artero, J. Pecaut, M. Fontecave, *Proc. Natl. Acad. Sci. U. S. A.* 2009, 106, 20627-20632.
[40] C. Baffert, V. Artero, M. Fontecave, *Inorg. Chem.* 2007, 46, 1817-1824.
[41] X. Hu, B.M. Cossairt, B.S. Brunschwig, N.S. Lewis, J.C. Peters, *Chem. Commun.* 2005, 4723-4725.
[42] M. Razavet, V. Artero, M. Fontecave, *Inorg. Chem.* 2005, 44, 4786-4795.
[43] N. Kaeffer, A. Morozan, V. Artero, *J. Phys. Chem. B* 2015, 119, 13707-13713.
[44] R. Tatematsu, T. Inomata, T. Ozawa, H. Masuda, *Angew. Chem.* 2016, 55, 5247-5250.
[45] P. Tong, W. Xie, D. Yang, B. Wang, X. Ji, J. Li, J. Qu, *Dalton Trans.* 2016, 45, 18559-18565.
[46] P. Zhang, M. Wang, Y. Yang, D. Zheng, K. Han, L. Sun, *Chem. Commun.* 2014, 50, 14153-14156.
[47] C. Fliedel, P. Braunstein, *J. Organomet. Chem.* 2014, 751, 286-300.
[48] S. Diez-Gonzalez, N. Marion, S.P. Nolan, *Chem. Rev.* 2009, 109, 3612-3676.
[49] R.H. Crabtree, *J. Organomet. Chem.* 2005, 690, 5451-5457.
[50] J.-N. Luy, S.A. Hauser, A.B. Chaplin, R. Tonner, *Organometallics* 2015, 34, 5099-5112.
[51] X.-B. Lan, F.-M. Chen, B.-B. Ma, D.-S. Shen, F.-S. Liu, *Organometallics* 2016, 35, 3852-3860.

[52] P. de Fremont, N. Marion, S.P. Nolan, *Coord. Chem. Rev.* 2009, 253, 862-892.
[53] A. Kruger, L.J.L. Haller, H. Muller-Bunz, O. Serada, A. Neels, S.A. Macgregor, M. Albrecht, *Dalton Trans.* 2011, 40, 9911-9920.
[54] K.V. Tan, J.L. Dutton, B.W. Skelton, D.J.D. Wilson, P.J. Barnard, *Organometallics* 2013, 32, 1913-1923.
[55] J.-Y. Lee, J.-Y. Lee, Y.-Y. Chang, C.-H. Hu, N.M. Wang, H.M. Lee, *Organometallics* 2015, 34, 4359-4368.
[56] W.A. Herrmann, M. Elison, J. Fischer, C. Köcher, G.R.J. Artus, *Angew. Chem. Int. Ed.* 1995, 34, 2371-2374.
[57] E. Peris, R.H. Crabtree, *Coord. Chem. Rev.* 2004, 248, 2239-2246.
[58] J.A. Mata, M. Poyatos, E. Peris, *Coord. Chem. Rev.* 2007, 251, 841-859.
[59] A.T. Normand, K.J. Cavell, *Eur. J. Inorg. Chem.* 2008, 2781-2800.
[60] W.A. Herrmann, Fritz E. Kühn, *J. Organomet. Chem.* 2015, 775, 101-102.
[61] L.P. Bheeter, M. Henrion, L. Brelot, C. Darcel, M.J. Chetcuti, J.-B. Sortais, V. Ritleng, *Adv. Synth. Catal.* 2012, 354, 2619-2624.
[62] R.J. Keaton, J.M. Blacquiere, R.T. Baker, *J. Am. Chem. Soc.* 2007, 129, 1844-1845.
[63] L. Postigo, B. Royo, *Adv. Synth. Catal.* 2012, 354, 2613-2618.
[64] J. Berding, T.F. van Dijkman, M. Lutz, A.L. Spek, E. Bouwman, *Dalton Trans.* 2009, 6948-6955.
[65] J. Berding, M. Lutz, A.L. Spek, E. Bouwman, *Organometallics* 2009, 28, 1845-1854.
[66] P. Guan, C. Cao, Y. Liu, Y. Li, P. He, Q. Chen, G. Liu, Y. Shi, *Tetrahedron Lett.* 2012, 53, 5987-5992.
[67] W.-J. Guo, Z.-X. Wang, *J. Org. Chem.* 2013, 78, 1054-1061.
[68] F.-S. Han, *Chem. Soc. Rev.* 2013, 42, 5270-5298.
[69] D. Yuan, H. Tang, L. Xiao, H.V. Huynh, *Dalton Trans.* 2011, 40, 8788-8795.
[70] S. Burling, B.M. Paine, D. Nama, V.S. Brown, M.F. Mahon, T.J. Prior, P.S. Pregosin, M.K. Whittlesey, J.M.J. Williams, *J. Am. Chem. Soc.* 2007, 129, 1987-1995.
[71] K. Matsubara, H. Yamamoto, S. Miyazaki, T. Inatomi, K. Nonaka, Y. Koga, Y. Yamada, L.F. Veiros, K. Kirchner, *Organometallics* 2017, 36, 255-265.
[72] Y. Kim, Y. Kim, M.Y. Hur, E. Lee, *J. Organomet. Chem.* 2016, 820, 1-7.
[73] Z. Xi, X. Zhang, W. Chen, S. Fu, D. Wang, *Organometallics* 2007, 26, 6636-6642.
[74] A.F. Hill, C.M.A. McQueen, *Organometallics* 2014, 33, 1909-1912.
[75] A.F. Hill, C.M.A. McQueen, *Organometallics* 2012, 31, 8051-8054.
[76] P. Nägele, U. Herrlich, F. Rominger, P. Hofmann, *Organometallics* 2013, 32, 181-191.
[77] S. Hameury, P. de Frémont, P.-A.R. Breuil, H. Olivier-Bourbigou, P. Braunstein, *Inorg. Chem.* 2014, 53, 5189-5200.
[78] D. Yuan, H. Han Vinh, *Inorg. Chem.* 2013, 52, 6627-6634.
[79] M. Dangalov, M. Stoyanova, P. Petrov, M. Putala, N.G. Vassilev, *J. Organomet. Chem.* 2016, 817, 1-14.
[80] K. Kawano, K. Yamauchi, K. Sakai, *Chem. Commun.* 2014, 50, 9872-9875.
[81] M. van der Meer, E. Glais, I. Siewert, B. Sarkar, *Angew. Chem. Int. Ed.* 2015, 54, 13792-13795.
[82] D.J. Nelson, *Eur. J. Inorg. Chem.* 2015, 2012-2027.
[83] J.C. Bernhammer, H.V. Huynh, *Organometallics* 2014, 33, 5845-5851.
[84] D. Yuan, H.V. Huynh, *Organometallics* 2010, 29, 6020-6027.

[85] J. Guo, L. Lv, X. Wang, C. Cao, G. Pang, Y. Shi, *Inorg. Chem. Commun.* 2013, 31, 74-78.
[86] H. Song, D. Fan, Y. Liu, G. Hou, G. Zi, *J. Organomet. Chem.* 2013, 729, 40-45.
[87] D. Zhang, S. Zhou, Z. Li, Q. Wang, L. Weng, *Dalton Trans.* 2013, 42, 12020-12030.
[88] A.G. Tennyson, V.M. Lynch, C.W. Bielawski, *J. Am. Chem. Soc.* 2010, 132, 9420-9429.
[89] P.F. Huo, C. Uyeda, J.D. Goodpaster, J.C. Peters, T.F. Miller, *ACS Catalysis* 2016, 6, 6114-6123.
[90] C. Costentin, J.-M. Saveant, *Chemelectrochem* 2014, 1, 1226-1236.
[91] E.S. Rountree, B.D. McCarthy, T.T. Eisenhart, J.L. Dempsey, *Inorg. Chem.* 2014, 53, 9983-10002.
[92] P. Zhang, M. Wang, Y. Yang, T. Yao, L. Sun, *Angew. Chem. Int. Ed.* 2014, 53, 13803-13807.
[93] J. Wang, C. Li, Q. Zhou, W. Wang, Y. Hou, B. Zhang, X. Wang, *Catal. Sci. Technol.* 2016, 6, 8482-8489.
[94] S. Luo, M.A. Siegler, E. Bouwman, *Eur. J. Inorg. Chem.* 2016, 4693-4700.

CHAPTER 2

Dinuclear Nickel Complexes of Thiolate-Functionalized Carbene Ligands and their Electrochemical Properties

*Four dimeric nickel(II) complexes $[Ni_2Cl_2(BnC_2S)_2]$ [**1**], $[Ni_2Cl_2(BnC_3S)_2]$ [**2**], $[Ni_2(PyC_2S)_2]Br_2$ [**3**]Br_2 and $[Ni_2(PyC_3S)_2]Br_2$ [**4**]Br_2 of four different thiolate-functionalized N-heterocyclic carbene (NHC) ligands were synthesized and their structures have been determined by single crystal X-ray crystallography. The four ligands differ by the alkyl chain length of the thiolate group (two – C_2 − or three – C_3 − carbon atoms) and the second functionality at the NHC being a benzyl (Bn) or a pyridylmethyl (Py) group. The nickel(II) ions are coordinated to the NHC carbon atom and bridged by the pendant thiolate groups. Additionally, in compounds [**1**] and [**2**] the fourth coordination position of the square-planar Ni(II) centers is occupied by the halide ions, whereas in [**3**]$^{2+}$ and [**4**]$^{2+}$ the additional pendant pyridylmethyl groups complete the coordination spheres of the nickel ions. The electrochemical properties of the four complexes were studied using CV (cyclic voltammetry) and CPC (controlled-potential coulometry) methods. Unfortunately, the thiolate-functionalized carbene complexes [**1**] and [**2**] appear to be poor electrocatalysts for the hydrogen evolution reaction (HER); the complexes [**3**]Br_2 and [**4**]Br_2, bearing an extra pyridylmethyl group, show higher catalytic activity in proton reduction, indicating the pyridine group to play an important role in the catalytic cycle.*

This chapter will be published. S. Luo, M.A. Siegler, and E. Bouwman, submitted

2.1 Introduction

Dihydrogen is a promising fuel which can be used to meet the rapidly increasing global energy demands. It has emerged as a sustainable alternative for fossil fuel resources as upon combustion only water is generated.[1] In general platinum-based electrodes are efficient catalysts for the hydrogen evolution reaction (HER).[2] However, the reserves and price of this noble metal might restrict its application in the future. Hydrogenases are enzymes that efficiently catalyze the transformation between protons and dihydrogen.[3] The abundantly available, non-expensive first row transition metals nickel and iron are present in the catalytic center of these hydrogenases. The coordination of a thiolate sulfur of cysteine to the metal ions in the active site of hydrogenases is likely to play an important role in the activity of the enzyme. Based on this knowledge, chemists worldwide focus their research efforts on mimicking the structure of the active site of hydrogenases. Either two thiolate bridges,[4-8] or a single thiolate bridge[9] are often incorporated in the biomimetic systems. In the search for efficient electrocatalysts for the proton reduction reaction researchers do not limit their investigations to iron and nickel compounds, but also have turned their attention to cobalt,[4] ruthenium,[5] and manganese.[10] Although these systems, such as nickel-bis(diphosphane) catalysts[11-15] and cobaloxime-based catalysts,[16-19] do not mimic the hydrogenase active site, generally these functional models show better electrocatalytic activity than the traditional structural models.[20]

Recently transition metal complexes bearing pyridine-functionalized carbene ligands have been reported as catalysts for HER.[21-23] However, only a few electrochemical studies are related to sulfur-functionalized metal-carbene complexes.[24] In this chapter, we report the synthesis of the dinuclear complexes $[Ni_2Cl_2(BnC_2S)_2]$ [**1**], $[Ni_2Cl_2(BnC_3S)_2]$ [**2**], $[Ni_2(PyC_2S)_2]Br_2$ [**3**]Br_2 and $[Ni_2(PyC_3S)_2]Br_2$ [**4**]Br_2 bearing four different thiolate-functionalized N-heterocyclic carbene (NHC) ligands (Figure 2.1). The thiolate group functions as a bridge between two nickel ions to form dinuclear compounds. The redox properties and electrocatalytic activity in HER of these four compounds are reported.

2.2 Results and Discussion

2.2.1 Synthesis of ligands and complexes

The benzimidazolium precursor salts $[HBnC_2Br]Br$ (**A**) and $[HBnC_3Br]Br$ (**B**),[25] $[HBnC_2SAc]Br$ (**C**) and $[HBnC_3SAc]Br$ (**D**),[26] $[HPyC_2Br]Br$ (**E**) and $[HPyC_3Br]Br$ (**F**)[27] were synthesized following literature methods. The benzimidazolium salts $[HPyC_2SAc]Br$ (**G**) and $[HPyC_3SAc]Br$ (**H**) were synthesized based on literature methods with small modifications (see experimental section).[25, 26] The dimeric nickel compounds $[Ni_2Cl_2(BnC_2S)_2]$ [**1**], $[Ni_2Cl_2(BnC_3S)_2]$ [**2**], $[Ni_2(PyC2S)_2]Br_2$ [**3**]Br_2 and $[Ni_2(PyC_3S)_2]Br_2$ [**4**]Br_2 were obtained from a melt of nickel acetate with the respective acyl-protected ligand precursor (**C**, **D**, **G** and **H**) in tetrabutylammonium bromide under vacuum at 120 °C (see Figure 2.1). The chloride ions in compounds [**1**] and [**2**] are derived from the solvent dichloromethane during the recrystallization process.

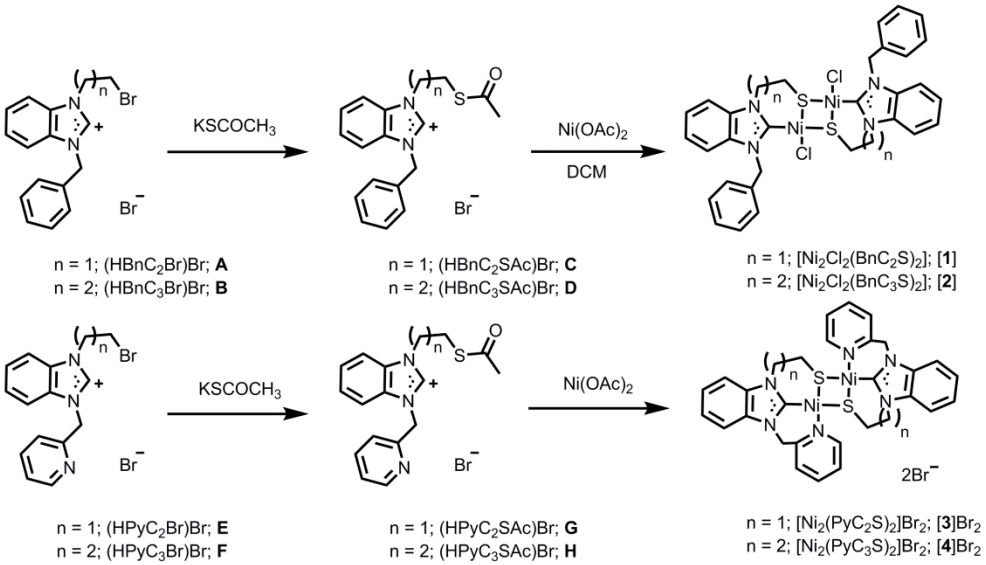

Figure 2.1. Synthesis route of the nickel compounds described in this Chapter.

Deprotonation of the benzimidazolium salt and in situ hydrolysis of the thioester group occurs during the reaction with the nickel salt and the resulting thiolate group bridges between two nickel ions to form the dinuclear Ni-NHC complexes. The four complexes were obtained as red powders. The absence of a ^{1}H NMR signal for the acidic NCHN proton (at ~ 10 ppm) confirmed formation of the desired Ni-carbene bond. The low-spin state of the Ni^{II} ions in compounds [**1**], [**2**] and [**4**]Br_2 is evidenced by their diamagnetic ^{1}H NMR spectra. In contrast, the ^{1}H NMR spectrum of compound [**3**]Br_2 in DMSO-d_6 shows rather broad signals (Figure AII.1). Low temperature NMR spectra could not be obtained as the solvent DMSO-d_6 is not suitable. ESI-MS analysis of the four compounds shows the presence of dicationic fragment ions $[M-2X]^{2+}$ and $[M-X]^+$. Despite the fact that recrystallized samples of the Ni compounds were dried in vacuo before elemental analysis was performed, the analytical data still show the presence of the solvents that were used in recrystallization.

2.2.2 Structural characterization of the complexes

Single crystals of [**1**] and [**2**] suitable for X-ray structure determination were obtained from slow evaporation of dichloromethane solutions of the compounds. Solutions of the complexes [**3**]Br_2 and [**4**]Br_2 are not stable in air (Figure AII.2); the compounds slowly decompose as apparent by a color change. Single crystals of these two complexes suitable for X-ray structure determination were obtained by slow evaporation of degassed methanol solutions under a flow of argon. The crystallographic data of compounds [**1**], [**2**], [**3**]Br_2 and [**4**]Br_2 are collected in Table AII.1 in Appendix II; selected bonds lengths and angles are given in Table 2.1. Projections of the structures are shown in Figure 2.2.

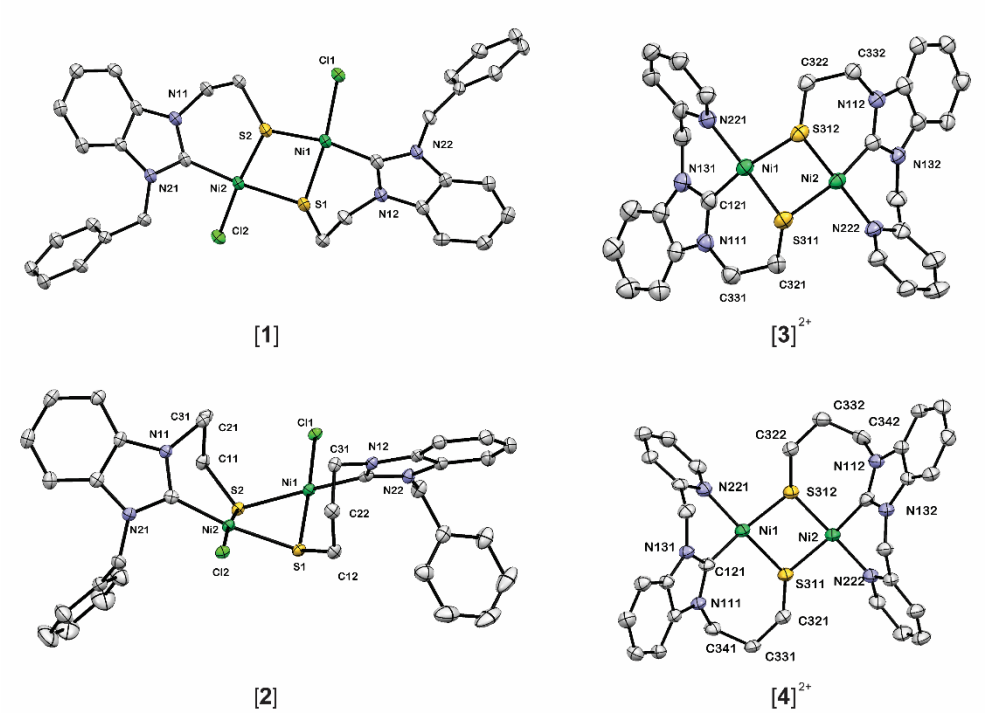

Figure 2.2. Displacement ellipsoid plots of the cationic compounds: [1], [2], $[3]^{2+}$ and $[4]^{2+}$ drawn at 50% probability level with selected atom numbering. Hydrogen atoms, non-coordinated bromide ions and lattice solvent molecules are omitted for clarity.

In the structures of compounds [**1**] and [**2**], each Ni center is coordinated by the bidentate ligand via the NHC carbon atom and the thiolate sulfur of the pendant arm as well as one chloride ion; the coordination sphere of the Ni^{II} ions is completed by a bridging thiolate donor of a second monomeric unit, resulting in the observed dinuclear structure. Thus the coordination geometry of the nickel ions in compounds [**1**] and [**2**] can be described as slightly distorted square planar (τ_4 = ~0.16 for [**1**], τ_4 = ~0.13 for [**2**]; τ_4 = 0 being the theoretical value for an ideal square-planar geometry).[28]

The nickel ions in [**3**]Br_2 and [**4**]Br_2 are coordinated by the tridentate ligand, bound via the pyridyl nitrogen, the NHC carbon and thiolate sulfur atom; the coordination sphere of the nickel centers is completed by a bridging thiolate sulfur atom of a second nickel center, thus forming the dinuclear complexes. The square-planar geometry of the nickel centers in $[\mathbf{3}]^{2+}$ and $[\mathbf{4}]^{2+}$ is even less distorted than those in [**1**] and [**2**] as evidenced by the smaller τ_4 values (τ_4 = ~0.10 for $[\mathbf{3}]^{2+}$, ~0.07 for $[\mathbf{4}]^{2+}$).

The crystal structure of compound [**1**] with two bromide ions instead of chlorides has been reported in the non-centrosymmetric orthorhombic $P2_12_12_1$ space group,[29] while compound [**1**] crystallized in the centrosymmetric triclinic *P-1* space group even though the environments of the nickel centers are highly similar. The bond distances and angles in [**1**]

are comparable with those in the published structure,[29] with the logical exception that the Ni─Cl bond is shorter than the Ni─Br distance. The complexes [**2**], [**3**]Br_2, and [**4**]Br_2 present similar Ni─C and Ni─S bond lengths. The Ni─C bond lengths in the four complexes are all around 1.89 Å and the Ni─S bond lengths within the chelating ligand are around 2.15 ~ 2.18 Å. The Ni─S bond distances to the thiolate sulfur of the other nickel center are slightly longer, namely around 2.19 ~ 2.22 Å. The Ni─N bond lengths in $[\mathbf{3}]^{2+}$ and $[\mathbf{4}]^{2+}$ are 1.929 Å and 1.922 Å, respectively.

*Table 2.1. Selected bond distances (Å) and angles (°) of the compounds [**1**], [**2**], [**3**]Br_2 and [**4**]Br_2.*[a]

	[**1**]	[**2**]	[**3**]Br_2	[**4**]Br_2
Ni1–S	2.1736(9)	2.1743(7)	2.153(3)	2.1829(15)
Ni1–S'	2.2312(9)	2.2227(6)	2.227(4)	2.2084(16)
Ni1–C	1.883(4)	1.887(2)	1.889(9)	1.882(6)
Ni1–Cl1	2.1943(9)	2.2046(6)	/	/
Ni1–N	/	/	1.930(8)	1.922(4)
Ni1…Ni2	3.0847(8)	3.0413(6)	2.960(4)	3.068(1)
S–Ni1–S'	77.77(4)	78.15(2)	79.22(14)	79.92(6)
S–Ni1–C	90.72(11)	94.00(7)	94.8(3)	97.34(16)
S'–Ni1–C	165.60(11)	169.67(7)	165.4(4)	169.03(17)
S–Ni1–Cl	172.34(4)	172.32(3)	/	/
S'–Ni1–Cl	96.03(4)	96.61(2)	/	/
C–Ni1–Cl	96.06(11)	91.84(7)	/	/
S–Ni1–N	/	/	163.5(3)	167.46(15)
S'–Ni1–N	/	/	96.1(3)	95.13(15)
C–Ni1–N	/	/	93.2(4)	89.6(2)
Dihedral angle α	44.5(3)	66.9(2)	10.6(5)	24.9(6)
Hinge angle β	128.24(5)	125.99(4)	119.54(7)	130.44(8)

[a] *S = S1 ([**1**] and [**2**]), S311 ([**3**]Br_2 and [**4**]Br_2); S' = S2 ([**1**] and [**2**]), S312 ([**3**]Br_2 and [**4**]Br_2); C = C91 ([**1**]), C101 ([**2**]), C121 ([**3**]Br_2 and [**4**]Br_2); Cl = Cl1 ([**1**] and [**2**]); N = N221 ([**3**]Br_2 and [**4**]Br_2);.*

In order to compare the surroundings of the four complexes in detail, the dihedral angle α and hinge angle β are defined (Figure 2.3). The dihedral angle α is the torsion angle N–C–Ni–S, describing the angle between the plane of the benzimidazolidene ring and the square plane of the nickel center, indicating the orientation of the carbene ligand with respect to the plane of coordination. The hinge angle β is the torsion angle Ni–S–S'–Ni', describing the dihedral angle between the two adjacent coordination planes of the nickel centers, indicating the bent nature of the dinuclear molecule. Of the four complexes, the complexes [**3**]Br_2 and [**4**]Br_2 show much smaller dihedral angles α than [**1**] and [**2**], indicating that the presence of the third donor atom (the pendant pyridyl group) forces the NHC ring to orient itself in a more co-planar fashion with the plane of coordination. In general, the NHC carbene ligand preferentially is oriented perpendicular to the plane of coordination with dihedral angles α between 40-90°.[28, 30-34] Few exceptions have been reported for complexes bearing certain type of tridentate pincer ligands.[35-37]

Notably, the complex $[Ni_2(PyC2S)_2]Br_2$ [**3**]Br_2 not only displays the smallest torsion angle α (10.6(5)°), but also smallest hinge angle β (119.54(7)°). This means that this molecule is

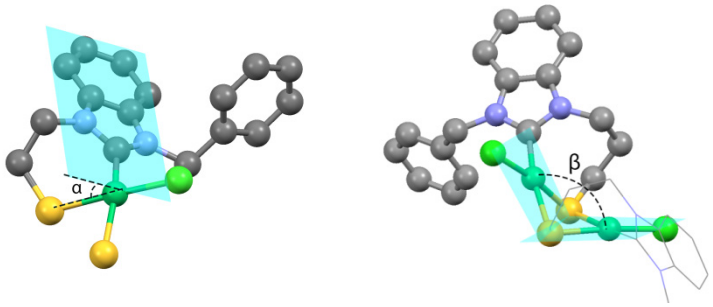

Figure 2.3. Schematic diagrams of the dihedral angle α and hinge angle β.

equipped with two nearly flat "wings", but that the overall structure is significantly bent. The crystal packing of compound [**3**]Br_2 shows an interesting interaction between one of the bromide ions with two dinuclear cations: two bent dinuclear molecules form a Ni_4S_4 "box" encapsulating the bromide ion (see Figure 2.4). This bromide ion is located near the apical position of each square-planar nickel center, with Ni to Br distances ranging between 3.4 to 3.6 Å (Ni1…Br1 = 3.616(3) Å, Ni2…Br1 = 3.668(5) Å, Ni3…Br1 = 3.422(5) Å, Ni4…Br1 = 3.403(6) Å). This interaction between four Ni centers and the bromide ions holds the Br^- ion in the center of a distorted "Ni_4 tetrahedron". If this supramolecular interaction is retained in solution it might be the cause of the broadening observed in the proton NMR spectrum of this compound.

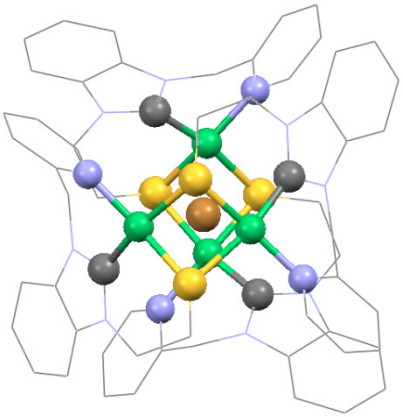

*Figure 2.4. Projection of the interaction between two [**3**]$^{2+}$ cations and one bromide ion in the crystal structure of compound [**3**]Br_2. Different elements are distinguished by color: nickel (green), sulfur (yellow),nitrogen (blue), carbon (grey), and bromide (brown).*

2.2.3 Electrochemical properties of the complexes

The redox properties of the two compounds $[Ni_2Cl_2(BnC_2S)_2]$ [**1**] and $[Ni_2Cl_2(BnC_3S)_2]$ [**2**] were first investigated with cyclic voltammetry in dry DMF solutions containing 0.1 M

tetrabutylammonium hexafluoridophosphate (TBAP) as the supporting electrolyte under a stream of argon. The CV of complex [**1**] shows one large irreversible reductive peak at −1.20 V followed by a more or less reversible couple at $E_{1/2}$ = −1.96 V vs Ag/AgCl. In between these reduction events two smaller reduction peaks are present (Figure 2.5). The CV of complex [**2**] shows a similar irreversible reductive peak at −1.28 V vs Ag/AgCl, at a slightly more negative potential compared to the C_2 analogue.

With the aim to study the electrocatalytic activity of these compounds in HER, subsequently acetic acid was added into the solutions of [**1**] and [**2**]. As a result, an increase in the current with an onset potential around −1.60 V was observed, but in both experiments only weak catalytic currents were observed (Figure 2.6).

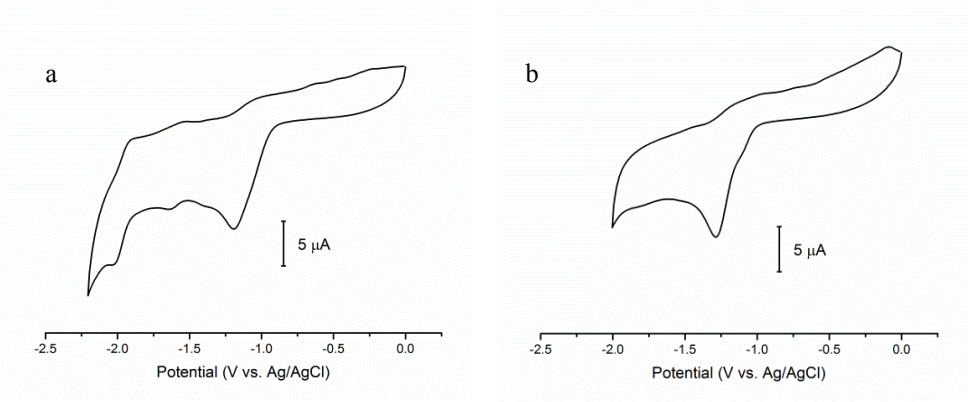

*Figure 2.5. The CVs of complexes [**1**] (a) and [**2**] (b) recorded in DMF containing 0.1 M TBAP as supporting electrolyte at scan rate 0.1 V/s, using glass carbon as working electrode.*

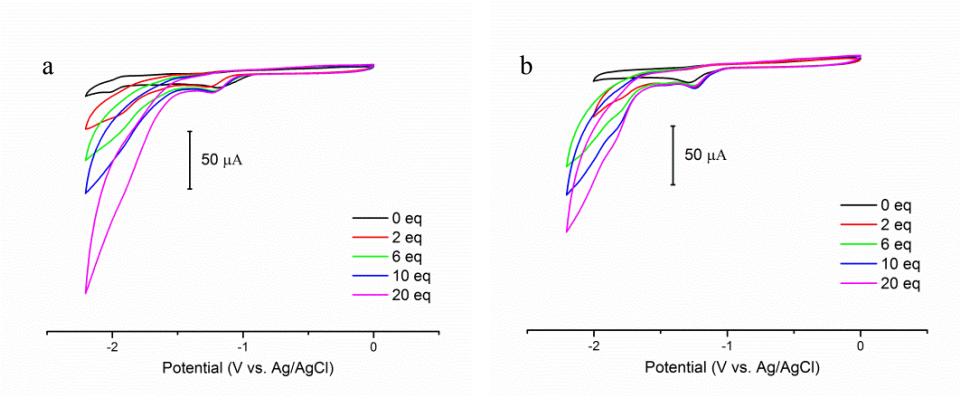

*Figure 2.6. The CVs of complexes [**1**] (a) and [**2**] (b) recorded in presence of various equivalents of acetic acid in DMF containing 0.1 M TBAP as supporting electrolyte at scan rate 0.1 V/s, using a glassy carbon working electrode.*

The redox properties of the pyridyl-containing complexes [**3**]Br_2 and [**4**]Br_2 were also investigated with cyclic voltammetry. In absence of acid, complex [**3**]Br_2 showed a number

of irreversible peaks with similar current intensities located in the range of −0.7 to −1.6 V, followed by a more or less reversible reduction at $E_{1/2}$ = −1.95 V vs. Ag/AgCl (Figure AII.4). The first reductive peak at −0.9 V becomes more reversible upon increasing scan rates (Figure 2.7). The complex [**4**]Br_2 with the longer alkyl chain shows a similar complicated CV (Figure AII.4). Similar to complex [**3**]Br_2, the first reductive peak becomes more reversible at higher scan rates (Figure 2.7). Notably, the first redox event of [**3**]Br_2 ($E_{1/2}$ = −0.88 V) occurs at more positive potential compared to the one of [**4**]Br_2 ($E_{1/2}$ = −0.98 V).

The complicated irreversible CVs of complex [**3**]Br_2 and [**4**]Br_2 might be due to solvation reactions in solution, resulting in an equilibrium of dimeric and monomeric species as shown in Figure 2.8. The dimeric structure might partly break up in solution after which the nickel ion coordinates with a bromide ion or solvent molecule to form a monomeric compound. The dimeric species and the different monomeric species will be reduced at different potentials, resulting in the multiple reductive waves. Alternatively, two Ni(II) ions in the dinuclear structure may successively be reduced to Ni(I) and then to Ni(0) instead of simultaneously.

Upon addition of acetic acid into the DMF solutions containing complex [**3**]Br_2 or [**4**]Br_2, a totally different electrochemical response is obtained compared to the complexes [**1**] and [**2**]. Whereas for complex [**1**] or [**2**] no obvious catalytic current was observed, upon addition of acetic acid into the DMF solution containing complex [**3**]Br_2, the reductive current after the onset potential of −0.91 V gradually increased; a large reductive current peak is observed at around −2 V. The solution of complex [**4**]Br_2 showed a similar result in presence of acetic acid with a onset potential at −1.08 V (Figure 2.9). In both situations, with increasing concentrations of acid the reductive current increased linearly (Figure 2.10). The i_c/i_p ratio is 100 for [**3**]Br_2 and 85 for [**4**]Br_2 in presence of 130 mM acid. Here, i_c is the maximum current of the catalytic peak, and i_p is the plateau current of the non-catalytic reduction wave.

Plots of i_c/i_p versus the square root of acid concentration for complexes [**3**]Br_2 and [**4**]Br_2 show a non-linear relationship (Figure AII.5). Instead, a linear relationship is found between i_c/i_p versus the acid concentration (Figure 2.10); thus the reaction is second order in acid, indicating that two protons are involved in the rate-determining catalytic step. The rate constant k_{obs} of the compounds cannot be calculated using equation (1)[6, 12, 13, 38-40] or the foot-of-the-wave method, as the preceding reduction wave is not reversible.[41-44]

$$\frac{i_c}{i_p} = \frac{n}{0.4463}\sqrt{\frac{RTk_{obs}}{Fv}} \quad (1)$$

By comparison of the i_c/i_p ratio it seems that complex [**3**]Br_2 shows higher catalytic activity in HER. However, complex [**3**]Br_2 also presents a redox process at $E_{1/2}$ = −1.95 V, which significantly overlaps with the catalytic current. Considering this redox event of the complex, the catalytic activity in this case might be lower than expected from the i_c/i_p ratio.

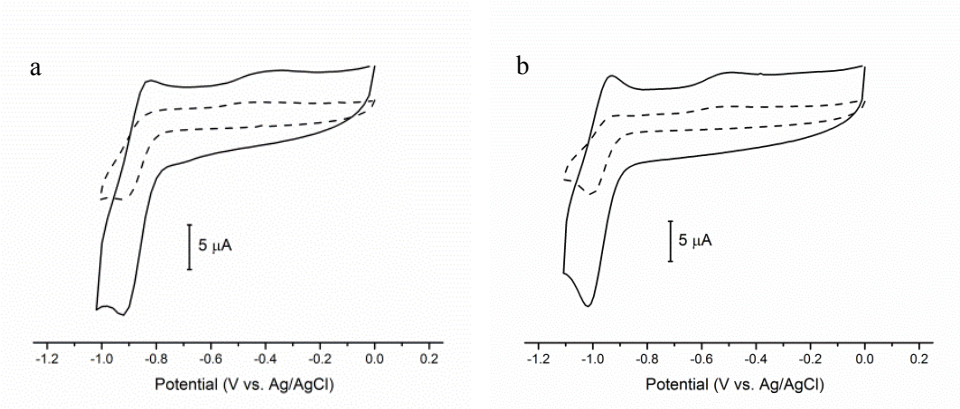

*Figure 2.7. Cyclic voltammograms of 1 mM [**3**]Br_2 (a) and [**4**]Br_2 (b) recorded in DMF containing 0.1 M TBAP as supporting electrolyte at different scan rates (dashed line = 0.1 V/s; solid line = 0.5 V/s), using a glassy carbon working electrode.*

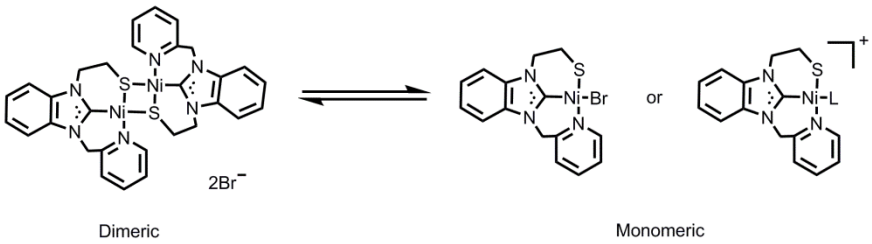

*Figure 2.8. Proposed dimer-monomer equilibrium of [**3**]Br_2 in solution (L = N,N-dimethylformamide).*

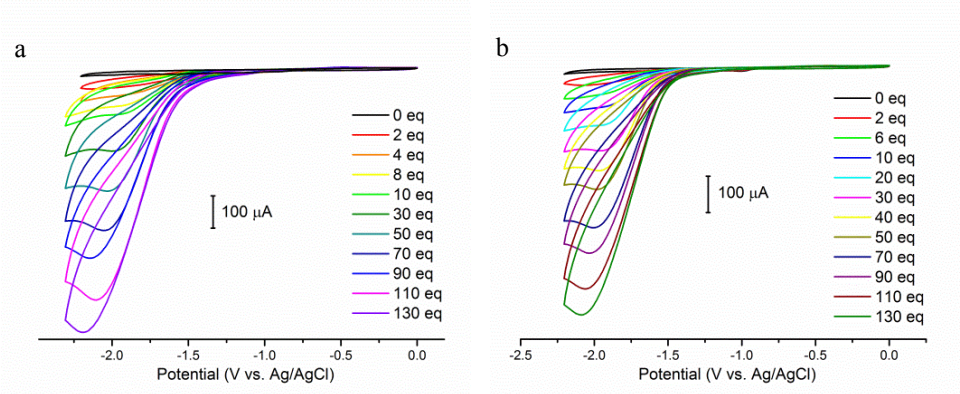

*Figure 2.9. The CVs of complexes [**3**]Br (a) and [**4**]Br (b) recorded in presence of various equivalents of acetic acid in DMF containing 0.1 M TBAP as supporting electrolyte at scan rate 0.1 V/s, using a glassy carbon working electrode.*

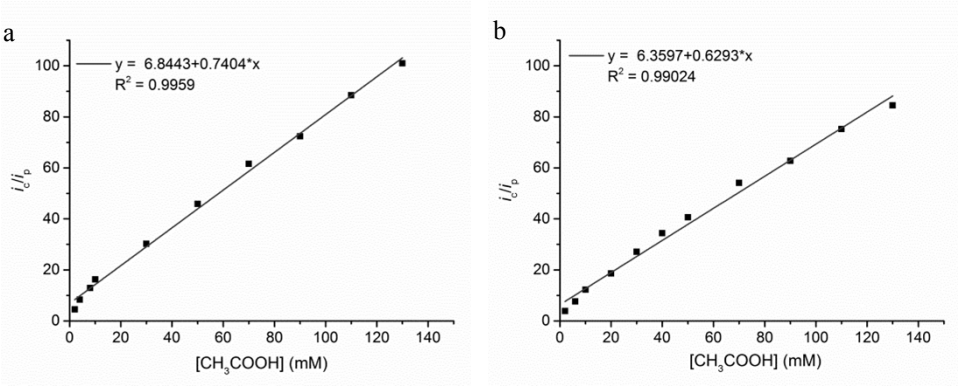

*Figure 2.10. Plot of i_c/i_p vs. [CH_3COOH] (mM) for [**3**]Br_2 (a) and [**4**]Br_2 (b). Conditions:1 mM complex in DMF containing 0.1 M TBAP as supporting electrolyte at 0.1 V/s, using a glassy carbon working electrode.*

With the aim to compare the electrocatalytic activity of the four compounds in a more quantitative way, controlled-potential coulometry experiments (CPC) were carried out. The charge consumptions over time of solutions containing just the pure acid or each of the catalysts were also recorded separately as references. The charge accumulation graphs show that over a period of 10 minutes charge consumption is negligible for the solutions containing only acid or only the nickel compounds (Figure 2.11 and Figure AII.6). In contrast, for solutions containing both acid and one of the nickel catalysts continuous charge consumption was recorded. Although no clear catalytic peaks were observed in the CV experiments for complex [**1**] or [**2**] in the presence of acid (Figure 2.6), relatively high charge consumptions were observed in the CPC experiments (Figure 2.11 and Figure AII.6). As expected, the pyridine-functionalized compounds [**3**]Br_2 and [**4**]Br_2 resulted in higher charge consumptions, indicating higher catalytic activities. The quantity of dihydrogen generated during the CPC experiments can be estimated from the charge consumption of solutions containing both the nickel compound and the acid after subtraction of the charge consumption of the blanks; the results are listed in Table 2.2 (assuming that all electrons are used in proton reduction). Among the four complexes, the compound $[Ni_2(PyC_3S)_2]Br_2$ [**4**]Br_2 shows the highest catalytic activity, which is estimated to produce 5×10^{-4} mmol H_2 gas in 10 min in presence of 6×10^{-3} mmol catalyst at a potential of −1.80 V. These compounds can hardly be considered to be good catalysts for HER; even so, it is apparent that the pyridine-functionalized complexes $[Ni_2(PyC_2S)_2]Br_2$ [**3**]Br_2 and $[Ni_2(PyC_3S)_2]Br_2$ [**4**]Br_2 as catalysts perform better than their benzyl-substituted analogues.

Table 2.2. Estimated amount of dihydrogen generated by the four compounds in 10 minutes ($n_{catalyst}$ = 6×10^{-3} mmol).

Compound	$[Ni_2Cl_2(BnC_2S)_2]$ [**1**]	$[Ni_2Cl_2(BnC_3S)_2]$ [**2**]	$[Ni_2(PyC_2S)_2]Br_2$ [**3**]Br_2	$[Ni_2(PyC_3S)_2]Br_2$ [**4**]Br_2
n (H_2) (mmol)	1.5×10^{-4}	1.5×10^{-4}	4×10^{-4}	5×10^{-4}

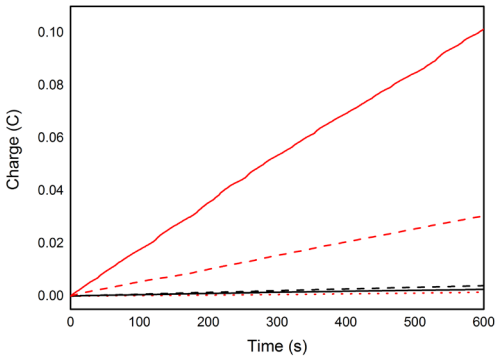

*Figure 2.11. Charge vs. time plot over 600 s during CPC at a potential of −1.8 V. Black line: compounds in absence of acid; Red line: compounds in presence of 50 mM acetic acid (dashed = 1 mM [$Ni_2Cl_2(BnC_3S)_2$] [**2**], solid = 1mM [$Ni_2(PyC_3S)_2$]Br_2 [**4**]Br_2); Dotted red line: 50 mM acetic acid only.*

2.3 Conclusion

In this Chapter, the synthesis and characterization is reported of the compounds [$Ni_2Cl_2(BnC_2S)_2$] [**1**], [$Ni_2Cl_2(BnC_3S)_2$] [**2**], [$Ni_2(PyC_2S)_2$]Br_2 [**3**]Br_2 and [$Ni_2(PyC_3S)_2$]Br_2 [**4**]Br_2, comprising four different thiolate-functionalized N-heterocyclic carbene ligands. CV and CPC experiments were used to investigate the redox properties and electrocatalytic activity of these complexes. In this Chapter, for thiolate-functionalized carbene compounds [**1**] and [**2**], we observed their weak catalytic activity on HER. However, it was found that compounds [**3**]Br_2 and [**4**]Br_2 containing pyridine groups show better catalytic activity in HER than their benzyl-containing analogues. Unfortunately, the limited stability of solutions of the complexes [**3**]Br_2 and [**4**]Br_2 in presence of air and the low electrocatalytic efficiency limit their potential application as proton reduction catalysts. Meanwhile understanding of the role of thiolate and pyridine group in catalytic cycle still requires further related research, which may help the design of efficient biomimic catalysts on HER.

2.4 Experimental

2.4.1 Materials

Commercial chemicals were used without further purification. Acetonitrile and diethyl ether were obtained from a PureSolv MD5 solvent dispenser. Dry dimethylformamide were prepared by adding molecular sieves into commercial anhydrous solvent. The rest commercial solvents were used without further purification. All air-sensitive reactions were performed under argon or dinitrogen gas using standard Schlenk techniques unless mentioned otherwise.

2.4.2 Analytical methods

^{1}H and ^{13}C spectra were recorded on a Bruker 300 DPX spectrometer. Mass spectra were obtained using a Finnigan Aqua Mass Spectrometer (MS) with electro spray ionization (ESI). UV-vis spectra were obtained using a transmission dip probe using an Avantes Avaspec-2048 spectrometer with an Avalight-DH-S-BAL light source. Elemental analyses were performed by the Kolbe Mikroanalytisches Laboratorium, Germany.

Cyclic voltammetry was recorded with an Autolab PGstat10 potentiostat controlled by GPES4 software under argon. A 3 mm diameter glassy carbon electrode was used as working electrode and platinum as the counter electrode. The cyclic voltammetry was performed in dry DMF with 0.1 M tetrabutylammonium hexafluoridophosphate (TBAP) as the supporting electrolyte under a stream of argon at room temperature. The experimental reference was an Ag/AgCl (3 M KCl) electrode in the electrolyte solution (TBAP). Ferrocene was added at the end of each measurement as an internal standard. Under these conditions the Fc/Fc^{+} couple was located at 0.510 V vs Ag/AgCl with a ΔE_p of 95 mV. The surface of the working electrode was polished, sonicated and rinsed before each single CV measurement.

Controlled-potential coulometry (CPC) experiments were carried out with an Autolab PGstat10 potentiostat controlled by GPES4 software under argon. A 3 mm diameter glassy carbon electrode was used as working electrode and platinum as the counter electrode. 0.006mmol complex (1 mM) and 17.5 µL acetic acid (50 mM) were added in 6 mL dry degassed DMF with 0.1 M tetrabutylammonium hexafluoridophosphate (TBAP) as the supporting electrolyte under a stream of argon at room temperature. A CPC experiment was run at −1.8 V for 600 s, while the solution was stirred continuously. The blank and reference CPC experiments (only acid or only catalyst added) were performed using the same conditions.

3.4.3 Single Crystal X-ray Crystallography

All reflection intensities were measured at 110(2) K using a SuperNova diffractometer (equipped with Atlas detector) with Cu *K*α radiation (λ = 1.54178 Å) under the program CrysAlisPro (Versions 1.171.36.32, 1.171.37.31 or 1.171.37.35 Agilent Technologies, 2013-2014). The same program was used to refine the cell dimensions and for data reduction. The structure was solved with the program SHELXS-2013,[45] and was refined on F^2 with SHELXL-2013.[45] Analytical numeric absorption corrections based on a multifaceted crystal model were applied using CrysAlisPro. The temperature of the data collection was controlled using the system Cryojet (manufactured by Oxford Instruments). The H atoms were placed at calculated positions (unless otherwise specified) using the instructions AFIX 23, AFIX 43, AFIX 137 or AFIX 147 with isotropic displacement parameters having values 1.2 or 1.5 *U*eq of the attached C atoms. For [**4**]Br_2, the H atoms attached to O1W were found from difference Fourier maps, and their coordinates were refined freely.

$[Ni_2Cl_2(BnC_2S)_2]$ [**1**]: The structure is disordered. The crystal that was mounted on the diffractometer was non-merohedrally twinned. The twin components are related by a twofold axis around the vector 0.0034a* + 0.7058b* + 0.7084c*. Data integration of the twinned data was performed using CrysAlisPro, and a HKLF 5 file was made. The BASF scale factor refines to 0.2245(18).

$[Ni_2Cl_2(BnC_3S)_2]$ [**2**]: The structure is partly disordered. The two crystallographically independent dichloromethane solvent molecules in the asymmetric unit are found to be disordered over two orientations. The occupancy factors of the major components of the disorder refine to 0.864(2) and 0.881(3).

$[Ni_2(PyC_2S)_2]Br_2$ [**3**]Br_2: The asymmetric unit contains four crystallographically independent dinuclear cations and eight bromide anions. The structure is partly disordered. Two of the four dimers are disordered over two orientations, and the occupancy factors of the major components of the disorder refine to 0.643(8) and 0.722(5), respectively. Four of the eight Br^- counter ions are fully occupied (and ordered), whereas the remaining counter ions are found to be disordered over two, three or four positions. For those counterions, the sum of the occupancy factors was restrained to be equal to four using the SUMP instruction. The crystal lattice also contains some amount of unresolved electron density (most likely disordered and/or partially occupied lattice solvent molecules), whose contribution has been taken out in the final refinement.[46]

$[Ni_2(PyC_2S)_2]Br_2$ [**4**]Br_2: The structure is partly disordered. One of the two Br^- counter ions is disordered over two positions, and the occupancy factor of the major component of the disorder refines to 0.74(3). The crystal lattice also contains one very disordered MeOH lattice solvent molecule per asymmetric unit found at sites of twofold axial symmetry; its contribution has been taken out in the final refinement.[46] The crystal was not single but rather a composite of three crystals stuck together, and the two BASF scale factors refine to 0.146(2) and 0.1023(19).

2.4.4 Ligand precursors synthesis

N-Pyridylmethylbenzimidazole,[47] and the benzimidazolium ligand precursor salts $[HBnC_2Br]Br$ (**A)** and $[HBnC_3Br]Br$ (**B**)[25], $[HBnC_2SAc]Br$ (**C**) and $[HBnC_3SAc]Br$ (**D**),[26], $[HPyC_2Br]Br$ (**E**) and $[HPyC_2Br]Br$ (**F**)[27] were synthesized following literature methods.

$[HPyC_2SAc]Br$ (**G**):
A mixture of salt **E** (0.625 g, 1.6 mmol) and $KSCOCH_3$ (0.200 g, 1.8 mmol) in acetonitrile (10 mL) was stirred at room temperature for 16 h. The suspension was filtered, yielding a white powder. The white powder was washed with diethyl ether to get the pure product in a yield of 0.44 g (72%). ^{1}H NMR (300 MHz, DMSO-d_6) δ 10.02 (s, 1H, NCHN), 8.49 (d, J = 4.8 Hz, 1H, Ar-*H*), 8.17 (d, J = 8.4 Hz, 1H, Ar-*H*), 7.99 – 7.85 (m, 2H, Ar-*H*), 7.75 – 7.57 (m, 3H, Ar-*H*), 7.43 – 7.32 (m, 1H, Ar-*H*), 5.95 (s, 2H, N-CH_2-Py), 4.77 (t, J = 6.4 Hz, 2H,

NCH_2), 3.43 (t, J = 6.6 Hz, 2H, CH_2S), 2.28 (s, 3H, COCH_3). ^{13}C NMR (75 MHz, DMSO-d_6) δ = 149.63, 143.30, 137.57, 126.80, 126.71, 123.74, 122.74, 113.93, 113.84, 50.87, 46.19, 30.50, 27.83. The resonances of the four quaternary carbon atoms were not detected. ESI-MS found (calculated): $[M-Br]^+$ m/z 312.1 (312.1).

[HPyC$_3$SAc]Br (**H**):
A mixture of salt **F** (0.500 g, 1 mmol) and KSCOCH$_3$ (0.170 g, 1.2 mmol) in acetonitrile (10 mL) was stirred at room temperature for 48 h. The suspension was filtered, yielding a white powder, which was washed with a mixture of the filtrate and diethyl ether. The white powder was purified by column chromatography (Al_2O_3, dichloromethane, dichloromethane/methanol = 3:1) giving a yield of 0.37 g (75%). ^{1}H NMR (300 MHz, DMSO-d_6) δ 10.00 (s, 1H, NCHN), 8.48 (d, J = 5.6 Hz, 1H, Ar-H), 8.10 (d, J = 7.0 Hz, 1H, Ar-H), 8.00 – 7.84 (m, 2H, Ar-H), 7.74 – 7.60 (m, 3H, Ar-H), 7.38 (dd, J = 7.0, 5.3 Hz, 1H, Ar-H), 5.92 (s, 2H, N-CH_2-Py), 4.62 (t, J = 7.0 Hz, 2H, NCH_2), 2.93 (t, J = 7.3 Hz, 2H, CH_2S), 2.32 (s, 3H, COCH_3), 2.19 (p, J = 7.1 Hz, 2H, CH$_2$-CH_2-CH$_2$). ^{13}C NMR (75 MHz, DMSO-d_6) δ = 149.57, 137.54, 126.77, 126.63, 123.72, 122.75, 113.89, 113.79, 50.86, 45.77, 28.68, 25.23. The resonances of the four quaternary carbon atoms were too weak to be detected. ESI-MS found (calculated): $[M-Br]^+$ m/z 316.1 (316.1).

2.4.4 Synthesis of the nickel compounds

[Ni$_2$Cl$_2$(BnC$_2$S)$_2$] [**1**]:
Ligand precursor **C** (0.390 g, 1.0 mmol), anhydrous Ni(OAc)$_2$ (0.090 g, 0.5 mmol) and tetrabutylammonium bromide (2 g) were weighed into a 10 mL round-bottomed flask and dried for 3 hours at 60 ^{o}C under vacuum. Then the temperature of the flask was increased to 120 ^{o}C and kept constant for 24 hours. The mixture was allowed to cool to room temperature and then was triturated with H_2O (10 ml) and DCM (20 ml). The organic layer was separated, washed with brine and dried on sodium sulfate. Removal of the solvent resulted in a red solid in a yield of 85 mg (24%). Single crystals suitable for X-ray structure determination were obtained from a DCM solution of the complex. ^{1}H NMR (300 MHz, chloroform-d) δ 7.63 (d, J = 6.1 Hz, 4H, Ar-H), 7.47 – 7.01 (m, 14H, Ar-H), 6.68 (d, J = 15.5 Hz, 2H, N-CHH-Py), 5.69 (d, J = 15.6 Hz, 2H, N-CHH-Py), 5.07 (t, J = 13.0 Hz, 2H, CHHS), 4.78 (d, J = 13.4 Hz, 2H, NCHH), 2.89 (d, J = 12.4 Hz, 2H, NCHH), 1.36 (t, J = 11.8 Hz, 2H, CHHS). ^{13}C NMR (75 MHz, chloroform-d) δ 174.30, 136.45, 134.95, 133.94, 128.95, 128.10, 127.97, 123.28, 123.24, 111.39, 110.07, 52.32, 49.34, 24.19. Elemental analysis: $C_{32}H_{30}N_4S_2Ni_2Cl_2 \cdot CH_2Cl_2$: Calcd. C 49.06, H 3.99, N 6.93; Found 49.26, H 4.17, N 6.75. ESI-MS found (calculated): $[M-2Cl]^{2+}$ m/z 325.0 (325.03); $[M-Cl]^+$ m/z 685.3 (685.03).

[Ni$_2$Cl$_2$(BnC$_3$S)$_2$] [**2**]:
Ligand precursor **D** (0.405 g, 1.0 mmol), anhydrous Ni(OAc)$_2$ (0.177 g, 1.0 mmol) and tetrabutylammonium bromide (2 g) were weighed into a 10 mL round-bottomed flask and dried for 3 hours at 60 ^{o}C under vacuum. Then the temperature was increased to 120 ^{o}C and kept constant for 24 hours. The mixture was allowed to cool to room temperature and then

was triturated with H_2O (10 ml) and DCM (20 ml). The organic layer was separated, washed with brine and dried on sodium sulfate. Removal of the solvent resulted in a red solid, which was washed with diethyl ether, giving a yield of 50 mg (13%). Single crystals suitable for X-ray structure determination were obtained from a DCM solution. ^{1}H NMR (300 MHz, Dichloromethane-d_2) δ 7.85 (td, J = 13.6, 5.9 Hz, 2H, CH*H*S), 7.55 (d, J = 6.8 Hz, 4H, Ar-*H*), 7.49 – 7.29 (m, 8H, Ar-*H*), 7.25 – 7.07 (m, 6H, Ar-*H*), 6.56 (d, J = 15.6 Hz, 2H, N-CH*H*-Py), 5.53 (d, J = 15.6 Hz, 2H, N-C*H*H-Py), 5.12 (dd, J = 14.3, 6.6 Hz, 2H, NCH*H*), 2.93 (m, 2H, CH_2-CH*H*-CH_2), 2.12 (m, 4H, CH_2-C*H*H-CH_2, NC*H*H), 0.63 (td, J = 13.5, 4.9 Hz, 2H, C*H*HS). ^{13}C NMR (75 MHz, Dichloromethane-d_2) δ = 176.08, 136.67, 135.54, 133.79, 129.18, 128.39, 128.21, 123.40, 123.17, 111.40, 109.96, 51.94, 44.51, 23.84, 22.59. Elemental analysis: $C_{34}H_{34}N_4S_2Ni_2Cl_2 \cdot C_4H_{10}O$: Calcd. C 55.31, H 5.37, N 6.79; Found C 55.15, H 5.09, N 6.54. ESI-MS found (calculated): $[M-Cl]^+$ *m*/*z* 713.3 (713.06).

$[Ni_2(PyC_2S)_2]Br_2$ [**3**]Br_2:
Ligand precursor **G** (0.380 g, 0.8 mmol), anhydrous $Ni(OAc)_2$ (0.140 g, 0.8 mmol) and tetrabutylammonium bromide (1.5 g) were weighed into a 10 mL round bottom flask and dried for 3 hours at 80 °C under vacuum. Then the temperature was increased to 120 °C and kept for 48 hours. The mixture was allowed to cool to room temperature and then was triturated with H_2O (10 ml) resulting in a red solid. The solid was washed with a small amount of DCM and dried in vacuum, giving a yield of 75 mg of a red solid (18%). Crystals suitable for X-ray structure determination were obtained by slow evaporation of a degassed methanol solution under a flow of argon. ^{1}H NMR showed broad signals. ^{1}H NMR (300 MHz, DMSO-d_6) δ = 9.09, 8.13, 8.00, 7.91, 7.75, 7.57, 7.43, 6.16, 4.53, 2.13. Elemental analysis: $C_{30}H_{28}N_6S_2Ni_2Br_2 \cdot 1.5H_2O$: Calcd. C 42.85, H 3.72, N 9.99; Found C 42.55, H 3.40, N 9.99. ESI-MS found (calculated): $[M-2Br]^{2+}$ *m*/*z* 326.1 (326.03); [1/2M-Br+MeOH]$^+$ (mononuclear) *m*/*z* 358.1 (358.05).

$[Ni_2(PyC_3S)_2]Br_2$ [**4**]Br_2:
Ligand precursor **H** (0.405 g, 1.0 mmol), anhydrous $Ni(OAc)_2$ (0.180 g, 1.0 mmol) and tetrabutylammonium bromide (1.9 g) were weighed into a 10 mL round bottom flask and dried for 3 hours at 80 °C under vacuum. Then the temperature was increased to 130 °C and kept for 24 hours. The mixture was allowed to cool to room temperature and then was triturated with H_2O (10 ml) resulting in a red solid. The solid was washed with a small amount of DCM and dried in vacuum, giving a yield of 42 mg (10%). Crystals suitable for X-ray structure determination were obtained by slow evaporation of a degassed methanol solution under a flow of argon. ^{1}H NMR (300 MHz, DMSO-d_6) δ 8.88 (d, *J* = 5.3 Hz, 2H), 8.09 – 8.00 (m, 4H, Ar-*H*), 7.88 (d, *J* = 7.7 Hz, 2H, Ar-*H*), 7.76 (d, *J* = 8.0 Hz, 2H, Ar-*H*), 7.51 – 7.39 (m, 6H, Ar-*H*), 6.58 (d, *J* = 15.4 Hz, 2H, N-CH*H*-Py), 6.29 (d, *J* = 15.1 Hz, 2H, N-C*H*H-Py), 4.84 (broad, 2H), 4.67 (d, *J* = 12.8 Hz, 2H), 1.92 (broad, 4H), 1.43 (broad, 4H). ^{13}C NMR (75 MHz, DMSO-d_6) δ = 171.14, 154.93, 154.70, 140.08, 133.51, 133.33, 125.47, 125.29, 123.76, 111.31, 110.96, 50.25, 42.37, 27.18, 24.53. $C_{32}H_{32}N_6S_2Ni_2Br_2$

$3CH_3OH{\cdot}3H_2O$: Calcd. C 42.37, H 5.08, N 8.47; Found C 42.76, H 5.13, N 8.41. ESI-MS found (calculated): $[M-2Br]^{2+}$ *m*/*z* 340.0 (340.04); $[M-Br]^{+}$ *m*/*z* 759.0 (759.00).

2.5 Acknowledgement

S. Luo gratefully acknowledges a grant from the Chinese Scholarship Council (no. 201306410011). We thank Mr. J.M.M van Brussel for ESI-MS measurements.

2.6 References

[1] B. Rausch, M.D. Symes, G. Chisholm, L. Cronin, *Science* 2014, 345, 1326-1330.
[2] D.L. DuBois, *Inorg. Chem.* 2014, 53, 3935-3960.
[3] T.R. Simmons, G. Berggren, M. Bacchi, M. Fontecave, V. Artero, *Coord. Chem. Rev.* 2014, 270, 127-150.
[4] P. Tong, W. Xie, D. Yang, B. Wang, X. Ji, J. Li, J. Qu, *Dalton Trans.* 2016, 45, 18559-18565.
[5] S. Canaguier, V. Fourmond, C.U. Perotto, J. Fize, J. Pecaut, M. Fontecave, M.J. Field, V. Artero, *Chem. Commun.* 2013, 49, 5004-5006.
[6] L. Gan, T.L. Groy, P. Tarakeshwar, S.K.S. Mazinani, J. Shearer, V. Mujica, A.K. Jones, *J. Am. Chem. Soc.* 2015, 137, 1109-1115.
[7] D. Brazzolotto, M. Gennari, N. Queyriaux, T.R. Simmons, J. Pecaut, S. Demeshko, F. Meyer, M. Orio, V. Artero, C. Duboc, *Nat Chem* 2016, 8, 1054-1060.
[8] I.K. Pandey, S.M. Mobin, N. Deibel, B. Sarkar, S. Kaur-Ghumaan, *Eur. J. Inorg. Chem.* 2015, 2875-2882.
[9] A. Mondragón, M. Flores-Alamo, P.R. Martínez-Alanis, G. Aullón, V.M. Ugalde-Saldívar, I. Castillo, *Inorg. Chem.* 2015, 54, 619-627.
[10] K. Hou, H.T. Poh, W.Y. Fan, *Chem. Commun.* 2014, 50, 6630-6632.
[11] L.-C. Song, H. Tan, F.-X. Luo, Y.-X. Wang, Z. Ma, Z. Niu, *Organometallics* 2014, 33, 5246-5253.
[12] E.I. Musina, V.V. Khrizanforova, I.D. Strelnik, M.I. Valitov, Y.S. Spiridonova, D.B. Krivolapov, I.A. Litvinov, M.K. Kadirov, P. Lonnecke, E. Hey-Hawkins, Y.H. Budnikova, A.A. Karasik, O.G. Sinyashin, *Chem. -Eur. J.* 2014, 20, 3169-3182.
[13] R.M. Stolley, J.M. Darmon, M.L. Helm, *Chem. Commun.* 2014, 50, 3681-3684.
[14] M.L. Helm, M.P. Stewart, R.M. Bullock, M.R. DuBois, D.L. DuBois, *Science* 2011, 333, 863-866.
[15] D. Morvan, J.-F. Capon, F. Gloaguen, A. Le Goff, M. Marchivie, F. Michaud, P. Schollhammer, J. Talarmin, J.-J. Yaouanc, R. Pichon, N. Kervarec, *Organometallics* 2007, 26, 2042-2052.
[16] C.C. McCrory, C. Uyeda, J.C. Peters, *J. Am. Chem. Soc.* 2012, 134, 3164-3170.
[17] P.A. Jacques, V. Artero, J. Pecaut, M. Fontecave, *Proc. Natl. Acad. Sci. U. S. A.* 2009, 106, 20627-20632.
[18] N. Kaeffer, A. Morozan, V. Artero, *J. Phys. Chem. B* 2015, 119, 13707-13713.
[19] S.M. Laga, J.D. Blakemore, L.M. Henling, B.S. Brunschwig, H.B. Gray, *Inorg. Chem.* 2014, 53, 12668-12670.
[20] P.D. Tran, J. Barber, *Phys. Chem. Chem. Phys.* 2012, 14, 13772-13784.
[21] K. Kawano, K. Yamauchi, K. Sakai, *Chem. Commun.* 2014, 50, 9872-9875.
[22] M. van der Meer, E. Glais, I. Siewert, B. Sarkar, *Angew. Chem. Int. Ed.* 2015, 54, 13792-13795.

[23] S. Luo, M.A. Siegler, E. Bouwman, *Eur. J. Inorg. Chem.* 2016, 4693-4700.
[24] S. Jiang, T. Zhang, X. Zhang, G. Zhang, L. Hai, B. Li, *RSC Advances* 2016, 6, 84139-84148.
[25] D. Yuan, H.V. Huynh, *Organometallics* 2010, 29, 6020-6027.
[26] D. Yuan, Q. Teng, H.V. Huynh, *Organometallics* 2014, 33, 1794-1800.
[27] A.K. Lal, M.D. Milton, *Tetrahedron Lett.* 2014, 55, 1810-1814.
[28] M.H. Reineke, M.D. Sampson, A.L. Rheingold, C.P. Kubiak, *Inorg. Chem.* 2015, 54, 3211-3217.
[29] D. Yuan, H.V. Huynh, *Inorg. Chem.* 2013, 52, 6627-6634.
[30] R. Jothibasu, K.-W. Huang, H.V. Huynh, *Organometallics* 2010, 29, 3746-3752.
[31] T. Kosterke, T. Pape, F.E. Hahn, *Chem. Commun.* 2011, 47, 10773-10775.
[32] H. Vinh Huynh, R. Jothibasu, *Eur. J. Inorg. Chem.* 2009, 1926-1931.
[33] H.V. Huynh, C. Holtgrewe, T. Pape, L.L. Koh, E. Hahn, *Organometallics* 2006, 25, 245-249.
[34] J.C. Bernhammer, H.V. Huynh, *Organometallics* 2014, 33, 5845-5851.
[35] E.M. Matson, G. Espinosa Martinez, A.D. Ibrahim, B.J. Jackson, J.A. Bertke, A.R. Fout, *Organometallics* 2015, 34, 399-407.
[36] D.H. Brown, B.W. Skelton, *Dalton Trans.* 2011, 40, 8849-8858.
[37] G.E. Martinez, C. Ocampo, Y.J. Park, A.R. Fout, *J. Am. Chem. Soc.* 2016, 138, 4290-4293.
[38] P. Zhang, M. Wang, Y. Yang, T. Yao, L. Sun, *Angew. Chem. Int. Ed.* 2014, 53, 13803-13807.
[39] M.P. Stewart, M.-H. Ho, S. Wiese, M.L. Lindstrom, C.E. Thogerson, S. Raugei, R.M. Bullock, M.L. Helm, *J. Am. Chem. Soc.* 2013, 135, 6033-6046.
[40] R. Tatematsu, T. Inomata, T. Ozawa, H. Masuda, *Angew. Chem. Int. Ed.* 2016, 55, 5247-5250.
[41] C. Costentin, J.-M. Saveant, *Chemelectrochem* 2014, 1, 1226-1236.
[42] J.M. Saveant, *Chemelectrochem* 2016, 3, 1967-1977.
[43] E.S. Wiedner, R.M. Bullock, *J. Am. Chem. Soc.* 2016, 138, 8309-8318.
[44] C. Costentin, S. Drouet, M. Robert, J.-M. Savéant, *J. Am. Chem. Soc.* 2012, 134, 11235-11242.
[45] G.M. Sheldrick, *Acta Cryst. A* 2008, 64, 112-122.
[46] A.L. Spek, *Acta Cryst. D* 2009, 65, 148-155.
[47] J. Dinda, S.D. Adhikary, S.K. Seth, A. Mahapatra, *New J. Chem.* 2013, 37, 431-438.

CHAPTER 3

Nickel Complexes of Pyridine-Functionalized N-heterocyclic Carbenes: Syntheses, Structures, and Activity in Electrocatalytic Hydrogen Production

*Two bis-(benz)imidazolium salts alkylated with pyridyl side arms, H_2**L1**Br_2 (1,2-bis[(1-(2-pyridylmethyl)-benzimidazolium-3-yl)-methyl]benzene bromide) and H_2**L2**Br_2 (1,2-bis[(1-(2-pyridylmethyl)-imidazolium-3-yl)-methyl]benzene bromide) have been prepared and were used as precursors in the synthesis of novel nickel compounds of N-heterocyclic carbenes (Ni-NHC). The four Ni-NHC complexes [Ni(**L1**)Br]Br (**1a**), [Ni(**L1**)]$(PF_6)_2$ (**1b**), [Ni(**L2**)]Br_2 (**2a**) and [Ni(**L2**)]$(PF_6)_2$ (**2b**) were isolated and characterized by various methods, and the X-ray crystal structures of **1a**, **2a** and **2b** are reported. The nickel ion in **1a** is in a square-pyramidal geometry with one of the bromide ions in the apical position, the nickel ions in **2a** and **2b** are in square-planar geometries. The compounds of the ligand with an imidazole-based carbene revealed much higher activity in electrocatalytic proton reduction and better acid tolerance, although their overpotentials are higher than those of the benzimidazole-based compounds. The presence of bromide ions has an adverse effect on the redox potentials as well as the overpotentials for proton reduction. Complex **2b**, having the most planar coordination geometry, appeared to have the highest catalytic efficiency for proton reduction in DMF (i_c/i_p = 50, k_{obs} = 490 s^{-1} at 0.1 V/s) when using acetic acid as the proton source.*

This chapter has been published as a full paper: S. Luo, M.A. Siegler, E. Bouwman, Eur. J. Inorg. Chem. **2016**, 2016, 4693-4700.

3.1 Introduction

Dihydrogen is an environmentally friendly energy carrier as upon combustion it only produces H_2O.[1, 2] In order to enable the establishment of a society based on dihydogen as an energy source, for many years researchers have focused on the search for efficient proton-reduction catalysts, notably for catalysts that are not based on noble metals.[3-7] In the field of bioinorganic chemistry the synthesis of structural models of hydrogenases is a common strategy to devise molecular catalysts for proton reduction.[8, 9] However, the so-called 'functional models' of hydrogenases, which do not exhibit exactly similar structures, appear to result in more active and more stable catalytic systems. The two-electron donor ligands such as phosphanes and amines have been widely used in combination with Co[10-12] and Ni[7, 13] metal centers. The N-heterocyclic carbene (NHC) ligand is also a two-electron donor, with strong binding properties comparable to that of phosphane ligands.[14] Although Ni-NHC complexes have found various applications in organometallic chemistry,[15-21] the electrocatalytic properties of this kind of compounds so far mostly have been neglected.

NHC ligands functionalized with pyridine groups have been used to synthesize nickel and palladium complexes that were found to be efficient catalysts for the Kumada cross-coupling[22] and Heck-type coupling reactions.[23] Recently, the group of Kubiak reported a study of nickel compounds with four carbene ligands including their electrochemical characterization, but their activity in electrocatalysis was not discussed.[24] A series of nickel N-heterocyclic carbene-pyridine complexes was reported by Thoi *et al*.[25, 26] to selectively reduce carbon dioxide to carbon monoxide. Nevertheless, the number of studies in the area of electrocatalysis using Ni-NHC compounds is limited. In this Chapter, we report four novel Ni-NHC complexes obtained with the ligand precursors H_2**L1**Br_2 and H_2**L2**Br_2, which are based on bis(benz)imidazolium salts bridged by a xylyl linker (Figure 3.1). We have studied their redox properties and electrocatalytic activity for proton reduction in an organic solvent.

3.2 Results and Discussion

3.2.1 Synthesis of complexes

The two bis(benz)imidazolium salts 1,2-bis[(1-(2-pyridylmethyl)-benzimidazolium-3-yl)-methyl]benzene bromide (H_2**L1**Br_2) and 1,2-bis[(1-(2-pyridylmethyl)-imidazolium-3-yl)-methyl]benzene bromide (H_2**L2**Br_2) were synthesized following published procedures with small modifications (details in chapter 3.4).[27, 28] The nickel bromide compounds [Ni(**L1**)Br]Br (**1a**) and [Ni(**L2**)]Br_2 (**2a**) were obtained as yellow-colored powders from a melt of nickel acetate with the ligand in tetrabutylammonium bromide (TBAB) in good yields (74% and 55%, respectively). The color of complex **1a** turned to orange once dried under vacuum overnight. Whereas the benzimidazole-based complex **1a** is poorly soluble in water, the imidazole-based compound **2a** is soluble in water. Compounds **1b** and **2b** were obtained from **1a** and **2a** via anion exchange by adding a solution of the complex in

methanol to a boiling methanol solution of NH_4PF_6. All complexes are air and moisture stable in the solid state for at least several months. The low-spin character of the Ni^{II} ion in all compounds is evidenced by their diamagnetic ^1H NMR spectra, indicating that the square-planar geometry of the Ni centers is retained in solution. The ESI-MS analysis of the four compounds shows the presence of monocationic (with one coordinated bromide anion, or as an ion pair) as well as dicationic fragment ions. Recrystallized samples of the Ni compounds were dried in vacuo before elemental analysis was performed; however, the results still show the presence of the corresponding solvents that were used in recrystallization.

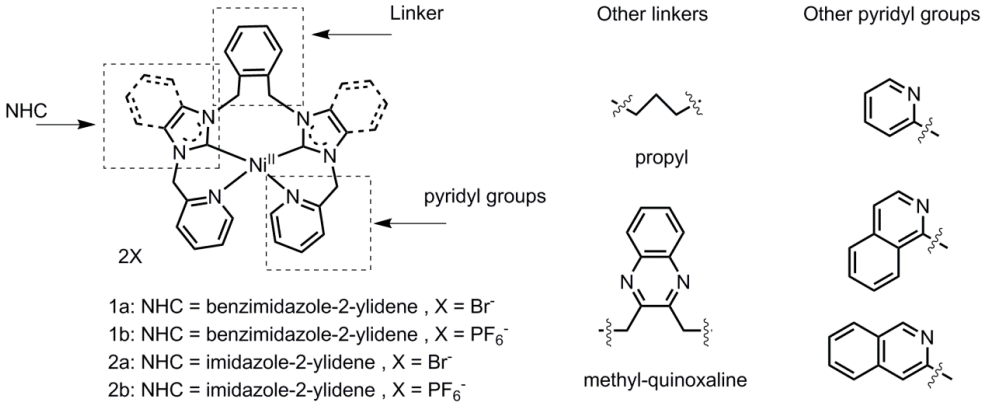

Figure 3.1. Complexes reported in this paper (linker = xylyl) and related compounds previously reported (with linker = propyl[26] or methyl-quinoxaline[29]).

3.2.2 Structural characterization of the complexes

Single crystals of **1a**, **2a**, and **2b** suitable for X-ray diffraction were obtained using the liquid-liquid diffusion method (MeCN/ether). The crystallographic data are provided in Table AIII.1; selected bonds lengths and bond angles are given in Table 3.1.

Compound **1a** crystallizes as a monocationic complex with one uncoordinated bromide ion and 1.5 water molecules per asymmetric unit. The nickel ion in complex **1a** is coordinated in a square-pyramidal geometry, with the donor atoms of the tetradentate ligand in the equatorial plane and one coordinating bromide ion at the apical position (Figure 3.2). The bond distance to the apical bromide (Ni1–Br2) is 3.0800(8) Å. This distance is rather long and could be considered as a normal van der Waals contact; however, also the coordination angles (between 86 - 99°), the small torsion angle of the equatorial plane and the low τ_5 value (see below) are indicative of a stronger interaction. The tetradentate ligand is wrapped around the nickel ion with the aromatic groups orientated in a zig-zag fashion with respect to each other. The ligand donor atoms form an approximate plane with only a small torsion angle (N22-N52-C42-C12 = 5.18(8)°), with Ni–N and Ni–C bond lengths in the range of 1.882 – 1.963 Å, consistent with the typical distances reported for this type of structures.[21, 29] The N–Ni–C and C–Ni–C bond angles are slightly smaller than the ideal

right angles (87.42 – 88.86°), but the 'open' N52–Ni1–N22 angle is slightly larger (95.85(9)°). The 5-coordinate geometry is characterized with a τ_5 value of 0.09, indicating that the nickel ion is coordinated in a near ideal square pyramid.[30]

The five-coordinate geometry of the nickel ion in **1a** is not rare; 5-coordinated geometries can be divided into two categories: the trigonal bipyramid[31] and the tetragonal pyramid.[32] The square-pyramidal geometry is commonly formed with pentadentate chelating ligands,[33] or from a combination of tridentate and bidentate chelating ligands.[34, 35] Square-pyramidal structures formed by a tetradentate ligand with an additional halide ion are rather rare.[36, 37] The non-coordinating bromide ion and the lattice water molecules are connected with the coordinating bromide ion via hydrogen bonding interactions.

Compounds **2a** and **2b** crystallize as dicationic complexes with the non-coordinating bromide ions and the solvent molecules (**2a**) or the hexafluoridophosphate ions (**2b**) in the crystal lattice. The nickel ion in these complexes is coordinated in a square-planar geometry, with the donor atoms of the tetradentate ligand wrapped around the nickel ion (Figure 3.2). The Ni–N bond lengths in **2a** and **2b** are slightly shorter than those in **1a**, whereas the Ni–C bond distances are rather similar (Table 3.1).

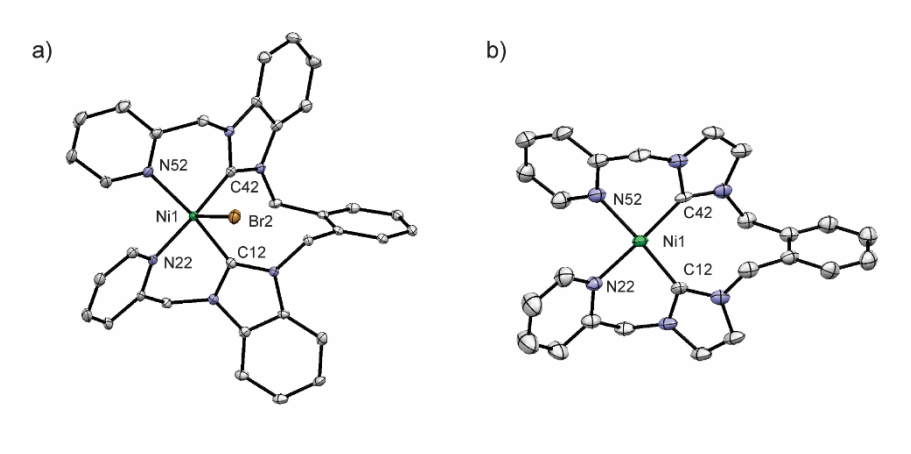

*Figure 3.2. Displacement ellipsoid plots (50% probability level) of the cations: a) [Ni(**L1**)Br]$^+$ in **1a** and b) [Ni(**L1**)]$^{2+}$ in **2b** at 110(2) K. Atom numbering scheme for the first coordination sphere is provided. Hydrogen atoms, the non-coordinated bromide ion, the hexafluoridophosphate ion and the lattice water molecules are omitted for clarity.*

The square-planar geometry of the nickel ion in **2a** was evaluated with an equation[24] derived from a report by Yang:[38]

$$\tau_4 = \frac{360-(\alpha+\beta)}{2\alpha}\delta;\ \delta = \frac{\beta}{\alpha}$$

The largest (α) and second-largest (β) L–Ni–L angles in **2a** are 171.7(3) and 167.7(2)°, resulting in a τ_4 value of 0.06. For compound **2b**, a τ_4 value of 0.04 is calculated,

indicating that the geometry of the central ion in both compounds is close to the ideal square-planar geometry. The structures of the nickel(II) compounds have been compared with those earlier reported (Table 3.1 and Table AIII.2);[26] it appears that ligands containing pyridylmethyl pendant arms result in nickel(II) compounds with longer Ni─C bond distances than ligands with pyridyl side groups. The donor atoms of tetradentate ligands containing the more flexible pyridylmethyl groups are arranged in a more planar fashion around the nickel ions with lower τ_4 values (τ_4 = 0.09 for pyridylmethyl groups and 0.14 for pyridyl groups). The different linkers in the dicarbene chelating structure may also affect the planarity of the arrangement of donor atoms around the nickel centers. Ligands with rigid linkers containing an aromatic group such as xylene (**2a** τ_4 = 0.06; **2b** τ_4 = 0.04) or dimethylquinoxaline[29] (τ_4 = 0.03) present smaller τ_4 values than the ligands with alkyl linkers (τ_4 = 0.12~0.14, see Table AIII.2).[26]

*Table 3.1. Selected bond distances (Å) and angles (°) of compounds **1a**, **2a**, and **2b**.*

	1a	**2a**	**2b**
Ni1–N22	1.962(2)	1.946(7)	1.942(3)
Ni1–N52	1.963(2)	1.929(2)	1.932(3)
Ni1–C12	1.879(2)	1.877(5)	1.879(4)
Ni1–C42	1.882(2)	1.876(3)	1.887(4)
Ni1–Br2	3.080(8)		
N22-Ni1-C12	87.42(9)	87.29(3)	87.8(2)
N22-Ni1-C42	176.72(9)	171.7(3)	172.7(1)
N22-Ni1-N52	87.86(8)	86.5(3)	89.4(1)
C12-Ni1-C42	95.8(1)	99.1(2)	95.0(2)
C12-Ni1-N52	171.03(9)	167.7(2)	173.4(2)
C42-Ni1-N52	88.86(9)	88.2(1)	88.5(1)

3.2.3 UV-vis absorption studies

Electronic absorption spectroscopy of the four nickel compounds as well as the precursor ligands H_2**L1**Br_2 and H_2**L2**Br_2 was performed both in the solid state and in DMF solutions (see Table 3.2 and Figure AIII.3-4).

Table 3.2. Parameters of the electronic spectra of Ni complexes and ligands.

	Solid state optical spectra (nm)	Absorption bands, λ_{max} nm (ε/$M^{-1}cm^{-1}$)[a]
1a	264, 305, 355, 433sh	276 (2540), 285 (5000), 303 (5680), 312 (6140), 361sh (1040)
1b	262, 298, 324, 390	280 (4450), 314 (5860), 389sh (360)
2a	260, 308, 351	274 (4000), 305 (4860), 378sh (1950)
2b	258, 299, 384, 556sh	273 (2860), 307 (3860), 381sh (180)
H_2L1Br_2	259	275 (3220)
H_2L2Br_2	258	267 (2370)

The solid-state absorption spectra of the ligand precursors H_2**L1**Br_2 and H_2**L2**Br_2 show one absorption around 260 nm ascribed to π-π* transitions of the pyridyl groups.[39] The absorption bands in the solid-state spectrum of **1a** at 305 and 355 nm are assigned to ligand-to-metal charge-transfer (LMCT) transitions, and the absorption at 433 nm is assigned to a d-d transition. Similar assignments are proposed for the spectra of the other compounds (Figure AIII.3).

Compounds **2a**, **1b** and **2b** readily dissolve in dry DMF resulting clear (pale) yellow solutions (within 1 min). However, the solubility of **1a** is lower, initially resulting in a cloudy solution; only after stirring for 1 h the solution became clear. The limited solubility of **1a** in DMF may be related to the coordination of one of the bromide ions; perhaps only upon dissociation of this bromide ion the compound is fully soluble. The UV-Vis spectra in DMF again show the intense π-π* transition of the pyridyl groups at around 275 nm and an intense transition around 310 nm, which has been ascribed to a ligand-to metal charge transfer (LMCT of carbene to nickel).[40] All compounds show a d-d transition in the region of 360 – 380 nm common for square-planar nickel(II) complexes (Figure AIII.4).

3.2.4 Redox properties of Ni complexes

Electrochemical analysis of the four nickel complexes in dry DMF was performed with 0.1 M tetrabutylammonium hexafluoridophosphate (TBAP) as the supporting electrolyte under a stream of argon. An Ag/AgCl reference electrode was used, ferrocene was added at the end of each measurement as an internal standard. The potentials reported in this chapter are versus the ferrocene/ferrocinium ($Fc^{0/+}$) couple. The electrochemical data of the nickel compounds are collected in Table 3.3.

The cyclic voltammogram of complex **1a** shows the presence of three reductive waves, two of which are reversible (Figure 3.3). The two reversible waves are tentatively assigned to the Ni^{II}/Ni^{I} and Ni^{I}/Ni^{0} redox couples ($E_{1/2}$ = −1.55 V and −1.80 V). However, the formation of a Ni(I) species with a ligand-centred radical is also possible, although the voltammogram of the ligand does not have a reduction wave coinciding with the second reversible reduction of the complex. Without a full spectro-electrochemical study the true nature of the reduction process occurring at –1.8 V is unknown. The first reversible redox wave at −1.55 V vs $Fc^{0/+}$, is characterized by a peak current ratio i_{pa}/i_{pc} of 0.99. A plot of the reductive peak current i_{pc} displays a linear relationships with the square root of the scan rate (Figure AIII.5), which demonstrates this first electrochemical reduction to be diffusion-controlled.[41] In addition, the current also increases linearly with the concentration of the nickel compound (Figure AIII.5). The third small reductive peak at −2.04 V is tentatively attributed to a ligand-based process, forming a ligand-centered radical, as its position coincides with a peak observed in the CV of H_2**L1**Br_2 (Figure 3.3).

Compound **2a** reveals a similar cyclic voltammogram with three reduction processes at −1.76, −1.96 and −2.27 V, and two oxidation processes at −1.67 and −1.86 V. However, the redox processes are significantly less reversible; the peak-current ratio i_{pa}/i_{pc} of the first

reduction event is 0.75 indicating a quasi-reversible redox process (Figure AIII.6). The voltammograms of the hexafluoridophosphate species **1b** and **2b** show similar patterns compared to their bromide analogs, but with the redox processes occurring at less negative redox potentials (~20 to 50 mV); the presence of the potentially coordinating anions apparently stabilizes the Ni(II) oxidation state.

It appears that the nickel compounds with a benzimidazole-based carbene ligand are more readily reduced with less negative half-wave potentials (−1.53 V ~ −1.55 V) than those with the imidazole-based carbenes (−1.66 V ~ −1.71 V), indicating the imidazole-based ligands to be slightly more electron donating. The redox potentials of these nickel compounds with the relatively hard pyridyl ligands occur at rather negative potentials compared to Ni centers that are coordinated with softer phosphane ligands.[13, 32]

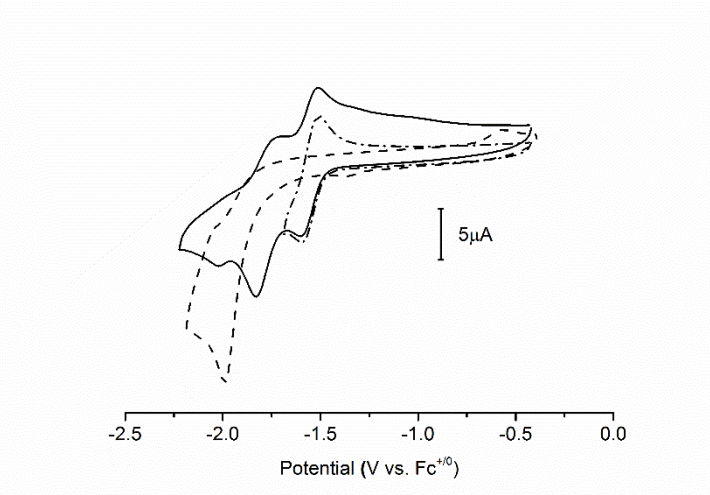

*Figure 3.3. Cyclic voltammograms of **1a** (1 mM, solid line and dash-dotted line) and H_2**L1**Br_2 (1 mM, dashed line) recorded in DMF in different scan ranges. Conditions: scan rate = 0.1 V/s, TBAP (0.1 M), glassy-carbon working electrode.*

Table 3.3. Electrochemical data of the nickel compounds.[a]

	E_{pc1} [V]	E_{pa1} [V]	$E_{1/2}$ [V] (ΔE_p [mV])	E_{pc2} [V]	E_{pa2} [V]	$E_{1/2}$ [V] (ΔE_p [mV])	E_{pc3} [V]
1a	−1.59	−1.51	−1.55 (82)	−1.84	−1.76	−1.80 (79)	−2.04
1b	−1.58	−1.49	−1.53 (84)	−1.80	−1.72	−1.76 (80)	−2.00
2a	−1.76	−1.67	−1.71 (82)	−1.96	−1.86	−1.91 (100)	−2.27
2b	−1.70	−1.63	−1.66 (75)	−1.90	−1.82	−1.86 (84)	−2.23

[a] All voltammograms were recorded in DMF; the potentials are referenced to the $Fc^{+/0}$ couple. Conditions: scan rate = 0.1 V/s, compound (1 mM), TBAP (0.1 M), glassy-carbon working electrode. Under these conditions we found $\Delta E_p(Fc^{+/0})$ = 78 mV.

3.2.5 Catalytic activity for proton reduction in non-aqueous solution

The four compounds have been investigated for their catalytic activity in the electrocatalytic proton reduction in DMF, using either acetic acid (HOAc) or trifluoroacetic acid (Htfa) as the proton source. For each scan the working electrode was freshly polished.

When using the acid Htfa as the proton source (pKa in DMF = 6.0[42]), two new reductive waves (−1.9 V and −2.4 V) appeared after two irreversible peaks at −1.6 V and −1.8 V (Figure 3.4a), consistent with the report of Canaguier *et al*.[6] The catalytic current i_c is the maximum current of the catalytic proton-reduction peak, and i_p is the plateau current of the non-catalytic reduction waves. The current of the catalytic wave is dependent on the acid concentration, but saturates at a concentration of 40 mM (Figure AIII.7). This saturation indicates that at this acid level the main rate-controlling process is no longer acid diffusion, but rather the catalytic efficiency of the Ni complex. In addition, in the acid-dependent region, the i_c/i_p ratio increases linearly with the square root of the acid concentration (Figure 3.4b). The i_c/i_p value is 43 in the acid-independent region (at a scan rate of 0.1 V/s) which corresponds to a rate constant (k_{obs}) of 360 s^{-1}.[7, 43]

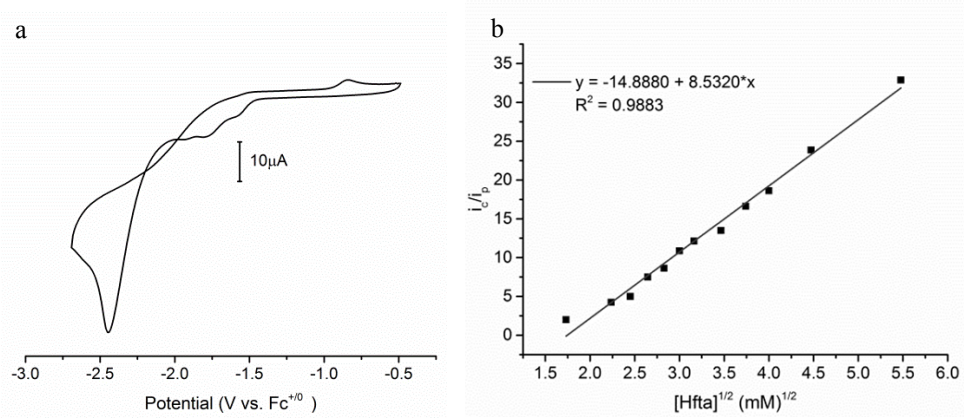

*Figure 3.4. (a) Cyclic voltammogram of **1a** (1 mM) in presence of Htfa (10 mM) recorded in DMF. (b)* Plot of i_c/i_p vs. $[Htfa]^{1/2}$ $(mM)^{1/2}$ for ***1a*** in presence of various concentrations of acid in DMF, *Conditions: scan rate = 0.1 V/s, TBAP (0.1 M), glassy-carbon working electrode.*

Activity for proton reduction is also observed when the weaker acetic acid is added to a solution of **1a** in DMF. The two reversible redox couples as well as the third irreversible reductive wave combine into one irreversible wave at −1.8 V. Meanwhile only one new reduction peak is observed at −2.6 V. The current of this peak is dependent on the acid concentration; this behavior is ascribed to the electrocatalytic reduction of protons by the nickel compound. The appearance of bubbles on the glassy carbon working electrode during the experiment is another visible indication for H_2 production. No obvious current enhancement is observed in a blank experiment using the same quantity of acid in the absence of nickel complex (see Figure AIII.8). The other three analogous nickel compounds show similar CVs in presence of acid: with the sequential addition of the acid,

the reductive current gradually increased (Figure 3.5). Moreover, we observed an acid-independent region after 20 mM acid for the benzimidazole-based compounds **1a** and **1b**.

In case of such similar structures those four compounds have, we initially assumed a first-order or pseudo-first order H_2 evolving reaction happened in the solution. Comparison of the catalytic activity of the four Ni complexes using acetic acid as the proton source revealed that the i_c/i_p value of compound **2b** is the highest, reaching 50 (corresponding to k_{obs} = 490 s^{-1} at 0.1 V/s) at an acid concentration of 80 mM (Table 3.4). The overpotential for electrocatalytic proton reduction at an acetic acid concentration of 10 mM of the four molecular catalysts has been calculated taking homoconjugation of the acid into account (Table 3.4).[44] The imidazole-based complex **2b**, which is the most efficient electrocatalyst of the four compounds, unfortunately displays a higher overpotential (1.28 V) than the benzimidazole-based carbene complexes (~1.15 V). Furthermore, the presence of bromide ions in complexes **1a** and **2a** results in slightly higher overpotentials (30 ~ 50 mV difference).

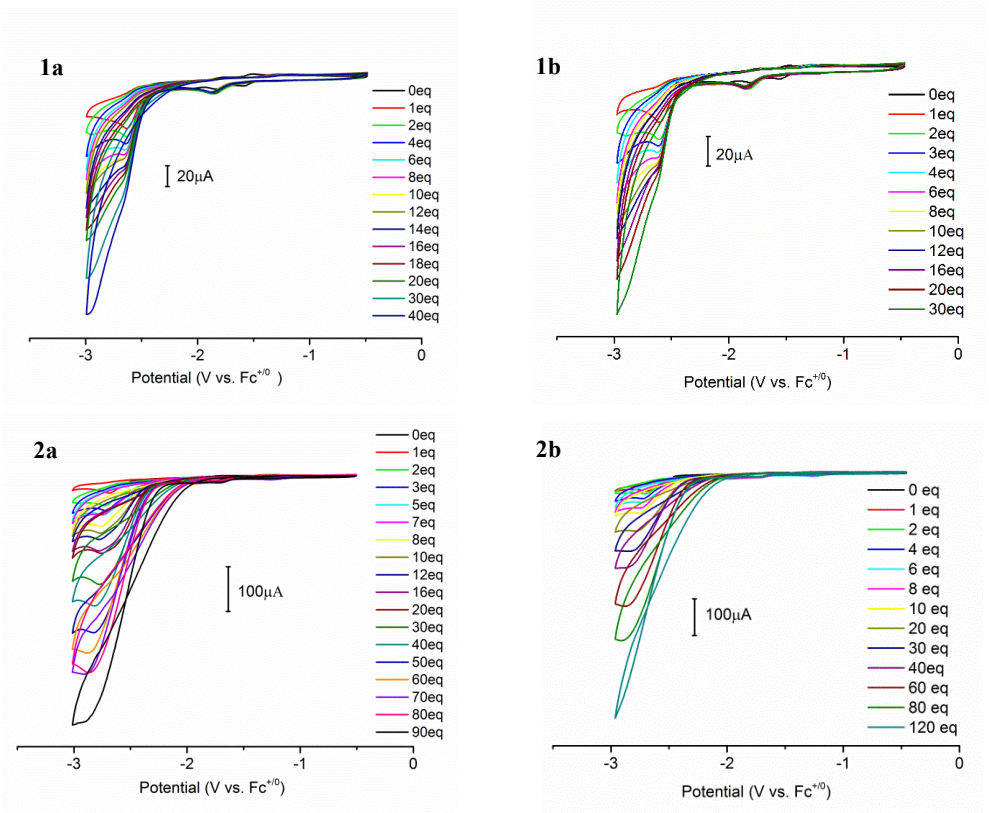

*Figure 3.5. The CVs of complexes **1a**, **1b**, **2a** and **2b** recorded in presence of various equivalents of acetic acid in DMF containing 0.1 M TBAP as supporting electrolyte at scan rate 0.1 V/s, using a glassy carbon working electrode.*

Table 3.4. Summary of the electrocatalytic properties of the compounds.[a]

	1a	**1b**	**2a**	**2b**
[HOAc] (mM)	16	16	80	80
i_c/i_p	11	9	40	50
k_{obs}	25	16	310	490
Overpotential (V)[b]	1.17	1.14	1.33	1.28

[a] The i_c/i_p value, k_{obs} and overpotentials of the reductive waves of the four complexes(1 mM) at the maximum concentration of acetic acid at a scan rate of 0.1 V/s (vs. $Fc^{+/0}$). [b] Overpotentials of proton reduction catalyzed by the complexes were calculated in the presence of 10 mM acetic acid.

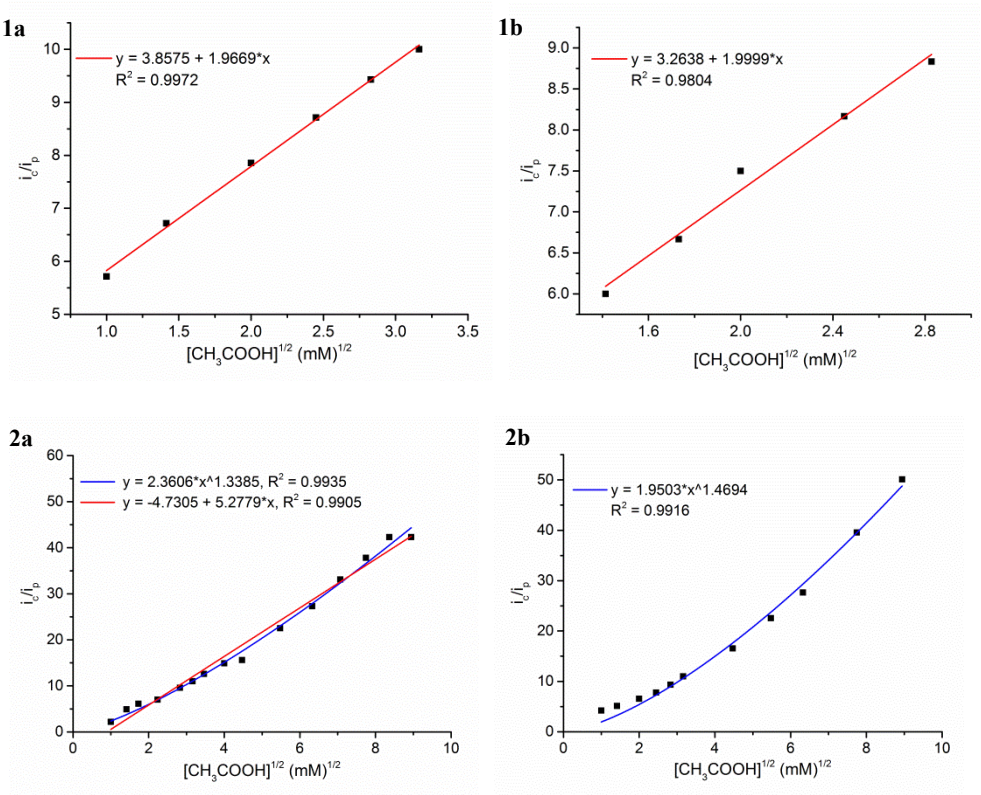

*Figure 3.6. Plots of i_c/i_p vs. $[CH_3COOH]^{1/2}$ $(mM)^{1/2}$ for four complexes (**1a** to **2b**) in presence of various acid concentration in DMF containing 0.1 M TBAP as supporting electrode at 0.1 V/s, using glassy carbon working electrode.*

The large difference in catalytic activity between the benzimidazole-based nickel-carbene compounds and the imidazole-based nickel-carbene compounds might be due to the difference in electron-donating properties of the ligands. The more electron-donating ligand based on imidazole results in better catalytic efficiency of its nickel compounds, but at the expense of larger overpotentials for proton reduction. Plots of the catalytic current i_c/i_p versus the square root of the acid concentration at the acid-dependent region (Figure 3.6) reveal a large difference in correlation between the benzimidazole-based species (**1a**, **1b**) and the imidazole-based compounds (**2a**, **2b**). For compounds **1a** and **1b** plots of i_c/i_p versus

the acid concentration in the acid-dependent region show a linear relationship, indicating that the reaction is first-order with respect to proton concentration.[7, 13, 32, 43, 45, 46] However, for compounds **2a** and **2b**, especially **2b**, the correlation between i_c/i_p versus $[H^+]^{½}$ is less linear. Especially for compound **2b**, which can be regarded as the best electrocatalyst of the four, a plot of i_c/i_p gives a linear relationship with acid concentration, instead of with square root of acid concentration (Figure 3.7). This relationship indicates that in the case of **2b**, two protons are involved in the rate-determining step of the reaction. Based on these data we propose that the rate-determining step in the catalytic mechanism of the benzimidazole-based species may be different from that of the imidazole-based compounds, which may also affect the efficiency of the catalysts. However, a DFT study needs to be carried out in order to understand the relationship between the catalyst's structure and its mechanism in detail.

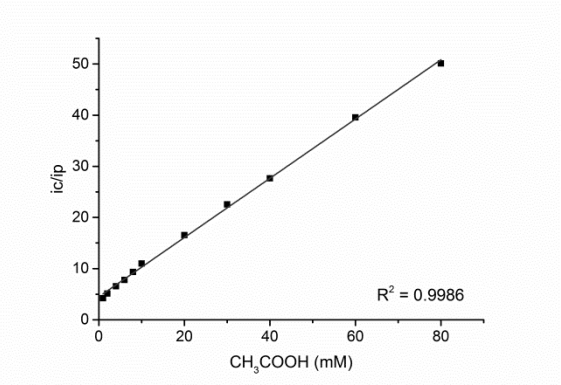

*Figure 3.7. Plots of i_c/i_p vs. [CH_3COOH] (mM) for complex **2b** in presence of various acid concentration in DMF containing 0.1 M TBAP as supporting electrode at 0.1 V/s, using a glassy carbon working electrode.*

3.3 Conclusion

In this chapter we report four novel pyridine-functionalized Ni-NHC complexes and their redox and electrocatalytic properties. The type and length of the linker between the carbenes as well as to the pyridine group influences the geometry of the complexes, as characterized by their τ_4 values. It appears that a rigid linker based on an aromatic group in combination with a methylenepyridine pendent group attributes to more ideal square-planar geometries. In addition, we found that the use of imidazole-based carbenes result in more negative Ni^{II}/Ni^{I} and Ni^{I}/Ni^{0} redox couples, although these compounds revealed much higher catalytic activity in electrocatalytic reduction of protons, as well as better acid tolerance. The most planar complex **2b** (with the smallest τ_4 value) shows the highest catalytic efficiency ($i_c/i_p = 50$, $k_{obs} = 490$ s^{-1} at 0.1 V/s) of all complexes investigated in this study for the catalytic proton reduction using acetic acid, although the overpotential at which dihydrogen is produced is sizeable. To the best of our knowledge, these are the first Ni-NHC complexes reported to catalyze proton reduction. Only a few recent reports relate to proton reduction with metal-NHC compounds, but these concern cobalt-NHC complexes.[14, 47] Furthermore, it was shown that the presence of halide ions results in more

negative potentials for the Ni^{II}/Ni^{I} and Ni^{I}/Ni^{0} redox couples, and also leads to larger overpotentials for proton reduction.

The experiments of catalytic proton reduction in organic solvents provide a starting point for analysis; however, water is the ideal solvent for H_2 production. Considering the higher solubility of the hexafluoridophosphate salts in aqueous solutions and the adverse effect of the bromide ions on the catalytic activity of the nickel compounds, further investigations to proton reduction catalysis with this type of molecular catalysts will be carried out in acid-buffered aqueous solutions. Although the observed overpotentials are not outstanding, the reported nickel compounds are attractive: the synthesis route of the complexes is straightforward and the complexes are air and moisture stable due to the presence of the bis-carbene donor.

3.4 Experimental

3.4.1 Materials

Commercial chemicals were used without further purification. Acetonitrile, tetrahydrofuran, dichloromethane and diethyl ether were obtained from a PureSolv MD5 solvent dispenser. Dry dimethylformamide was prepared by adding molecular sieves into commercial anhydrous solvent. The rest commercial solvents were used without further purification. *N*-Pyridylmethyl(benz)imidazole was synthesized following literature methods.[27] All air-sensitive reactions were performed under argon using standard Schlenk techniques unless mentioned otherwise.

3.4.2 Analytical methods

^{1}H, ^{13}C and ^{31}P NMR spectra were recorded on a Bruker 300 DPX spectrometer. Mass spectra were obtained using a Finnigan Aqua Mass Spectrometer (MS) with electro spray ionization (ESI). UV-vis spectra were obtained using either a transmission dip probe or a solid-state reflection probe on a Avantes Avaspec-2048 spectrometer with a Avalight-DH-S-BAL light source. Elemental analyses were performed by the Kolbe Mikroanalytisches Laboratorium, Germany.

Cyclic voltammetry was recorded with an Autolab PGstat10 potentiostat controlled by GPES4 software under argon. A 3 mm diameter glassy carbon electrode was used as working electrode and plantuim as the counter electrode. The experimental reference was an Ag/AgCl electrode in the electrolyte solution (TBAP). Ferrocene was added at the end of each measurement as an internal standard. All electrode potentials reported in this publication are given versus the potential of the ferrocene/ferrocenium redox couple ($[Fc^{+/0}]$, $E^{o} = 0.00$ V) as the reference.

The apparent rate constant (k_{obs}) can be regarded as turn-over frequency (TOF) when a first-order or pseudo-first order H_2 evolving reaction is catalyzed by a freely diffusing molecular catalyst.[43] The corresponding equation is provided below: [7, 43]

$$\frac{i_c}{i_p} = \frac{n}{0.4463}\sqrt{\frac{RTk_{obs}}{Fv}}$$

Here, i_c is the maximum current of the catalytic peak, and i_p is the plateau current of the non-catalytic reduction wave. F is Faraday's constant, T is 295 K, R is the universal gas constant, v is the scan rate, n is 2 in the case of the H_2 evolution process.

3.4.3 Single crystal x-ray crystallography

All reflection intensities were measured at 110(2) K using a SuperNova diffractometer (equipped with Atlas detector) with Mo *K*α radiation (λ = 0.71073 Å)) (**1a**) or Cu *K*α radiation (λ = 1.54178 Å) (**2a**, **2b**) under the program CrysAlisPro (Version 1.171.36.32 Agilent Technologies, 2013). The same program was used to refine the cell dimensions and for data reduction. The structure was solved with the program SHELXS-2013[48] and was refined on F^2 with SHELXL-2013.[48] Analytical numeric absorption corrections based on a multifaceted crystal model were applied using CrysAlisPro. The temperature of the data collection was controlled using the system Cryojet (manufactured by Oxford Instruments). The H atoms were placed at calculated positions (unless otherwise specified, see below) using the instructions AFIX 23 or AFIX 43 with isotropic displacement parameters having values 1.2 times *U*eq of the attached C atoms.

1a: The H atoms attached to O1W and O2W (*i.e.*, lattice water molecules) were found from difference Fourier maps, and their coordinates were refined freely. The structure is ordered. The crystal lattice also contains some amount of very disordered solvent molecules. Their contribution has been taken out using the SQUEEZE procedure[49] in the final refinement.

2a: The H atoms attached to O1W, O2W (O2W is found at sites of twofold axial symmetry) and O3W were found from difference Fourier maps, and their coordinates were refined freely. The H atoms attached to the lattice water solvent molecules O3W' (minor component of the disordered water lattice molecule) and O4W (partially occupied with occupancy factor = 0.292(9)) could not be retrieved from difference Fourier maps. The structure is partly disordered. One part of the Ni complex and one lattice water solvent molecule (O3W/O3W') is disordered over two orientations, and the occupancy factors of the major components of the disorder refine to 0.649(11) and 0.861(4), respectively. One of the two counterions (Br2) is disordered over three orientations, and the occupancy factors of the three components refine to 0.779(2), 0.180(2) and 0.0410(8).

2b: The structure is ordered, except for some amount of disordered lattice solvent molecules, whose contribution has been taken out using the SQUEEZE procedure[49] in the final refinement.

3.4.4 ligand precursors synthesis

H_2**L1**Br_2 and H_2**L2**Br_2[28] were synthesized following literature methods with small modifications.

*H_2**L1**Br_2*:
N-Pyridylmethylbenzimidazole (4 mmol, 0.836 g) and α,α′-dibromo-o-xylene (2 mmol, 0.57 g) were added into a 25 ml round-bottomed flask containing 10 ml toluene. The mixture was stirred for 24 h at 110 °C, after which time the product was collected by filtration. The white powder was washed with THF and ether, and dried under vacuum. Yield: 1.32g (97%). ^{1}H NMR (300 MHz, DMSO-d_6) δ = 10.07 (s, 2H, NC*H*N), 8.48 (d, *J* = 4.77 Hz, 2H, Ar-*H*), 8.04 (s, 1H, Ar-*H*), 8.02 (d, *J* = 3.17 Hz, 2H, Ar-*H*), 7.98 (d, *J* = 2.60 Hz, 1H, Ar-*H*), 7.95 (t, *J* = 2.18, 2.18 Hz, 2H, Ar-*H*), 7.92 (d, *J* = 1.74 Hz, 1H, Ar-*H*), 7.90 (d, *J* = 1.76 Hz, 1H, Ar-*H*), 7.74 (s, 1H, Ar-*H*), 7.72 (s, 1H, Ar-*H*), 7.66 (m, 4H, Ar-*H*), 7.44 (dd, *J* = 3.33, 5.70 Hz, 2H, Ar-*H*), 7.38 (dd, *J* = 5.35, 7.05 Hz, 2H, Ar-*H*), 7.19 (dd, *J* = 3.46, 5.58 Hz, 2H, Ar-*H*), 6.16 (s, 2H, N-CH_2-Py), 6.00 (s, 2H, NCH_2). ^{13}C NMR (75 MHz, DMSO-d_6) δ = 152.87, 149.55, 148.05, 143.87, 137.58, 132.06, 131.55, 131.07, 129.37, 128.25, 127.07, 126.80, 123.74, 122.77, 114.07, 50.85, 47.53. ESI-MS found (calculated): $[M–2Br]^{2+}$ *m/z* 261.3 (261.1); $[M–Br]^+$ *m/z* 601.1 (601.2).

*H_2**L2**Br_2*:
N-Pyridylmethylimidazole (4 mmol, 0.836 g) and α,α′-dibromo-o-xylene (2 mmol, 0.57 g) were added into a 25 ml round-bottomed flask containing 10 ml toluene. The mixture was stirred for 48 h at 110 °C, after which time the product was collected by filtration. The sticky solid was crushed and washed with THF until it became a brown powder, which was dried under vacuum. Yield: 0.90 g (76%). ^{1}H NMR (300 MHz, DMSO-d_6) δ = 9.48 (s, 2H, NC*H*N), 8.55 (d, *J* = 4.6 Hz, 2H, Ar-*H*), 7.93 (d, *J* = 1.5 Hz, 1H, Ar-*H*), 7.91 (d, *J* = 1.2 Hz, 1H, Ar-*H*), 7.88 (s, 2H, Ar-*H*), 7.82 (s, 2H, Ar-*H*), 7.55 (d, *J* = 8.1 Hz, 2H, Ar-*H*), 7.52 – 7.48 (m, 2H, Ar-*H*), 7.41 (dd, *J* = 4.8, 2.1 Hz, 2H, Ar-*H*), 7.32 (dd, *J* = 3.48, 5.44 Hz, 2H, Ar-*H*), 5.73 (s, 4H, N-CH_2-Py), 5.64 (s, 4H, NCH_2). ^{13}C NMR (75 MHz, DMSO-d_6) δ = 153.41, 149.57, 137.54, 137.48, 132.98, 129.64, 129.38, 123.75, 123.70, 122.69, 122.56, 53.09, 49.12. ESI-MS found (calculated): $[M–2Br]^{2+}$ *m/z* 211.2 (211.6); $[M–Br]^+$ *m/z* 501.0 (502.1)

3.4.4 complexes synthesis

*Synthesis of [Ni(**L1**)Br]Br (**1a**) and [Ni(**L2**)]Br_2 (**2a**)*
Tetrabutylammonium bromide (2 g), nickel acetate (0.18 g, 1 mmol) and H_2**L1**Br_2 (0.69 g, 1 mmol) or nickel acetate (0.15 g, 0.84 mmol) and H_2**L2**Br_2 (0.49 g, 0.84 mmol) were weighed into a 10 ml round-bottomed flask. The mixture was heated at 80 °C under vacuum for 3 h. Then the temperature was increased to 120-130 °C and the flask was heated for another 24 h under vacuum. After cooling to room temperature the residue was triturated with 50 ml distilled water, and kept overnight. The mixture was filtered yielding a yellow powder. The powder was thoroughly washed with diethyl ether. Yield: **1a** 0.55 g (74%), **2a** 0.29 g (45%). Single crystals were obtained by the liquid-liquid diffusion method (MeCN/ether).

1a ^{1}H NMR (300 MHz, DMSO-d_6) δ = 8.49 (d, *J* = 5.50 Hz, 2H, Ar-*H*), 8.13 (m, 6H, Ar-*H*), 7.885 (dd, *J* = 3.66, 5.20 Hz, 2H, Ar-*H*), 7.34 – 7.44 (m, 10H, Ar-*H*), 7.25 (t, *J* = 7.70, 7.70

Hz, 2H, N-CH*H*-Py), 6.465 (d, *J* = 15.22 Hz, 2H, N-C*H*H-Py), 5.45 (d, *J* = 16.06 Hz, 2H, NCH*H*), 5.32 (d, *J* = 15.93 Hz, 2H, NC*H*H). ^{13}C NMR (75 MHz, DMSO-d_6) δ = 168.43, 154.56, 153.16, 141.00, 134.30, 134.04, 132.86, 132.78, 128.81, 124.81, 124.64, 124.34, 124.04, 112.77, 111.35, 50.76, 50.12. ESI-MS found (calculated): $[M–2Br]^{2+}$ *m/z* 289.0 (289.1); $[M–Br]^{+}$ *m/z* 657.1 (657.1). Anal. Calcd for Ni $C_{34}H_{28}N_6Br_2 \cdot 0.5H_2O \cdot 0.7CH_3CN$: C 54.83, H 4.18, N 11.64; found C 54.57, H 3.93, N 11.80.

2a ^{1}H NMR (300 MHz, DMSO-d_6) δ = 8.30 (d, *J* = 5.27 Hz, 2H, Ar-*H*), 8.11 (t, *J* = 7.62, 7.62 Hz, 2H, Ar-*H*), 7.88 (d, *J* = 7.62 Hz, 2H, Ar-*H*), 7.71 (d, *J* = 1.56 Hz, 2H, Ar-*H*), 7.55 (m, 2H, Ar-*H*), 7.35 – 7.37 (m, 4H, Ar-*H*), 6.98 (m, Ar-*H,* 4H, N-C*H*H-Py), 5.81 (d, *J* = 14.99 Hz, 2H, N-C*H*H-Py), 5.01 (d, *J* = 15.46 Hz, 2H, NCH*H*), 4.69 (d, *J* = 15.30 Hz, 2H, NC*H*H). ^{13}C NMR (75 MHz, DMSO-d_6) δ = 155.56, 154.67, 152.64, 140.83, 135.54, 131.42, 129.04, 124.97, 124.84, 124.67, 122.80, 53.39, 51.50. ESI-MS found (calculated): $[M–2Br]^{2+}$ *m/z* 239.1 (239.1); $[M–Br]^{+}$ *m/z* 557.0 (557.1). Anal. Calcd for $NiC_{26}H_{24}N_6Br_2 \cdot H_2O$: C 47.53, H 3.99, N 12.79; found C 47.73, H 3.74, N 12.69.

*[Ni(**L1**)](PF$_6$)$_2$ (**1b**) and [Ni(**L2**)](PF$_6$)$_2$ (**2b**)*

NH_4PF_6 (128 mg, 0.4 mmol) was dissolved in 15 ml methanol and the solution was brought to a boil. The compounds **1a** (74 mg, 0.1 mmol) or **2a** (64 mg, 0.1 mmol) were added into this boiling methanol solution. The resulting suspension was stirred for 30 min during which time it cooled down. The product was collected by filtration and the pale yellow solid was washed with cold methanol and diethyl ether. Yield: **1b** 35 mg (55%), **2b** 55 mg (72%). Single crystals were obtained by the liquid-liquid diffusion method (MeCN/ether).

1b ^{1}H NMR (300 MHz, DMSO-d_6) δ = 8.42 (s, *J* = 5.26 Hz, 2H, Ar-*H*), 8.15 – 8.18 (m, 5H, Ar-*H*), 7.87 (dd, *J* = 3.61, 5.23 Hz, 2H, Ar-*H*), 7.40 – 7.46 (m, 6H, Ar-*H*), 7.37 (s, 1H, Ar-*H*), 7.27 (m, 2H, Ar-*H*), 7.02 (d, *J* = 15.23 Hz, 2H, N-CH*H*-Py), 6.43 (d, *J* = 15.32 Hz, 2H, N-C*H*H-Py), 5.48 (d, *J* = 15.99 Hz, 2H, NCH*H*), 5.17 (d, *J* = 15.83 Hz, 2H, NC*H*H). ^{13}C NMR (75 MHz, DMSO-d_6) δ = 168.11, 154.54, 152.65, 141.23, 134.23, 132.89, 132.76, 128.82, 124.97, 124.89, 124.40, 124.06, 112.86, 111.42, 101.22, 50.41, 49.89. ^{31}P NMR (122 MHz, DMSO-d_6) δ = –144.88. ESI-MS found (calculated): $[M–2PF_6]^{2+}$ *m/z* 289.9 (289.9); $[M–PF_6]^{+}$ *m/z* 723.2 (723.1). Anal. Calcd for $NiC_{34}H_{28}N_6(PF_6)_2 \cdot CH_3CN$: C 47.50, H 3.43, N 10.77; found C 47.78, H 3.43, N 10.80.

2b ^{1}H NMR (300 MHz, DMSO-d_6) δ = 8.25(d, *J* = 15.99 Hz, 2H, Ar-*H*), 8.12 (t, *J* = 7.41, 7.41 Hz, 2H, Ar-*H*), 7.89 (d, *J* = 7.57 Hz, 2H, Ar-*H*), 7.71 (s, 2H, Ar-*H*), 7.54 (m, 2H, Ar-*H*), 7.40 – 7.46 (m, 4H, Ar-*H*), 6.99 (s, 2H, Ar-*H*), 6.77 (d, *J* = 14.93 Hz, 2H, N-CH*H*-Py), 5.80 (d, *J* = 15.01 Hz, 2H, N-C*H*H-Py), 5.04 (d, *J* = 15.39 Hz, 2H, NCH*H*), 4.61 (d, *J* = 15.26 Hz, 2H, NC*H*H). ^{13}C NMR (75 MHz, DMSO-d_6) δ = 155.45, 154.62, 152.33, 141.01, 135.47, 131.44, 129.10, 125.17, 124.99, 124.88, 122.93, 53.28, 51.34. ^{31}P NMR (122 MHz, DMSO-d_6) δ = –144.87. ESI-MS found (calculated): $[M–2PF_6]^{2+}$ *m/z* 239.1 (239.6). Anal. Calcd for $NiC_{26}H_{24}N_6(PF_6)_2$: C 40.60, H 3.15, N 10.93; found C 40.64, H 3.18, N 10.92.

3.5 Acknowledgements

S. Luo gratefully acknowledges a grant from the Chinese Scholarship Council (no. 201306410011). We are grateful to Mr. John van Dijk for mass spectrometry.

3.6 Reference

[1] P.D. Tran, J. Barber, *Phys. Chem. Chem. Phys.* 2012, 14, 13772-13784.
[2] J.D. Holladay, J. Hu, D.L. King, Y. Wang, *Catal. Today* 2009, 139, 244-260.
[3] V. Khrizanforova, I. Knyazeva, V. Matveeva Sokolova, I. Nizameev, T. Gryaznova, M. Kadirov, A. Burilov, O. Sinyashin, Y. Budnikova, *Electrocatalysis* 2015, 6, 357-364.
[4] A. Lewandowska-Andralojc, T. Baine, X. Zhao, J.T. Muckerman, E. Fujita, D.E. Polyansky, *Inorg. Chem.* 2015, 54, 4310-4321.
[5] N. Queyriaux, R.T. Jane, J. Massin, V. Artero, M. Chavarot-Kerlidou, *Coord. Chem. Rev.* 2015, 304-305, 3-19.
[6] S. Canaguier, V. Fourmond, C.U. Perotto, J. Fize, J. Pecaut, M. Fontecave, M.J. Field, V. Artero, *Chem. Commun.* 2013, 49, 5004-5006.
[7] L. Gan, T.L. Groy, P. Tarakeshwar, S.K.S. Mazinani, J. Shearer, V. Mujica, A.K. Jones, *J. Am. Chem. Soc.* 2015, 137, 1109-1115.
[8] D.L. DuBois, R.M. Bullock, *Eur. J. Inorg. Chem.* 2011, 1017-1027.
[9] M.T.M. Koper, E. Bouwman, *Angew. Chem. Int. Ed.* 2010, 49, 3723-3725.
[10] S.M. Laga, J.D. Blakemore, L.M. Henling, B.S. Brunschwig, H.B. Gray, *Inorg. Chem.* 2014, 53, 12668-12670.
[11] L. Tong, R. Zong, R.P. Thummel, *J. Am. Chem. Soc.* 2014, 136, 4881-4884.
[12] D. Basu, S. Mazumder, X. Shi, H. Baydoun, J. Niklas, O. Poluektov, H.B. Schlegel, C.N. Verani, *Angew. Chem. Int. Ed.* 2015, 54, 2105-2110.
[13] R.M. Stolley, J.M. Darmon, M.L. Helm, *Chem. Commun.* 2014, 50, 3681-3684.
[14] M. van der Meer, E. Glais, I. Siewert, B. Sarkar, *Angew. Chem. Int. Ed.* 2015, 54, 13792-13795.
[15] J. Berding, T.F. van Dijkman, M. Lutz, A.L. Spek, E. Bouwman, *Dalton Trans.* 2009, 6948-6955.
[16] L.P. Bheeter, M. Henrion, L. Brelot, C. Darcel, M.J. Chetcuti, J.-B. Sortais, V. Ritleng, *Adv. Synth. Catal.* 2012, 354, 2619-2624.
[17] E.A. Bielinski, W. Dai, L.M. Guard, N. Hazari, M.K. Takase, *Organometallics* 2013, 32, 4025-4037.
[18] K. Fuji, S. Tamba, K. Shono, A. Sugie, A. Mori, *J. Am. Chem. Soc.* 2013, 135, 12208-12211.
[19] P. Guan, C. Cao, Y. Liu, Y. Li, P. He, Q. Chen, G. Liu, Y. Shi, *Tetrahedron Lett.* 2012, 53, 5987-5992.
[20] L. Postigo, B. Royo, Adv. *Synth. Catal.* 2012, 354, 2613-2618.
[21] Z. Xi, X. Zhang, W. Chen, S. Fu, D. Wang, *Organometallics* 2007, 26, 6636-6642.
[22] Z. Xi, B. Liu, W. Chen, *J. Org. Chem.* 2008, 73, 3954-3957.
[23] M.C. Jahnke, T. Pape, F.E. Hahn, *Eur. J. Inorg. Chem.* 2009, 1960-1969.
[24] M.H. Reineke, M.D. Sampson, A.L. Rheingold, C.P. Kubiak, *Inorg. Chem.* 2015, 54, 3211-3217.
[25] V.S. Thoi, C.J. Chang, *Chem. Commun.* 2011, 47, 6578-6580.

[26] V.S. Thoi, N. Kornienko, C.G. Margarit, P. Yang, C.J. Chang, *J. Am. Chem. Soc.* 2013, 135, 14413-14424.
[27] J. Dinda, S.D. Adhikary, S.K. Seth, A. Mahapatra, *New J. Chem.* 2013, 37, 431-438.
[28] J. Berding, M. Lutz, A.L. Spek, E. Bouwman, *Organometallics* 2009, 28, 1845-1854.
[29] Q.-X. Liu, Z.-Q. Yao, X.-J. Zhao, Z.-X. Zhao, X.-G. Wang, *Organometallics* 2013, 32, 3493-3501.
[30] A.W. Addison, T.N. Rao, J. Reedijk, J. Vanrijn, G.C. Verschoor, *J Chem Soc-Dalton Trans.* 1984, 1349-1356.
[31] R. Garcia-Bueno, M.D. Santana, G. Sanchez, J. Garcia, G. Garcia, J. Perez, L. Garcia, *Dalton Trans.* 2010, 39, 5728-5736.
[32] E.I. Musina, V.V. Khrizanforova, I.D. Strelnik, M.I. Valitov, Y.S. Spiridonova, D.B. Krivolapov, I.A. Litvinov, M.K. Kadirov, P. Lonnecke, E. Hey-Hawkins, Y.H. Budnikova, A.A. Karasik, O.G. Sinyashin, *Chem. -Eur. J.* 2014, 20, 3169-3182.
[33] M.D. Santana, A.A. Lozano, G. Garcia, G. Lopez, J. Perez, *Dalton Trans.* 2005, 104-109.
[34] H. Ma, S. Chattopadhyay, J.L. Petersen, M.P. Jensen, *Inorg. Chem.* 2008, 47, 7966-7968.
[35] H. Ma, J.L. Petersen, V.G. Young, G.T. Yee, M.P. Jensen, *J. Am. Chem. Soc.* 2011, 133, 5644-5647.
[36] S.F. Tyler, S.N. Natoli, B. Vlaisavljevich, P.E. Fanwick, T. Ren, *Inorg. Chem.* 2015, 54, 10058-10064.
[37] J.-i. Nishigaki, T. Matsumoto, K. Tatsumi, *Eur. J. Inorg. Chem.* 2010, 5011-5017.
[38] L. Yang, D.R. Powell, R.P. Houser, *Dalton Trans.* 2007, 955-964.
[39] E.C.M. Ording-Wenker, M.A. Siegler, M. Lutz, E. Bouwman, *Inorg. Chem.* 2013, 52, 13113-13122.
[40] M. Sheng, N. Jiang, S. Gustafson, B. You, D.H. Ess, Y. Sun, *Dalton Trans.* 2015, 44, 16247-16250.
[41] J. Heinze, *Angew. Chem. Int. Ed.* 1984, 23, 831-847.
[42] V. Fourmond, S. Canaguier, B. Golly, M.J. Field, M. Fontecave, V. Artero, *Energy Environ Sci.* 2011, 4, 2417-2427.
[43] P. Zhang, M. Wang, Y. Yang, T. Yao, L. Sun, *Angew. Chem.* 2014, 53, 13803-13807.
[44] V. Fourmond, P.-A. Jacques, M. Fontecave, V. Artero, *Inorg. Chem.* 2010, 49, 10338-10347.
[45] M.P. Stewart, M.-H. Ho, S. Wiese, M.L. Lindstrom, C.E. Thogerson, S. Raugei, R.M. Bullock, M.L. Helm, *J. Am. Chem. Soc.* 2013, 135, 6033-6046.
[46] R. Tatematsu, T. Inomata, T. Ozawa, H. Masuda, *Angew. Chem. Int. Ed.* 2016, 55, 5247-5250.
[47] K. Kawano, K. Yamauchi, K. Sakai, *Chem. Commun.* 2014, 50, 9872-9875.
[48] G.M. Sheldrick, *Acta Cryst. A* 2008, 64, 112-122.
[49] A.L. Spek, *Acta Cryst. D* 2009, 65, 148-155.

CHAPTER 4

Free Pyridyl Groups as Proton Shuttles in Pyridine-Functionalized Ni-NHC Complexes

*Two nickel(II) complexes [Ni(**L1**)$_2$]Br$_2$ and [Ni(**L2**)$_2$]Br$_2$ (H**L1**Cl = 1-benzyl-3-(pyridin-2-ylmethyl)benzimidazolium chloride; H**L2**Cl = 1,3-bis(pyridin-2-ylmethyl)benzimidazolium chloride) were synthesized as non-noble metal catalysts for the electrocatalytic hydrogen evolution reaction. Single crystal X-ray crystallography revealed that the nickel metal centers in both compounds are found in a square-planar geometry with like donor atoms of the two bidentate ligands in cis positions. The redox properties of the two compounds were studied using cyclic voltammetry. Electrocatalytic proton reduction experiments using these complexes were performed in DMF with acetic acid as the proton source. Compound [Ni(**L2**)$_2$]Br$_2$, containing two free pyridyl groups, not only exhibits higher electrocatalytic activity, but also has a smaller overpotential for the reduction of protons. The comparison of these two similar structures provides convincing experimental evidence for the pyridyl group acting as proton relay during the proton reduction process.*

This chapter will be published. S. Luo, D.F. Bruggeman, M.A. Siegler, and E. Bouwman, submitted

4.1 Introduction

Ligands with pendant, non-coordinating Lewis bases have received ample attention from inorganic chemists, because the additional Lewis base might affect the performance of molecular catalysts by providing binding sites for protons.[1-4] Notably, the introduction of base-functionalized pendant arms in the ligands of molecular catalysts has been quite popular in the electrochemical research area for assisting in proton-coupled electron-transfer processes.[5-8] For example, Ni-diphosphane complexes bearing pendant amines as proton-binding sites have been shown to exhibit extremely high activity (TOF > 100,000 s^{-1}) in electrocatalytic H_2 evolution.[9] The molecular design of catalysts using pendant Lewis bases is inspired by the structures of natural enzymes, in which nearby amino acids close to the active site play are involved in temporary proton storage.[8-11] With the aim to investigate the role of the pendant amine group in dihydrogen evolution, DuBois's group compared the electrocatalytic activity of the compound $[Co(P^{Ph}_2N^{Ph}_2)(CH_3CN)_3](BF_4)_2$ ($P^{Ph}_2N^{Ph}_2$ = 1,3,5,7-tetraphenyl-1,5-diaza-3,7-diphosphacyclooctane), incorporating pendant amines, with that of the compound $[Co(dppp)(CH_3CN)_3](BF_4)_2$ (dppp = 1,3-bis(diphenylphosphanyl)propane) without a pendant amine.[10] Although the two cobalt compounds are equipped with similar diphosphane ligands, the investigations showed that only the former one containing a pendant amine group possesses catalytic activity in proton reduction.

Not only secondary or tertiary amines but also the pyridyl group can realize the function as a proton relay.[7, 12-14] Recent DFT calculations on a pyridyl-functionalized cobalt diimine-dioxime catalyst have been proposed that the non-coordinated pyridyl pendant group may help to reduce the energetic barrier for hydride formation in electrolysis.[7] Indeed it has been suggested that the pyridyl group may facilitate the reaction of an intermediate metal-hydride with a nearby proton.[14]

In the research described in this paper, we aimed to explore the role of uncoordinated pyridyl groups in the proton reduction activity of nickel compounds with carbene ligands. N-heterocyclic carbenes (NHCs) are widely recognized as innocent ligands in organometallic chemistry.[15] In the absence of other redox-active functional groups, the influence of a pendant pyridine arm in electrocatalysis might be more readily understood.

In the design of metal-carbene complexes pyridine-functionalized (benz)imidazole-2-ylidene ligands have received a lot of attention. Coordination compounds of these functionalized carbenes have been reported for a large array of metal centers such as Ag, Hg, Pd, Au, Ni, Ru and Pt.[16-21] For one and the same ligand, the configuration of the complexes will largely depend on the properties of the metal center. Setting the ligand precursor 1,3-bis(pyridin-2-ylmethyl)benzimidazolium chloride H**L2**Cl as an example, Pt^{II} and Pd^{II} ions can coordinate with one ligand with both pyridines bound in square-planar geometries;[16, 21] Ru^{II} ions may bind two ligands without free pyridine arms in an octahedral geometry;[21] whereas Ag^{I} and Au^{I} ions can bind either one[18] or two ligands[20]

with both pyridine arms non-coordinated. However, none of these studies report the electrocatalytic properties of the compounds.

Herein, we report the synthesis and characterization of two new nickel complexes of pyridyl-functionalized carbene ligands based on benzimidazole and the study of their electrocatalytic activity in H_2 evolution. By comparing these two related compounds we sought to determine whether the presence of pendant pyridyl groups could enhance H_2 evolution by acting as an intramolecular proton shuttle in electrocatalysis.

4.2 Results and Discussion

4.2.1 Synthesis of the complexes

The ligand precursors 1-benzyl-3-(pyridin-2-ylmethyl)benzimidazolium chloride (H**L1**Cl)[22] and 1,3-bis(pyridin-2-ylmethyl)benzimidazolium chloride (H**L2**Cl),[21] were synthesized following literature methods with small modifications, in good yields of 77% and 87%, respectively. The nickel(II) bromide compounds [Ni(**L1**)$_2$]Br$_2$ and [Ni(**L2**)$_2$]Br$_2$ were obtained as yellow-colored powders from a melt of nickel acetate with these ligand precursors in tetrabutylammonium bromide (TBAB) in vacuum (Figure 4.1). The complexes were characterized by NMR spectroscopy and electrospray ionization mass spectrometry (ESI-MS). The absence in the ^{1}H NMR spectra of the characteristic downfield signals for the imidazolium NCHN protons (10 ~10.5 ppm) in both complexes indicates the successful creation of the carbene moieties and their coordination to the nickel(II) center. Whereas the sharp and clear ^{1}H NMR spectrum of [Ni(**L1**)$_2$]Br$_2$ is in agreement with a low-spin square-planar nickel ion, the ^{1}H NMR spectrum of [Ni(**L2**)$_2$]Br$_2$ showed broad peaks, indicating high-spin five-coordinate or octahedral nickel species (see Section 4.2.2. and Appendix IV Figure AIV.5). The ESI-MS spectra exhibit base peaks corresponding to the $[M - 2Br]^{2+}$ cationic complexes. Crystalline samples of the Ni compounds were dried in vacuo before elemental analysis was performed; however, the analysis results indicated that some amount of lattice water molecules found in the crystal lattice was not totally removed. During synthesis of the complexes the chloride counter ions of the ligands were replaced by the bromide from TBAB.

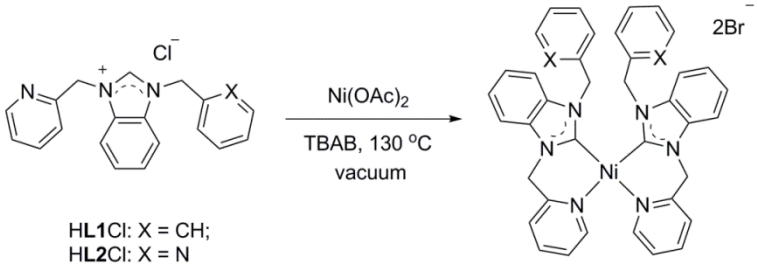

*Figure 4.1. Synthesis route of the compounds [Ni(**L1**)$_2$]Br$_2$ and [Ni(**L2**)$_2$]Br$_2$.*

4.2.2 Structural characterization of the complexes

Single crystals of [Ni(**L1**)$_2$]Br$_2$ and [Ni(**L2**)$_2$]Br$_2$ suitable for X-ray structure determination were obtained using the liquid-liquid diffusion method. The crystallographic and refinement data are collected in Appendix IV. Projections of the structures of the cationic nickel centers in [Ni(**L1**)$_2$]Br$_2$ and [Ni(**L2**)$_2$]Br$_2$ are shown in Figure 4.2. Selected bond distances and angles are provided in Table 4.1.

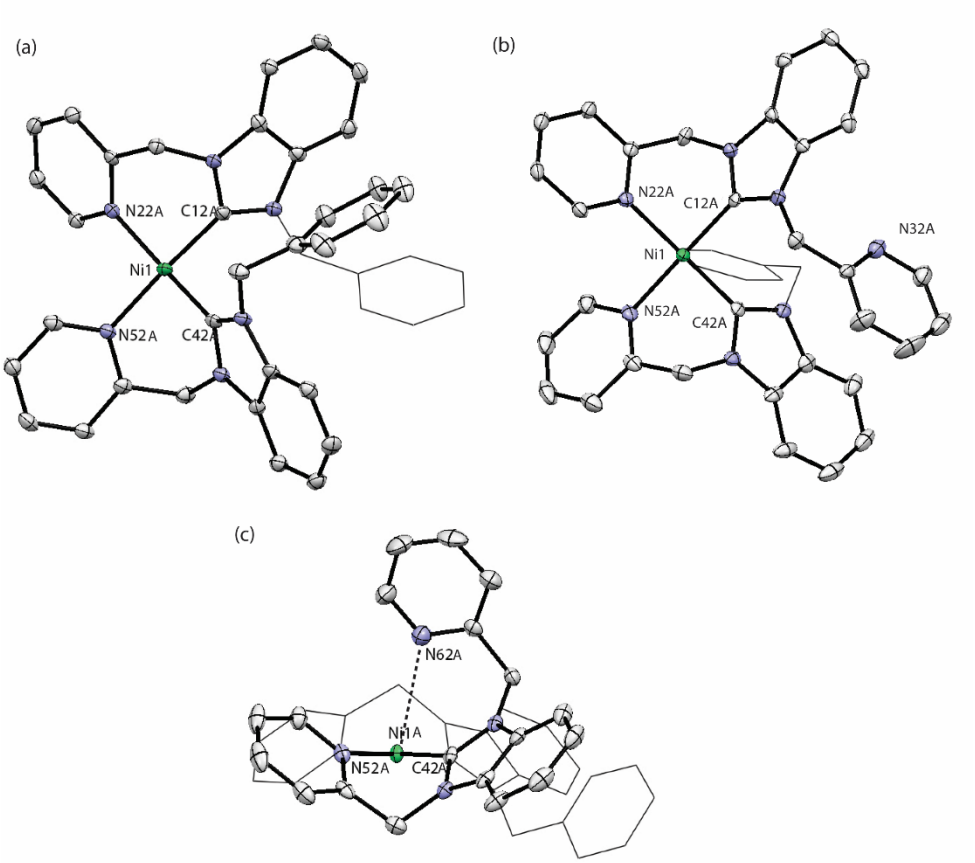

*Figure 4.2. Displacement ellipsoid plots of the cationic complexes (a) [Ni(**L1**)$_2$]Br$_2$, (b) and (c) [Ni(**L2**)$_2$]Br$_2$ are drawn at 50% probability level with selected atom numbering. For clarity the hydrogen atoms, bromide ions, solvent molecules and the lattice water molecules are omitted and parts of the ligands are displayed in wireframe.*

The compound [Ni(**L1**)$_2$]Br$_2$ crystallizes in the space group *P−1*, whereas the compound [Ni(**L2**)$_2$]Br$_2$ crystallizes in the monoclinic space group *Cc*. Both compounds crystallized with two independent cationic complexes, four bromide ions and some disordered solvent molecules in the asymmetric unit. The coordination environment of the nickel centers in the two independent molecules is very similar, and for both compounds, the relevant bond distances and angles from only one of the two molecules are provided. The nickel ion in [Ni(**L1**)$_2$]$^{2+}$ is found in a four-coordinate square planar geometry in which two ligands are

bound in a bidentate C, N fashion with the C and N donor atoms in mutual *cis* positions (Figure 4.2a). Although the ligand **L2** potentially is a tridentate ligand, in $[Ni(\mathbf{L2})_2]^{2+}$ the nickel ion is also found in a square-planar geometry with donor atoms of the two bidentate ligands in *cis* positions (see Figure 4.2b).

The Ni–C bond distances in the two compounds are around *ca.* 1.87 Å whereas the Ni–N bonds are *ca.* 1.94 Å. In comparison with the reported Ru,[21] Pd,[16, 17] and Au compounds,[20] both the Ni –C and Ni–N bond distances are shorter by 0.2 Å, which can be attributed to the smaller ionic radius of the nickel ion. In the compound $[Ni(\mathbf{L2})_2]Br_2$ the nitrogen atom of one of the pendant pyridyl groups resides in an apical position of the nickel center at a distance of *ca.* 2.98 Å; if this interaction is taken into account the geometry of the nickel ion may be regarded as a distorted square pyramid (Figure 4.2c). This additional binding of the pyridyl group may be the cause of the broad signals observed in the ^{1}H NMR spectra of this compound, as the nickel center in the five-coordinate (or octahedral in solution) species may be in the high-spin state.

The square-planar geometries of the nickel ions in $[Ni(\mathbf{L1})_2]Br_2$ and $[Ni(\mathbf{L2})_2]Br_2$ were evaluated with an equation derived from a report by Yang.[23, 24] The largest and second-largest L–Ni–L angles in $[Ni(\mathbf{L1})_2]Br_2$ are 171.7(1)° and 174.0(1)°, resulting in a τ_4 value of 0.100, indicative of only a very slight distortion of the square-planar geometry. For compound $[Ni(\mathbf{L2})_2]Br_2$ a τ_4 value of 0.023 is calculated, indicating that the geometry of the central ion (not taking into account the axial coordination of pyridine) is close to the ideal square-planar geometry.

Table 4.1. Selected bond distances (Å) and angles (°) of the compounds $[Ni(\mathbf{L1})_2]Br_2$ and $[Ni(\mathbf{L2})_2]Br_2$.

	$[Ni(\mathbf{L1})_2]Br_2$	$[Ni(\mathbf{L2})_2]Br_2$
Ni1–C12A	1.880(3)	1.860(4)
Ni1–C42A	1.872(2)	1.863(4)
Ni1–N22A	1.947(2)	1.938(4)
Ni1–N52A	1.953(2)	1.950(4)
Ni1…N62A	/	2.984(4)
N52A–Ni1–N22A	95.10(9)	91.25(15)
N52A–Ni1–C42A	86.47(10)	87.32(17)
C42A–Ni1–C12A	93.12(11)	94.33(18)
C12A–Ni1–N22A	86.15(10)	87.09(17)
N52A–Ni1−C12A	174.00(10)	178.08(18)
C42A–Ni1−N22A	171.71(11)	178.56(17)

Complexes of other metal ions bearing the ligand **L2** have been reported by Adhikary *et al*.[21] Pt(II) was found to coordinate with one ligand **L2** to form the complex $[Pt(\mathbf{L2})Cl]PF_6$ with the Pt(II) ion in a square-planar geometry, whereas the Ru(II) ion binds two ligands **L2** to form the compound $[Ru(\mathbf{L2})_2](PF_6)_2$ with the ruthenium center in an octahedral geometry. A structure has been reported of a nickel compound containing two 1,3-

bis(pyridin-2-ylmethyl)imidazolium ligands, in which similar to [Ni(**L2**)$_2$]Br$_2$ the ligands are arranged with like donor atoms in *cis* positions.[17] The nickel ion in this compound is also in a square-planar geometry and one of the pendant pyridyl groups resides in an apical position of the nickel center at a distance of 3.345 Å, significantly larger than the one in [Ni(**L2**)$_2$]Br$_2$.

4.2.3 Electrochemical properties of the complexes

The redox potentials of the nickel compounds were evaluated using cyclic voltammetry. The electrochemical potentials given in this Chapter are all referred to Ag/AgCl. The cyclic voltammogram (CV) of [Ni(**L1**)$_2$]Br$_2$ shows two reductive waves, the first of which is reversible at a scan rate of 0.1 V/s (Figure 4.3). The reversible redox process located at $E_{1/2}$ = −1.00 V vs. Ag/AgCl is diffusion controlled, as shown by the linear dependence of the peak current on the square root of the scan rate (Figure AIV.1). This redox wave is characterized by a peak-to-peak separation ΔE_p of 80 mV (in our conditions ΔE_p for the $Fc^{0/+}$couple was found to be 95 mV), indicating a one-electron transfer. Thus, we assign this first wave to the Ni(II)/Ni(I) redox process. The quasi-reversible reduction event at −1.29 V is tentatively ascribed to a Ni(I)/Ni(0) redox process. The assignment of these two redox waves to nickel-centered reduction events is supported by the fact that the ligand precursor H**L1**Cl is electrochemically inert in the range of 0 to −1.5 V. Upon increasing scan rate the second reductive wave at −1.29 V gradually becomes reversible, whereas with decreasing scan rates the wave becomes less reversible (see Figure AIV.2). This behavior indicates the occurrence of a dissociative electron transfer (DET) process,[25] meaning that after the reduction of $[Ni^{II}(\mathbf{L1})_2]^{2+}$ to $[Ni^{I}(\mathbf{L1})_2]^{+}$ a stepwise chemical reaction is coupled to the second electron transfer, generating a new product.

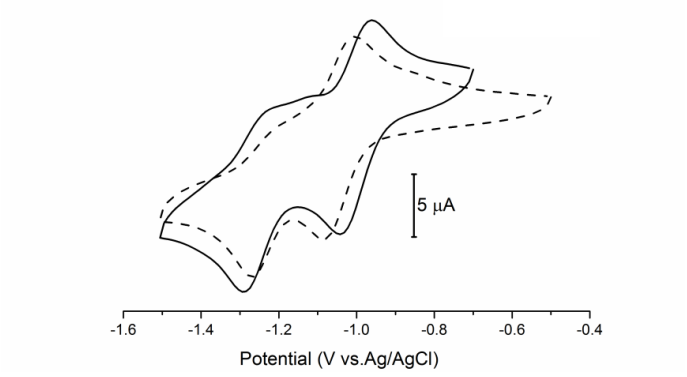

*Figure 4.3. CVs of the compounds [Ni(**L1**)$_2$]Br$_2$ (solid line) and [Ni(**L2**)$_2$]Br$_2$ (dashed line). Experiments were performed at a complex concentration of 1 mM in DMF with 100 mM TBAP as the supporting electrolyte at scan rate 0.1 V/s, using a glassy carbon working electrode.*

Similarly, the CV of compound [Ni(**L2**)$_2$]Br$_2$, containing two uncoordinated pyridyl groups, shows one reversible redox process at $E_{1/2}$ = −1.05 V followed by an irreversible reductive process at −1.27 V (Figure 4.3). The first reversible redox process of [Ni(**L2**)$_2$]Br$_2$ is at a slightly more negative potential compared to that of [Ni(**L1**)$_2$]Br$_2$, indicating a slightly

higher electron density at the nickel ion because of the interaction between the nickel center and one of the pendant pyridyl groups in solution. The reversibility of the second reductive wave at E_{pc2} = −1.29 V of this tetrapyridyl-functionalized compound [Ni(**L2**)$_2$]Br$_2$ appeared not to depend on the scan rate. Even when the scan rate was increased to 500 mV/s the second reductive process still was quasi-reversible (see Figure AIV.3). The electrochemical data are summarized in Table 4.2.

Table 4.2. Electrochemical data of the nickel compounds.[a]

	E_{pc1} [V]	E_{pa1} [V]	$E_{1/2}$ [V] (ΔE_p [mV])	E_{pc2}[V]
[Ni(**L1**)$_2$]Br$_2$	−1.04	−0.96	−1.00 (80)	−1.29
[Ni(**L2**)$_2$]Br$_2$	−1.09	−1.01	−1.05 (80)	−1.27

[a] Potentials are given vs. the Ag/AgCl electrode. All voltammograms were recorded in DMF. Conditions: scan rate = 0.1 V/s, compound (1 mM), TBAP (0.1 M), using glassy-carbon working electrode.

4.2.4 Electrocatalytic activity for proton reduction in DMF

The two compounds were examined for their activity in the electrocatalytic proton reduction in DMF, using acetic acid (HOAc) as a weak proton source. For each scan the working electrode was freshly polished.

Compared to the CV of acetic acid (10 mM) in DMF, after addition of either the complex [Ni(**L1**)$_2$]Br$_2$ or [Ni(**L2**)$_2$]Br$_2$ a relatively large current indicating the reduction of protons was observed at a potential around −2 V vs Ag/AgCl (Figure 4.4). Two small irreversible peaks appear before the electrocatalytic wave, approximately at −1.04 V and −1.17 V for [Ni(**L1**)$_2$]Br$_2$ and at −1.09 V and −1.20 V for [Ni(**L2**)$_2$]Br$_2$. These peaks were broad and close to each other making it difficult to identify them separately. Only a broad plateau can be recognized when showing these waves together with the following catalytic wave. A zoom of CVs (ranging from −0.5 V to −1.5 V) is provided in Figure AIV.4.

For both compounds the first small reductive wave occurs at the exact same potential where the metal-centered Ni^{II}/Ni^{I} reduction process was observed (Section 4.2.3 and Figure AIV.4). The second small reductive potential occurs at a more positive potential compared to the ones in the absence of acid, indicating that there is a chemical step before the second electron transfer takes place. The electrocatalysis therefore most likely proceeds via an ECEC mechanism.[26] The catalytic onset potential for proton reduction in presence of [Ni(**L2**)$_2$]Br$_2$ (at −1.6 V) occurs at a lower potential than in the presence of [Ni(**L1**)$_2$]Br$_2$ (at −1.8 V). Furthermore, in the same conditions the compound [Ni(**L2**)$_2$]Br$_2$ shows the larger catalytic current, indicating a higher electrocatalytic activity than that of [Ni(**L1**)$_2$]Br$_2$ (Figure 4.4).

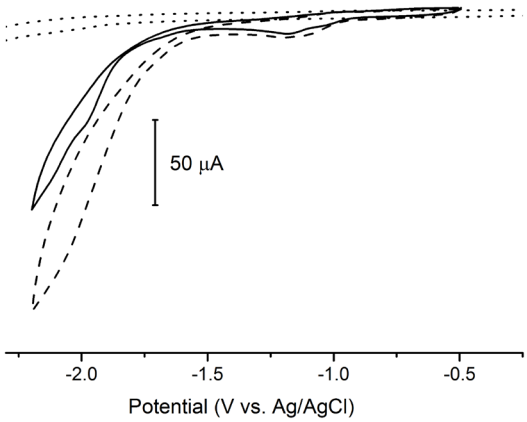

*Figure 4.4. CVs of 10 mM acetic acid in presence of 1mM complex [Ni(**L1**)$_2$]Br$_2$ (solid line), in the presence of 1mM complex [Ni(**L2**)$_2$]Br$_2$ (dashed line) and in the absence of a complex (dotted line) in DMF containing 0.1 M TBAP as supporting electrolyte at scan rate 0.1V/s, using glassy carbon working electrode.*

With the aim to compare the electrocatalytic activity of the two compounds in a more quantitative way, controlled-potential coulometry experiments (CPC) were carried out. The charge consumptions over time of solutions containing just the pure acid or each of the catalysts were also recorded separately as references. The charge accumulation graphs show that over a period of 10 minutes charge consumption is negligible for the solutions containing only acid or only the nickel compounds (Figure 4.5). However, for solutions containing both acid and one of the nickel catalysts continuous charge consumption was recorded. The quantity of dihydrogen gas generated during the CPC experiments can be estimated from the charge consumption of solutions containing both the nickel compound and the acid, after subtraction of the charge consumption of the blanks. The two complexes [Ni(**L1**)$_2$]Br$_2$ or [Ni(**L2**)$_2$]Br$_2$ are estimated to produce 3×10^{-4} mmol and 5×10^{-4} mmol H_2 respectively in 10 min in presence of 6×10^{-3} mmol catalyst at a potential of −1.80 V (assuming that all electrons are used in proton reduction). The complex [Ni(**L2**)$_2$]Br$_2$ equipped with two additional pendant pyridine groups showed almost doubled charge consumption, indicating a higher catalytic activity.

4.2.5 Discussion of the proposed mechanism

Generally, the mechanism of a hydrogen-evolution process based on a metal-containing homogenous catalyst can be divided in three steps. The first step is the reduction of the metal center; if the metal center is equipped with an electron-withdrawing ligand, the metal center is more readily reduced. The second step is the formation of the metal hydride intermediate, which is facilitated by the presence of an electron-donating ligand. The third step is the generation of dihydrogen: the metal-hydride intermediate reacts with another proton and electron to release dihydrogen.[27] Based on this mechanism, generally a molecular catalyst will work at a small overpotential but with relatively low efficiency (for

electron-withdrawing ligands), or with high efficiency but at a relatively large overpotentials (for electron-donating ligands).

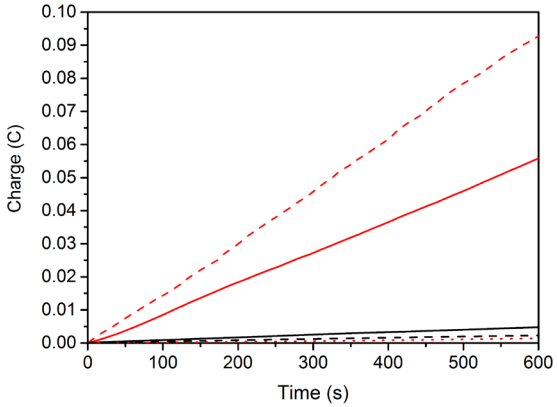

*Figure 4.5. Charge vs. time plot over 600 s during CPC at potential of −1.8 V. Black lines: compounds in absence of acid; Red lines: compounds in presence of 50 mM acetic acid (solid = [Ni(**L1**)$_2$]Br$_2$, dashed = [Ni(**L2**)$_2$]Br$_2$); Dotted red line: 50 mM acetic acid only.*

As discussed in the previous section, in absence of acid, the ligand **L2** is the more electron donating so that the nickel center in [Ni(**L2**)$_2$]Br$_2$ is reduced at more negative potentials. If the complex [Ni(**L1**)$_2$]Br$_2$ follows the aforementioned catalytic mechanism, it will show lower catalytic activity but at a smaller overpotential than the pyridine-substituted analogue [Ni(**L2**)$_2$]Br$_2$. Unexpectedly, the compound [Ni(**L2**)$_2$]Br$_2$ not only shows higher electrocatalytic activity but also a smaller overpotential (Figure 4.4). Thus, the presence of the free pyridyl pendant arms in the compound [Ni(**L2**)$_2$]Br$_2$ apparently reduces the overpotential for the electrocatalytic proton reduction. The additional pyridyl groups act as an intramolecular proton acceptor and proton shuttle assisting in the generation of dihydrogen.[7] Based on the assistance of the pyridyl groups for complex [Ni(**L2**)$_2$]Br$_2$ the catalytic mechanism probably can be described as shown in Figure 4.6. Firstly, in the presence of acid the non-coordinated pyridyl arms are protonated. Then the metal center is reduced to Ni^{I}, followed by the formation of a metal-hydride. Finally the hydride reacts with the proton on the pyridyl arm with the release of dihydrogen.

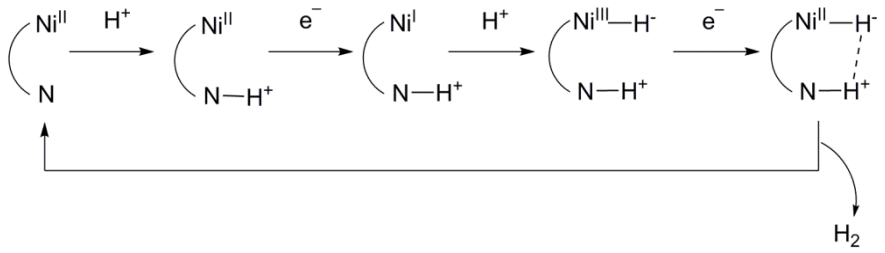

*Figure 4.6. Proposed mechanism of the electrocatalytic reduction of protons by [Ni(**L2**)$_2$]Br$_2$.*

4.3 Conclusion

Two nickel(II) complexes [Ni(**L1**)$_2$]Br$_2$ and [Ni(**L2**)$_2$]Br$_2$ with different ligands were synthesized as non-noble metal molecular catalysts for the hydrogen evolution reaction. The nickel center in both compounds is in a square-planar geometry with two bidentate ligands in *cis* arrangements. The binding of two potentially tridentate ligands in this configuration in the structure of [Ni(**L2**)$_2$]Br$_2$ results in the presence of two free pyridyl groups. The redox properties of the two complexes were determined using cyclic voltammetry and the electrocatalytic dihydrogen generation with these complexes in DMF was studied using acetic acid as the proton source. Of the two compounds, the complex [Ni(**L2**)$_2$]Br$_2$ containing two free pyridyl groups exhibited not only the higher activity in electrocatalysis, but also a smaller overpotential for proton reduction. This result indicates that the presence of the free pyridyl groups help to break the anti-correlation between the energy of the reduction and the catalytic activity. The comparison of the catalytic properties of these two related structures (both with redox-innocent carbene backbones) provide convincing experimental evidence of the pyridyl group acting as proton relay during the proton reduction process.

4.4 Experimental

4.4.1 Materials

Commercial chemicals were used without further purification. Acetonitrile and diethyl ether were obtained from a PureSolv MD5 solvent dispenser. Dry methanol and dimethylformamide were prepared by adding molecular sieves into commercial anhydrous solvent.. All air-sensitive reactions were performed under argon or dinitrogen gas using standard Schlenk techniques unless mentioned otherwise.

4.4.2 Analytical methods

^{1}H and ^{13}C spectra were recorded on a Bruker 300 DPX/Bruker 400 AV spectrometer. Mass spectra were obtained using a Finnigan Aqua Mass Spectrometer (MS) with electrospray ionization (ESI). Elemental analyses were performed by the Mikroanalytisches Laboratorium Kolbe, Germany.

Cyclic voltammetry was recorded with an Autolab PGstat10 potentiostat controlled by GPES4 software under argon. A 3 mm diameter glassy carbon electrode was used as working electrode and plantium as the counter electrode. The experimental reference was an Ag/AgCl electrode in the electrolyte solution (TBAP). Cyclic voltammety was performed in dry DMF with 0.1 M tetrabutylammonium hexafluoridophosphate (TBAP) as the supporting electrolyte under a stream of argon at room temperature. All potentials are given versus Ag/AgCl in this Chapter. Ferrocene was added after each experiment as an internal standard. Under these conditions the $Fc^{0/+}$ couple was located at $E_{1/2}$ = 0.510 V vs.

Ag/AgCl with a ΔE_p of 95 mV. The working electrode surface was polished, ultrasonically cleaned and rinsed before each single CV measurement.

Controlled-potential coulometry (CPC) experiments were carried out with an Autolab PGstat10 potentiostat controlled by GPES4 software under argon. A 3 mm diameter glassy carbon electrode was used as working electrode and platinum as the counter electrode. 1 mM complex and 50 mM acetic acid were added in 6 mL dry degassed DMF with 0.1 M tetrabutylammonium hexafluoridophosphate (TBAP) as the supporting electrolyte under a stream of argon at room temperature. A CPC experiment was run at −1.8 V for 600 s, while the solution was stirred continuously. The blank and reference CPC experiments (only acid or only catalyst added) were performed using the same conditions.

4.4.3 Single crystal X-ray crystallography

All reflection intensities were measured at 110(2) K using a SuperNova diffractometer (equipped with Atlas detector) with Mo *K*α radiation (λ = 0.71073 Å) under the program CrysAlisPro (Version 1.171.36.32 Agilent Technologies, 2013). The same program was used to refine the cell dimensions and for data reduction. The structure was solved with the program SHELXS-2014/7[28, 29] and was refined on F^2 with SHELXL-2014.[28, 29] Numerical absorption correction based on gaussian integration or analytical numeric absorption correction over a multifaceted crystal model was applied using CrysAlisPro. The temperature of the data collection was controlled using the system Cryojet (manufactured by Oxford Instruments). The H atoms were placed at calculated positions (unless otherwise specified) using the instructions AFIX 23 or AFIX 43 with isotropic displacement parameters having values 1.2 or 1.5 *U*eq of the attached C atoms. For [Ni(**L1**)$_2$]Br$_2$, the H atoms attached to O1W (ordered lattice water molecule) and O2W (only for the major component of the disorder) could be retrieved from difference Fourier maps. Their coordinates were refined freely but the O–H and H…H distances were restrained to be 0.84(1) and 1.33(1) Å, respectively. For [Ni(**L2**)$_2$]Br$_2$, the O–H and H…H distances were restrained to be 0.84(3) and 1.33(3) using the DFIX instruction. The atoms attached to O4W, O5W, O6W, O7W, O8W and O9W (partially occupied or disordered lattice water molecules) could not be retrieved.

Additional note:
The structure of [Ni(**L1**)$_2$]Br$_2$ is partly disordered. One phenyl group (C61A-C66A) and one Br^- counter ion are found disordered over two orientations; the occupancy factors of the major components of the disorder refine to 0.59(4) and 0.923(5), respectively. One of the three lattice water molecule (O2W) is disordered over three orientations, and the occupancy factors refine to 0.808(3), 0.109(3) and 0.083(3). The occupancy of the lattice water molecule O3W was refined freely, and its value refines to 0.639(8). The H atoms attached to O3W could not be retrieved. ADDSYM detects a pseudo translation of ½ **a** + ½ **c**. However, the conformations of the two crystallographically independent molecules are different as the orientations of the phenyl groups are significantly different.

The structure of [Ni(**L2**)$_2$]Br$_2$ is partly disordered. One of the pyridine rings (from molecule A) is found to be disordered over two orientations, and the occupancy factor of the major component of the disorder refines to 0.52(2). In the asymmetric unit, there are five Br^- sites with all occupancies lower than 1. Two sites (Br1 and Br2) are ordered, and their occupancy factors refine to 0.940(2) and 0.942(2), respectively. The remaining counter ions (Br3/Br3', Br4/Br4' and Br5/Br5') are disordered over two orientations. The occupancies factors for Br3, Br3, Br4, Br4', Br5 and Br5' refine to 0.853(3), 0.086(3), 0.624(2), 0.0494(15), 0.391(2) and 0.1149(16), respecitvely. The sum of all occupancies factors for the Br^- counterions was restrained to be 4 using the SUMP instruction. The occupancy factors for O4W/O4W' (disordered), O5W/O5W' (disordered), O6W, O7W, O8W and O9W refine to 0.434(11)/0.566(11), 0.715(8)/0.285(8), 0.674(15), 0.671(16), 0.429(18) and 0.41(2), respectively.

4.4.4 Ligand and complex synthesis

N-Pyridylmethyl-benzimidazole,[30] ligand precursors H**L1**Cl,[22] H**L2**Cl,[21] and the complexes [Ni(**L1**)$_2$]Br$_2$ and [Ni(**L2**)$_2$]Br$_2$[31] were synthesized following literature methods with small modifications.

[Ni(**L1**)$_2$]Br$_2$

H**L1**Cl (0.67 g, 2 mmol), anhydrous Ni(OAc)$_2$ (0.17 g, 1 mmol) and tetrabutylammonium bromide (1.5 g) were weighed into a 10 mL round-bottomed flask and dried for 4 hours at 80 °C in a Schlenk setup under vacuum. The reaction mixture was stirred for 48 hours at 130 °C under vacuum. The mixture was then cooled to room temperature and triturated with H_2O. The water layer was washed with DCM (3 × 20 mL) and evaporated to dryness. The remaining solid was dissolved in a mixture of MeCN and methanol and a yellow crystalline solid was obtained using liquid to liquid diffusion method with diethyl ether in 12% yield (90 mg). ^{1}H NMR (400 MHz, DMSO-d_6) δ 8.26 – 8.13 (m, 4H), 8.12 – 7.99 (m, 4H), 7.48 (q, J = 8.0, 7.1 Hz, 4H), 7.32 (dt, J = 15.3, 8.0 Hz, 4H), 7.10 – 6.94 (m, 10H), 6.82 (d, J = 15.5 Hz, 2H, N-C*H*H-Ph), 6.47 (d, J = 15.6 Hz, 2H, N-CH*H*-Ph), 5.53 (d, J = 16.4 Hz, 2H, N-C*H*H-Py), 5.05 (d, J = 16.4 Hz, 2H, N-CH*H*-Py).^{13}C NMR (400 MHz, DMSO-d_6) δ 170.32, 154.74, 153.15, 142.04, 141.29, 134.78, 134.05, 133.64, 133.54, 128.33, 127.59, 126.02, 125.06, 124.34, 124.15, 112.16, 111.52, 50.98, 50.54. ESI-MS found (calculated): $[M - 2Br]^{2+}$ m/z 328.1 (328.1). $C_{40}H_{34}N_6NiBr_2 \cdot C_4H_{10}O \cdot 1.5H_2O \cdot 0.5$ CH_3CN: Calcd. H 5.21, C 57.56, N 9.70; Found H 5.45, C 57.68, N 9.90.

[Ni(**L2**)$_2$]Br$_2$

H**L2**Cl (0.67 g, 2 mmol), anhydrous Ni(OAc)$_2$ (0.17 g, 1 mmol) and tetrabutylammonium bromide (1.5 g) were weighed into a 10 mL round-bottomed flask and dried for 4 hours at 80 °C in a Schlenk setup under vacuum. The mixture was stirred for 48 hours at 130 °C under vacuum, after which the mixture was let to cool and triturated with H_2O. The water layer was washed with DCM (3 × 20 mL), and a brown crystalline solid was obtained from the water solution in 5% yield (40 mg). ^{1}H NMR gave broad peaks. ^{13}C NMR spectrum was

not recorded. ^{1}H NMR (300 MHz, DMSO-d_6) δ = 8.53, 8.32, 8.07, 7.57, 7.45, 7.41, 7.31, 7.08, 6.99, 6.43, 5.75, 4.96. MS *m*/*z* found (calc): $[M - 2Br]^{2+}$ 329.1 (329.1). $C_{38}H_{32}N_8NiBr_2 \cdot 2.5H_2O$: Calcd. H 4.31, C 52.81, N 12.97; Found H 4.80, C 53.08, N 12.99.

4.5 Acknowledgements

S. Luo gratefully acknowledges a grant from the Chinese Scholarship Council (no. 201306410011). We thank Mr. J.M.M. van Brussel for ESI-MS measurements.

4.6 References

[1] V.G. Organo, A.S. Filatov, J.S. Quartararo, Z.M. Friedman, E.V. Rybak-Akimova, *Inorg. Chem.* 2009, 48, 8456-8468.
[2] P. Zhang, M. Wang, Y. Yang, D. Zheng, K. Han, L. Sun, *Chem. Commun.* 2014, 50, 14153-14156.
[3] E.I. Musina, V.V. Khrizanforova, I.D. Strelnik, M.I. Valitov, Y.S. Spiridonova, D.B. Krivolapov, I.A. Litvinov, M.K. Kadirov, P. Lonnecke, E. Hey-Hawkins, Y.H. Budnikova, A.A. Karasik, O.G. Sinyashin, *Chem. -Eur. J.* 2014, 20, 3169-3182.
[4] J. Berding, T.F. van Dijkman, M. Lutz, A.L. Spek, E. Bouwman, *Dalton Trans.* 2009, 6948-6955.
[5] R. Tatematsu, T. Inomata, T. Ozawa, H. Masuda, *Angew. Chem. Int. Ed.* 2016, 55, 5247-5250.
[6] A. Kochem, M. O'Hagan, E.S. Wiedner, M. van Gastel, *Chem. -Eur. J.* 2015, 21, 10338-10347.
[7] P.F. Huo, C. Uyeda, J.D. Goodpaster, J.C. Peters, T.F. Miller, *ACS Catalysis* 2016, 6, 6114-6123.
[8] D.L. DuBois, R.M. Bullock, *Eur. J. Inorg. Chem.* 2011, 1017-1027.
[9] M.L. Helm, M.P. Stewart, R.M. Bullock, M.R. DuBois, D.L. DuBois, *Science* 2011, 333, 863-866.
[10] G.M. Jacobsen, J.Y. Yang, B. Twamley, A.D. Wilson, R.M. Bullock, M.R. DuBois, D.L. DuBois, *Energy Environ Sci.* 2008, 1, 167-174.
[11] P.D. Tran, J. Barber, Phys. *Chem. Chem. Phys.* 2012, 14, 13772-13784.
[12] D.J. Martin, B.D. McCarthy, C.L. Donley, J.L. Dempsey, *Chem. Commun.* 2015, 51, 5290-5293.
[13] N. Queyriaux, R.T. Jane, J. Massin, V. Artero, M. Chavarot-Kerlidou, Coord. *Chem. Rev.* 2015, 304-305, 3-19.
[14] J. Wang, C. Li, Q. Zhou, W. Wang, Y. Hou, B. Zhang, X. Wang, *Catal. Sci. Technol.* 2016, 6, 8482-8489.
[15] J.-N. Luy, S.A. Hauser, A.B. Chaplin, R. Tonner, *Organometallics* 2015, 34, 5099-5112.
[16] Q.-X. Liu, H.-L. Li, X.-J. Zhao, S.-S. Ge, M.-C. Shi, G. Shen, Y. Zang, X.-G. Wang, *Inorg. Chim. Acta* 2011, 376, 437-445.
[17] C. Chen, H. Qiu, W. Chen, *J. Organomet. Chem.* 2012, 696, 4166-4172.
[18] X. Zhang, S. Gu, Q. Xia, W. Chen, *J. Organomet. Chem.* 2009, 694, 2359-2367.
[19] L.B. Munro, V.J. Catalano, *Eur. J. Inorg. Chem.* 2014, 4994-5007.
[20] K. Chen, M.M. Nenzel, T.M. Brown, V.J. Catalano, *Inorg. Chem.* 2015, 54, 6900-6909.

[21] S. Das Adhikary, T. Samanta, G. Roymahapatra, F. Loiseau, D. Jouvenot, S. Giri, P.K. Chattaraj, J. Dinda, *New J. Chem.* 2010, 34, 1974-1980.
[22] J. Liu, M. Liu, Y. Yue, M. Yao, K. Zhuo, *Chin. J. Chem.* 2012, 30, 644-650.
[23] M.H. Reineke, M.D. Sampson, A.L. Rheingold, C.P. Kubiak, *Inorg. Chem.* 2015, 54, 3211-3217.
[24] L. Yang, D.R. Powell, R.P. Houser, *Dalton Trans.* 2007, 955-964.
[25] G. Armendariz-Vidales, C. Frontana, *Phys. Chem. Chem. Phys.* 2015, 17, 29299-29304.
[26] C. Costentin, J.-M. Saveant, *Chemelectrochem* 2014, 1, 1226-1236.
[27] M.T.M. Koper, E. Bouwman, *Angew. Chem. Int. Ed.* 2010, 49, 3723-3725.
[28] G.M. Sheldrick, *Acta Cryst. A* 2008, 64, 112-122.
[29] G.M. Sheldrick, *Acta Cryst. C* 2015, 71, 3-8.
[30] J. Dinda, S.D. Adhikary, S.K. Seth, A. Mahapatra, *New J. Chem.* 2013, 37, 431-438.
[31] J. Berding, M. Lutz, A.L. Spek, E. Bouwman, *Organometallics* 2009, 28, 1845-1854.

CHAPTER 5

Nickel Compounds of Pyridine-Amide-Functionalized Carbene Ligands: Synthesis, Structure and Electrocatalytic Activity

*Two pyridyl-amide substituted (benz)imidazolium salts H_2**L1**Cl and H_2**L2**Cl were synthesized and successfully employed as ligand precursors for the syntheses of novel nickel(II) complexes [Ni(**L1**)]Cl and [Ni(**L2**)]PF_6 bearing tetradentate ligands including an N-heterocyclic carbene (NHC) functionality. Single crystal X-ray crystallography revealed that the nickel ions in both compounds are in slightly distorted square-planar geometries. Cyclic voltammetry of the two compounds showed irreversible reduction events. In the solvent dimethylformamide in presence of acetic acid, the imidazolidene-based complex [Ni(**L1**)]Cl shows higher catalytic activity in the electrocatalytic proton reduction than the nickel compound of the benzimidazolidene-based ligand. Moreover, the water-soluble complex [Ni(**L1**)]Cl appeared to be an active electrocatalyst for proton reduction in aqueous buffer solutions at pH 6.8. The stability of this complex in aqueous solutions is low.*

This chapter will be published. S. Luo, M.A. Siegler, and E. Bouwman, manuscript in preparation.

5.1 Introduction

Dihydrogen gas is a promising energy carrier and has emerged as a good alternative for fossil fuel resources, which can meet the rapidly increasing global energy demands.[1] Aiming to avoid the use of the expensive Pt-based catalyst, the study of the hydrogen evolution reaction (HER) using molecular catalysts based on non-noble metals has received extensive attention in recent decades. The development of an inexpensive catalyst with high catalytic turnover rates is the ultimate goal. However, a high stability and low overpotential of the catalyst are also of great significance. Hydrogenase enzymes act as effective catalysts in the hydrogen evolution reaction at ambient temperatures and pressures. But most of the hydrogenase enzymes only work in anaerobic conditions and suffer from oxidative deactivation.[2] On the other hand, synthetic molecular catalyst often suffer from decomposition in aqueous acidic media, resulting in the formation of heterogeneous catalyst systems.[3]

In the last decade the cobaloxime-type catalysts[4] and nickel-based catalysts with diphosphane ligands[5] have proven to have high activity in the electrocatalytic proton reduction reaction. Meanwhile, other molecular catalyst based on molybdenum,[6] zinc,[7] manganese,[8] and copper[9] have been reported to have outstanding activities. Our interest is in the development of novel nickel-based homogeneous catalysts supported by N-heterocyclic carbene (NHC) ligands.[10, 11] Such NHC ligands functionalized with pyridine groups have been used to synthesize nickel and palladium complexes that were found to be efficient catalysts for the Kumada cross-coupling[10-12] and Heck-type coupling reactions.[13] Nevertheless, so far metal-NHC complexes have received little attention regarding their potential electrochemical properties and activity in electrocatalysis.[14, 15] Herein, we report the synthesis and characterization of two novel nickel compounds supported by tetradentate N-functionalized carbene ligands. We report their redox properties in the solvent dimethylformamide as well as their electrocatalytic activity for proton reduction in weakly acidic aqueous conditions.

5.2 Results and Discussion

5.2.1 Synthesis of ligand precursors and the Ni-NHC complexes

The two new (benz)imidazolium salts H_2**L1**Cl and H_2**L2**Cl were designed for their use as ligand precursors for the formation of tetradentate anionic NHC ligands, comprising amide and pyridine donor moieties. Alkylation of N-pyridylmethyl(benz)imidazole didn't appeared to be straightforward. The relatively high reactivity of the pendant pyridyl group resulted in the formation of oligomeric side products (Figure 5.1), giving relatively low yields of the desired products (30%-50%). The (benz)imidazolium salts were characterized by NMR spectroscopy and electrospray ionization mass spectrometry (ESI-MS). In the ^{1}H NMR spectra the characteristic downfield signals for the imidazolium NCHN and amide NH protons were observed at 9.32 and 9.15 ppm for H_2**L1**Cl and at 10.02 and 9.44 ppm for

H_2**L2**Cl. The ESI-MS exhibited base peaks corresponding to the $[M - Cl]^+$ (benz)imidazolium cations.

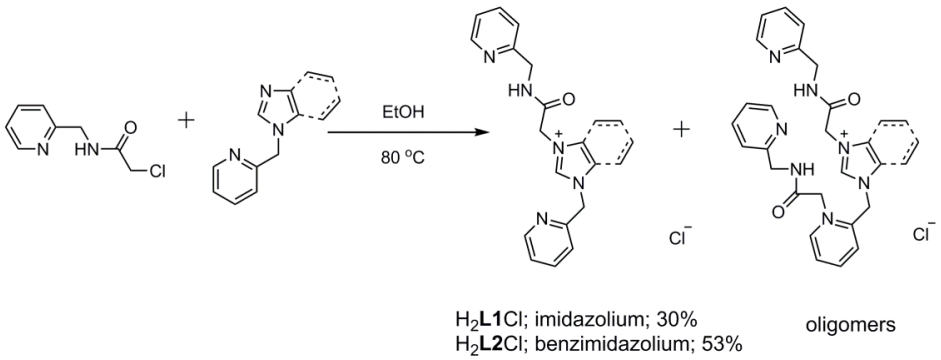

*Figure 5.1. Synthetic route of the ligand precursors H_2**L1**Cl and H_2**L2**Cl.*

Nickel(II) complexes were prepared by reacting the ligand precursors H_2**L1**Cl and H_2**L2**Cl with Ni(dme)Cl_2 in DMF in the presence of K_2CO_3 at room temperature and were isolated as yellow solids. The complex [Ni(**L1**)]Cl was obtained as a pure product after dilution of the reaction mixture with water and an extraction with dichloromethane (DCM). Unfortunately, this purification method did not work for the benzimidazole-based compound [Ni(**L2**)]Cl. Therefore, by addition of NH_4PF_6 the chloride anion was replaced with the hexafluoridophosphate counter ion. The crystalline yellow needle-shaped crystals of [Ni(**L2**)]PF_6 were obtained directly from the filtrate after the reaction. The absence in the ^{1}H NMR spectra of the nickel compounds of the characteristic downfield signals for the amide NH and imidazolium NCHN protons indicates the successful creation of the deprotonated amide and carbene moieties and their coordination to the nickel(II) center. The ESI-MS spectra exhibit base peaks corresponding to the $[M - Cl]^+$ or $[M - PF_6]^+$ cationic complexes. Recrystallized samples of the nickel compounds were dried in vacuo before elemental analyses were performed; however, the analysis result still showed the presence of small amounts of H_2O. Compound [Ni(**L1**)]Cl readily dissolves in water, whereas compound [Ni(**L2**)]PF_6 is soluble in DMF but hardly dissolves in water.

5.2.2 Structural characterization of Ni-NHC complexes

Single crystals of [Ni(**L1**)]Cl suitable for X-ray structure determination were obtained by vapor diffusion of diethyl ether into an acetonitrile solution of the complex. Single crystals of [Ni(**L2**)]PF_6 were picked from the yellow needle-like crystals that were obtained directly from the reaction mixture. Projections of the cationic complexes are shown in Figure 5.2. The crystallographic and refinement data are provided in Table AV.1, and selected bonds lengths and angles are given in Table AV.2. The imidazole-based compound [Ni(**L1**)]Cl crystallized in the space group $P2_1/c$. Apart from the cationic complex and the non-coordinating chloride anion the asymmetric unit contains three lattice water molecules. The

benzimidazole-based compound [Ni(**L2**)]PF_6 crystallized in the triclinic space group P$\bar{1}$, with one cationic complex and one PF_6 anion in the asymmetric unit.

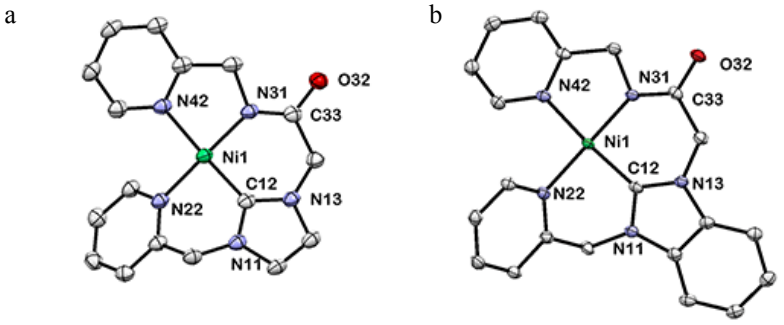

*Figure 5.2. Displacement ellipsoid plots (50% probability level) of the cations of compounds [Ni(**L1**)]Cl (a) and [Ni(**L2**)]PF_6 (b) at 110(2) K. Hydrogen atoms, counter ions and the lattice solvents are omitted for clarity.*

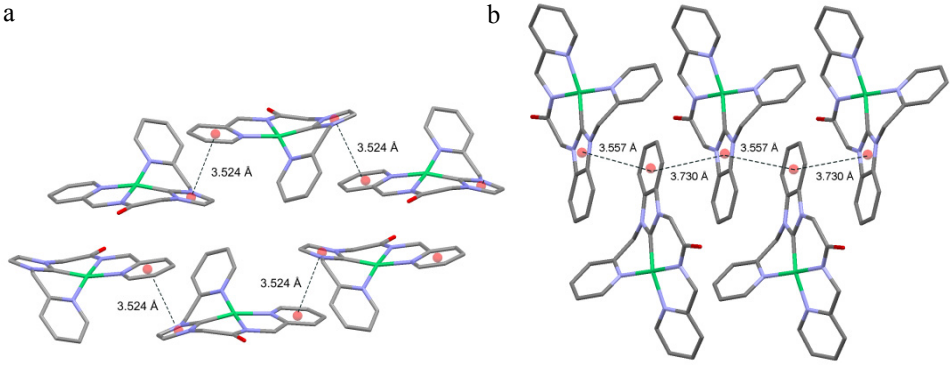

*Figure 5.3. View of π-stacking interactions in [Ni(**L1**)]Cl (a) and [Ni(**L2**)]PF_6 (b). Distances given are between ring centers.*

In both structures the nickel(II) ion is in a four-coordinate [$NiCN_3$] chromophore with short Ni–C (carbene) and Ni–N (amide) bonds, and two longer Ni–N (pyridine) bond distances. The nickel ions are in slightly distorted square-planar geometries (τ_4 = 0.178 for [Ni(**L1**)]Cl and τ_4 = 0.177 for [Ni(**L2**)]PF_6).[16] The Ni–N_{amide} bond in both complexes (1.873(3) Å and 1.856(2) Å, respectively) is slightly longer than in other reported nickel compounds with pyridylmethyl-amide groups (ranging from 1.81 to 1.85 Å).[17-19] The carbonyl C33–O32 bond in compound [Ni(**L1**)]Cl is slightly longer than the one in compound [Ni(**L2**)]PF_6, probably due to the presence of hydrogen bonds between the carbonyl O32 and lattice water molecules in [Ni(**L1**)]Cl. The structure [Ni(**L1**)]Cl is further stabilized by intermolecular π-π stacking interactions between pyridine and carbene rings with a distance of 3.524 Å. The chloride ion is at a distance of 3.443 Å of the nickel center.

Intermolecular π-π stacking interactions in the structure of [Ni(**L2**)]PF_6 occur between adjacent benzimidazole rings with distances of 3.525 and 3.677 Å (Figure 5.3).

5.2.2 Electrochemical studies in dimethylformamide

The redox properties of the two compounds were investigated with cyclic voltammetry in dry DMF solutions containing 0.1 M tetrabutylammonium hexafluoridophosphate (TBAP) as the supporting electrolyte, under a stream of argon. For the imidazole-based complex [Ni(**L1**)]Cl an irreversible reduction was found at −1.4 V vs. Ag/AgCl; in the anodic return scan one irreversible oxidative peak was found at −0.84 V (Figure AV.1.1). The benzimidazole-based complex [Ni(**L2**)]PF_6 showed the first irreversible reduction to occur at −1.27 V vs. Ag/AgCl. The less negative reductive potential of [Ni(**L2**)]PF_6 must be due to the benzimidazole-based carbene being a more electron-withdrawing group, which makes the nickel center relatively electron poor. The oxidative peak **c** in the return scan of [Ni(**L2**)]PF_6 is also located at a less negative potential at −0.75 V. Upon expanding the scan window down to −2.2 V, a second irreversible reductive peak is found at −2.02 V and three small oxidative waves **c**, **d** and **e** appeared at −0.75, −0.64 and −0.26 V, respectively (Figure 5.4). It indicate that the new oxidative processes **d** and **e** are related to the second reductive event **b**. Both complexes [Ni(**L1**)]Cl and [Ni(**L2**)]PF_6 show irreversible redox nature, indicating that electron transfer is immediately followed by a fast chemical reaction or structural rearrangement.[20]

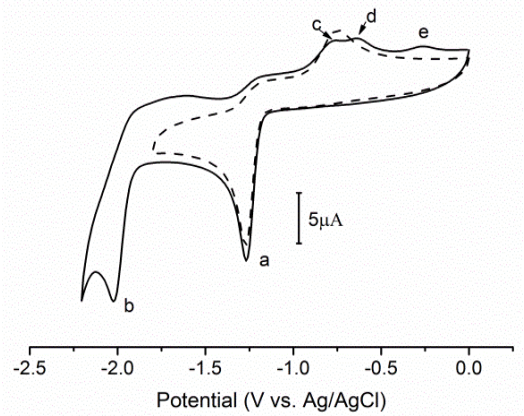

*Figure 5.4. Cyclic voltammograms of [Ni(**L2**)]PF_6 (1 mM) recorded in DMF containing 0.1 M TBAP as supporting electrolyte in different scan windows (dashed line = 0 to −1.8 V; solid line = 0 to −2.2 V) at scan rate 0.1 V/s, using a glassy carbon working electrode.*

The electrocatalytic activity of the two compounds for HER were studied in DMF solutions, using acetic acid as proton source. For compound [Ni(**L1**)]Cl a catalytic reductive current response appeared with an onset potential at −1.53 V in presence of 10 mM acid (Figure 5.5a). For compound [Ni(**L2**)]PF_6 a similar catalytic reductive current was observed with an onset potential of −1.69 V. However, before the catalytic wave of [Ni(**L2**)]PF_6 one small additional irreversible reduction appeared at −1.60 V (Figure 5.5b). With increasing acid

concentration this additional peak becomes invisible, as it overlaps with the following large catalytic peak (Figure AV.2).

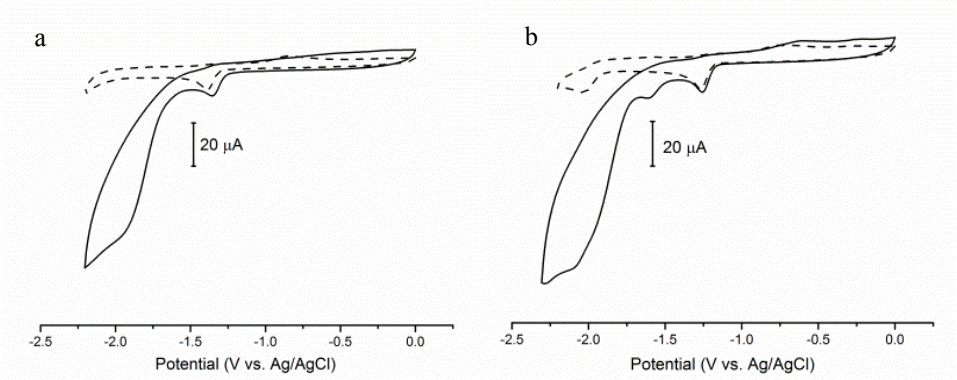

*Figure 5.5. Cyclic voltammograms of (a) 1 mM of [Ni(**L1**)]Cl and (b) 1 mM of [Ni(**L2**)]PF_6 recorded in DMF containing 0.1 M TBAP as supporting electrolyte at scan rate 0.1V/s in absence (dashed line) and in presence (solid line) of 10 mM acetic acid, using glassy carbon working electrode.*

In general, for an irreversible catalytic reaction following a reversible charge transfer (P + $e^- \rightleftharpoons$ Q; Q + A $\xrightarrow{k}$ P+B), the k_{obs} can be deduced from i_c.

$$i_c = n'FAC_P^0\sqrt{Dk_{obs}} \qquad (1)$$

If equation (1) is combined with the Randles-Sevcik equation (2), the relationship (3) is obtained.

$$i_p = 0.4463n'FAC_P^0\left(\frac{n\prime FvD}{RT}\right)^{1/2} \qquad (2)$$

$$\frac{i_c}{i_p} = \frac{1}{0.4463}\sqrt{\frac{RTk_{obs}}{n\prime Fv}} \qquad (3)$$

$$k_{obs} = kC_A^0 \qquad (4)$$

Where i_c is the maximum current of the catalytic peak, and i_p is the plateau current of the non-catalytic reduction wave, *n'* is the number of electrons transferred to P from the electrode, F is Faraday's constant, *A* is the area of the electrode, C_P^0 is the catalyst concentration, C_A^0 is the substrate concentration, *D* is the diffusion coefficient, *k* is the rate constant.

When specialized the reaction to the two electron transferred hydrogen evolution reaction (HER), the order of the reaction with respect to acid can be identified using the following equations:[21-23]

$$k_{obs} = k[H^+]^x \qquad (5)$$

$$\frac{i_c}{i_p} = \frac{n}{0.4463}\sqrt{\frac{RTk[\mathrm{H}^+]^x}{Fv}} \qquad (6)$$

Where x is the order of the reaction with respect to protons. n is the number of electrons involved in HER (n = 2).

According to equations (5) and (6), if a plot of i_c/i_p versus the square root of the proton concentration gives a linear correlation, a catalytic reaction has a first-order dependence on proton concentration. Many publications have cited this method to calculate k_{obs} and k for electrocatalytic reactions.[9, 22, 24-27]

Plots of i_c/i_p versus the square root of the acid concentration for the complexes [Ni(**L1**)]Cl and [Ni(**L2**)]PF_6 show a non-linear relationship (Figure AV.3). Instead, plots of i_c/i_p versus acid concentration do show a linear relationship (see Figure 5.6). This relationship reveals that two protons are involved in the rate-determining step of the reaction. Unfortunately, due to the irreversible redox property of both compounds, equation (6) is not suitable for k_{obs} determination for both complexes.[21, 23]

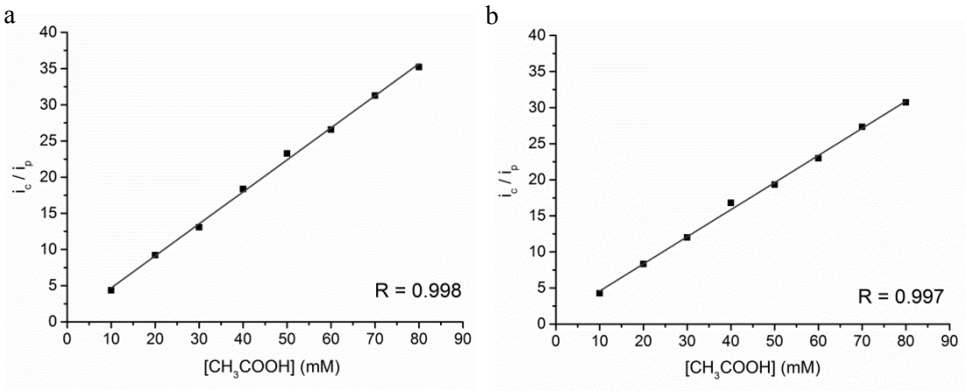

*Figure 5.6. Plot of i_c/i_p vs. [CH_3COOH] (mM) for [Ni(**L1**)]Cl (a) and [Ni(**L2**)]PF_6 (b) in presence of various acid concentration in DMF containing 0.1 M TBAP as supporting electrode at 0.1 V/s, using a glassy carbon working electrode.*

In the presence of 80 mM acetic acid the value of i_c/i_p reaches 35.2 and 30.7 for complex [Ni(**L1**)]Cl and [Ni(**L2**)]PF_6, respectively, indicating that the imidazole-based compound [Ni(**L1**)]Cl is the faster HER catalyst of the two. This difference in activity was confirmed with controlled-potential electrolysis (CPE) experiments (see below). The overpotential for proton reduction in our conditions is 860 mV for [Ni(**L1**)]Cl and 940 mV for [Ni(**L2**)]PF_6, taking homoconjugation of the acid into account.[28] In general, a more electron-donating group such as imidazolylidene will make the metal centre of complex more difficult to reduce, which might increase the overpotential in electrocatalysis. The cyclic voltammogrammes indeed show the reductive events of [Ni(**L1**)]Cl to occur at more

negative potentials compared to those of [Ni(**L2**)]PF_6. Surprisingly, the overpotential for proton reduction is lower for the imidazole-based compound.

Hydrogen production was further confirmed using gas chromatography (GC) monitoring the controlled-potential electrolysis at −1.8 V; the faradaic efficiencies were determined to be around 85% for both [Ni(**L1**)]Cl and [Ni(**L2**)]PF_6. After subtracting the results of a blank reaction (volume of H_2 produced at this potential in absence of catalyst, for data treatment see Appendix I), 185 µL and 105 µL H_2 were generated over 2 h electrolysis in presence [Ni(**L1**)]Cl and [Ni(**L2**)]PF_6, respectively, corresponding to a mere 1.5 and 0.9 mol H_2 per mol of catalyst. The better electrocatalytic activity of [Ni(**L1**)]Cl may tentatively be ascribed to the better electron-donating properties of the imidazole-based carbene, which might facilitate the formation of a metal hydride intermediate.

Thus, the imidazole-based compound [Ni(**L1**)]Cl not only shows higher activity in catalyzing HER, but is also active at a lower overpotential. This anti-correlation indicates that a proton delivery between the ligand and the metal center is operative, which breaks the correlation between energy costs and kinetic barriers.[29]

5.2.3 Electrochemical studies in aqueous solution

As the compound [Ni(**L1**)]Cl shows good solubility in water, the electrochemical properties of [Ni(**L1**)]Cl in aqueous solutions were also investigated. Voltammograms of [Ni(**L1**)]Cl in an 0.2 mM phosphate buffer solution (pH = 6.86) are shown in Figure 5.7a. Compared with the buffer solution without nickel complex, a small irreversible reductive process at −1.36 V is observed, which is followed by a large catalytic current at −1.82 V, which can be assign to HER process. The catalytic current increased with increasing of the scan rate (0.05 to 2 V/s), as shown in Figure 5.7b. At lower scan rate range, the catalytic current increases linearly; when scan rate reach ≥ 0.5 V/s, the current shows a saturated trend (Figure 5.7c).

It was observed that the bright yellow aqueous solution containing [Ni(**L1**)]Cl gradually faded to pale yellow during the electrochemical experiments. In order to investigate whether this color change is related to electrolysis or the stability of the compound in mildly acidic aqueous solutions, ^{1}H NMR spectra were recorded of [Ni(**L1**)]Cl in presence and absence of acid in deuterium oxide. The ^{1}H NMR spectra of a solution of [Ni(**L1**)]Cl in deuterium oxide did not change significantly over a period of more than four days. However, upon addition of an excess of acetic acid-*d*4 the color of the solution visibly faded within 1 hour, and the solution was colorless after one day. The ^{1}H-NMR spectra revealed that nearly 50% of the compound decomposed within 1 h (Figure AV.4). The composition of the colorless solution was investigated with ESI-MS (Figure AV.5). The MS peak located at m/z 309.3 can be assigned to the ligand precursor [HD**L1**]$^+$. Although we investigated the stability of compounds in organic solvent in presence of acid (see Figure AV.6), it appears that the presence of even a weak acid in aqueous solution is

sufficient to cause dissociation of the ligand from the nickel center by protonation of the amidate nitrogen and the carbene carbon atoms.

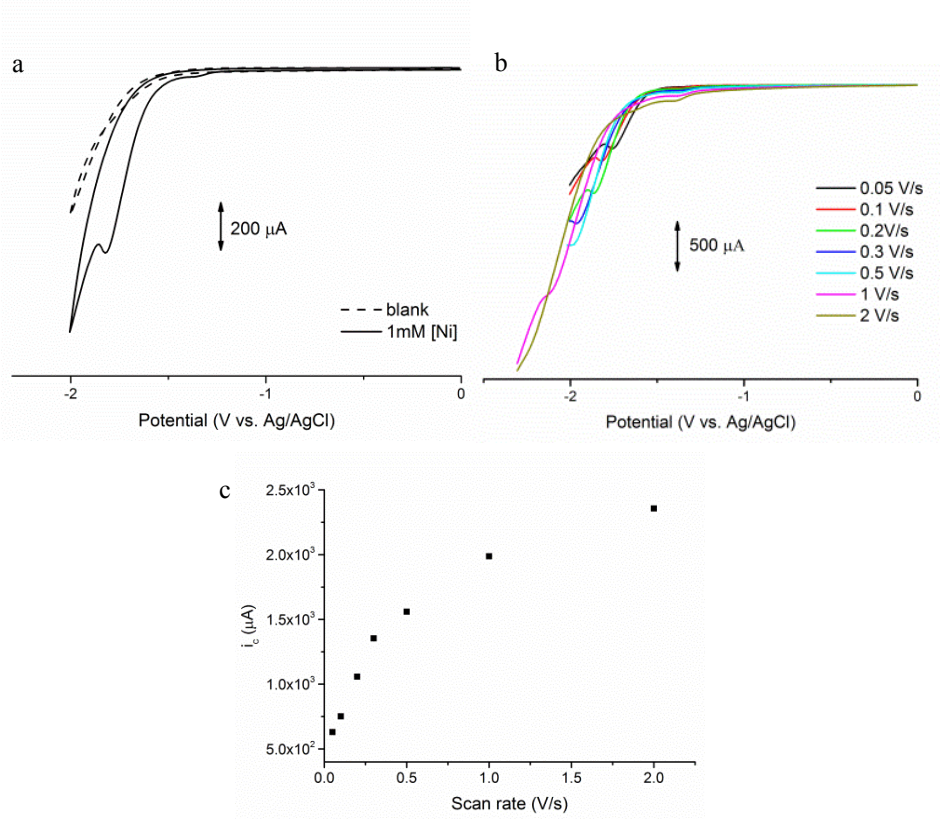

Figure 5.7. (a) *CVs of compound [Ni(**L1**)]Cl recorded in pH = 6.86 phosphate buffer solution (0.2 M) in absence (dashed line) and in presence (solid line) at a scan rate of 0.1 V/s; (b) Forward scans of 1 mM [Ni(**L1**)]Cl in phosphate buffer solution (0.2 M, pH = 6.86) at various scan rates from 0.05 to 2 V/s; (c) plots of catalytic current* vs. scan rate for compound *[Ni(**L1**)]Cl in phosphate buffer solution (0.2 M, pH = 6.86), using glassy carbon as the working electrode. For Ag/AgCl (3 M KCl) reference electrode, E^o = 0.223 V vs. NHE.*

5.3 Conclusion

The two new nickel(II) complexes [Ni(**L1**)]Cl and [Ni(**L2**)]PF_6 bearing pyridyl-amidate substituted tetradentate ligands based on N-heterocyclic carbenes, were isolated and characterized. X-ray structure analysis revealed that the nickel ions in both compounds are in slightly distorted square-planar geometries. Cyclic voltammetry of the two compounds showed irreversible redox events. In dimethylformamide in presence of acetic acid both complexes showed activity for the electrocatalytic reduction of protons into H_2 gas as confirmed by GC quantification. The imidazole-based complex [Ni(**L1**)]Cl shows slightly higher catalytic activity at lower overpotentials compared to the benzimidazole-based compound. Moreover, the water-soluble complex [Ni(**L1**)]Cl appears to be an active

electrocatalyst also in aqueous buffer solutions. Although the compounds appeared to be stable in acidic organic solution, the complex [Ni(**L1**)]Cl is not stable in acidic aqueous solution. Unfortunately, the activity of the compounds for proton reduction appeared to be low, and far from comparable with the well-developed cobaloxime-type and nickel-diphosphane type catalysts. If possible, the catalytic mechanism as well as rate-determining steps need to be identified and studied in priority. Further research needs to focus on finding an explanation for the low catalytic activity of the catalysts based on carbene-type ligands.

5.4 Experimental

5.4.1 Materials

Commercial chemicals were used without further purification. Acetonitrile, tetrahydrofuran, dichloromethane and diethyl ether were obtained from a PureSolv MD5 solvent dispenser. Dry ethanol and dimethylformamide were prepared by adding molecular sieves into commercial anhydrous solvent. The rest commercial solvents were used without further purification. All air-sensitive reactions were performed under argon or dinitrogen gas using standard Schlenk techniques unless mentioned otherwise. The compounds dichlorido(dimethoxyethane)nickel ([Ni(dme)Cl_2]),[30] 2-chloro-N-(pyridin-2-ylmethyl)acetamide,[31] and *N*-pyridin-2-ylmethyl(benz)imidazole[32] were prepared following published procedures.

5.4.2 Analytical methods

^{1}H and ^{13}C spectra were recorded on Bruker 300DPX /400DPX-liq spectrometer. Mass spectra were obtained using a Finnigan Aqueous Mass Spectrometer (MS) with electrospray ionization (ESI). Elemental analyses were performed by the Mikroanalytisches Laboratorium Kolbe, Germany. Cyclic voltammetry was recorded with an Autolab PGstat10 potentiostat controlled by GPES4 software under argon. A 3 mm diameter glassy carbon electrode was used as working electrode and plantium as the counter electrode. The experimental reference electrode was a commercially available Ag/AgCl electrode (E^o = 0.223 V vs. NHE). Ferrocene was added at the end of each measurement as an internal standard when experiments were carried out in organic solvents. Under the used conditions the redox couple of ferrocene was located at $E_{1/2}$ = 0.52 V vs Ag/AgCl with ΔE = 90 ~ 110 mV.

Controlled-potential electrolysis (CPE) experiments were carried out in an H-shaped double-compartment cell. A glassy carbon electrode with a surface area of 0.07 cm^2 was used as the working electrode for electrolysis. As the auxiliary electrode a platinum gauze electrode was used. The reference electrode was a commercially available aqueous Ag/AgCl electrode. The solution containing the sample was bubbled with helium gas for 10 min before measurement and the electrolysis was carried out under an atmosphere of helium. The solutions in both compartments were constantly stirred during electrolysis

experiments. The evolved H_2 gas produced during electrolysis measurements was quantified using gas chromatography, which was performed on a Shimadzu GC2010 at 35ºC fitted with a Supelco Carboxen 1010 molecular sieve column. Two separate experiments were done and the results of two experiments were averaged.

5.4.3 Single crystal x-ray crystallography

All reflection intensities were measured at 110(2) K using a SuperNova diffractometer (equipped with Atlas detector) with Cu *K*α radiation (λ = 1.54178 Å) under the program CrysAlisPro (Version 1.171.37.35 Agilent Technologies, 2014). The same program was used to refine the cell dimensions and for data reduction. The structure was solved with the program SHELXS-2014/7 and was refined on F^2 with SHELXL-2014/7.[33] Analytical numeric absorption correction using a multifaceted crystal model was applied using CrysAlisPro. The temperature of the data collection was controlled using the system Cryojet (manufactured by Oxford Instruments). The H atoms were placed at calculated positions (unless otherwise specified) using the instructions AFIX 23, AFIX 43 with isotropic displacement parameters having values 1.2 *U*eq of the attached C atoms.

Additional notes for the structures:
Compound [Ni(**L1**)]Cl*:* The structure is mostly ordered. The asymmetric contains three lattice water solvent molecules. Two are disordered over two orientations, and the occupancy factors of the major components of the disorder refine to 0.721(6) and 0.858(6). The H atoms for O3W' could not be retrieved. Apart from the hydrogen bonds between carbonyl and water molecules, there are specified hydrogen bonds between chloride ion and water molecules (hydrogen bond details are provided in Appendix V Table AV.3).

Compound [Ni(**L2**)]PF_6*:* The structure is partly disordered. The PF_6^- counter ion is found to be disordered over two orientations, and the occupancy factor of the major component of the disorder refines to 0.869(9).

5.4.4 Ligand and complex synthesis

H_2**L1**Cl:
N-pyridin-2-ylmethylimidazole (6 mmol, 0.960 g) and 2-chloro-*N*-(pyridin-2-ylmethyl)acetamide (5 mmol, 0.925 g) were added into a 100 ml round-bottomed flask containing 25 ml dry ethanol. The mixture was heated at 80 °C for 5 h, after which the solvent was removed by rotary evaporation. The residue was dissolved in THF and the solution was filtered. The filtrate was concentrated to 5 ml and acetone was added until a yellow precipitate appeared. The yellow-brownish powder was collected by filtration, washed with diethyl ether, and dried under vacuum. Yield: 0.92 g (54% based on the acetamide). ^{1}H NMR (300 MHz, DMSO-d_6) δ 9.32 (s, 1H, NC*H*N), 9.15 (t, *J* = 5.6 Hz, 1H, N*H*), 8.54 (dd, *J* = 11.4, 4.8 Hz, 2H, Py-*H*), 7.89 (td, *J* = 7.7, 1.8 Hz, 1H, Py-*H*), 7.78 (m, 3H, Py-*H*), 7.54 – 7.21 (m, 4H, Py-*H*, $C_{imidazole}$-*H*), 5.62 (s, 2H, Py-CH_2-$N_{imidazole}$), 5.17 (s, 2H, Py-CH_2-N_{Amide}), 4.44 (d, *J* = 5.8 Hz, 2H, C(O)-CH_2-$N_{imidazole}$). ^{13}C NMR (75 MHz, DMSO-d_6) δ = 165.13, 157.60, 153.57, 149.61, 148.94, 137.54, 136.79, 123.96, 123.68,

122.59, 122.49, 122.35, 121.32, 53.05, 50.65, 44.42. The signal of N-*C*H-N could not be found. ESI-MS found (calc): $[M–Cl]^+$ *m/z* 308.2 (308.15).

H_2**L2**Cl:
The same synthetic procedure of H**L1**Cl was followed, but with the starting material *N*-pyridin-2-ylmethylbenzimidazole (8.5 mmol, 1.78 g) and 2-chloro-*N*-(pyridin-2-ylmethyl)acetamide (8.5 mmol, 1.6 g) in 25 ml dry ethanol at 80 °C for 60 h. Yield: 0.90 g (30% based on the acetamide). ^{1}H NMR (300 MHz, DMSO-d_6) δ 10.02 (s, 1H, NC*H*N), 9.44 (s, 1H, N*H*), 8.56 (d, *J* = 4.7 Hz, 1H, Py-*H*), 8.49 (d, *J* = 4.6 Hz, 1H, Py-*H*), 8.02 (d, *J* = 7.1 Hz, 1H, Py-*H*), 7.98 – 7.81 (m, 3H, Py-*H*), 7.73 – 7.59 (m, 3H, Py-*H*, C_{benzim}-*H*), 7.46 (d, *J* = 7.8 Hz, 1H, C_{benzim}-*H*), 7.37 (q, *J* = 7.7 Hz, 2H, C_{benzim}-*H*), 5.99 (s, 2H, Py-CH_2-N_{benzim}), 5.55 (s, 2H, Py-CH_2-N_{Amide}), 4.51 (s, 2H, C(O)-CH_2-N_{benzim}). ^{13}C NMR (75 MHz, DMSO-d_6) δ = 165.07, 152.99, 149.67, 148.29, 144.16, 137.63, 131.65, 130.95, 126.76, 123.79, 122.81, 122.70, 121.71, 113.91, 50.92, 48.66, 44.14. ESI-MS found (calc): $[M–Cl]^+$ *m/z* 358.2 (358.17).

[Ni(**L1**)]Cl:
A Schlenk flask was charged with [Ni(dme)Cl_2] (0.5 mmol, 0.11 g), H_2**L1**Cl (0.5 mmol, 0.17 g), K_2CO_3 (1.9 mmol, 0.26 g) and dry DMF (10 mL) under an argon atmosphere. The dark green solution was stirred at room temperature overnight. The reaction mixture was filtered to remove the salts. To the solution 100 ml distilled water was added and the aqueous solution was washed with DCM (3×50 ml). The water layer was evaporated to dryness. The resulting yellow solid was collected and dried under vacuum. Crystals suitable for X-ray diffraction were obtained by vapor diffusion of diethyl ether into an acetonitrile solution of the complex. Yield: 28% (56 mg). ^{1}H NMR (300 MHz, DMSO-d_6) δ 9.09 (d, *J* = 5.5 Hz, 1H, Py-H), 8.22 (t, *J* = 7.1 Hz, 1H, Py-H), 8.10 (t, *J* = 7.3 Hz, 1H, Py-H), 7.86 (d, *J* = 7.6 Hz, 1H, Py-H), 7.70 (m, 3H, Py-H), 7.49 (d, *J* = 8.6 Hz, 3H, Py-H, NCH), 5.74 (s, 2H, Py-CH_2-N_{NHC}), 4.74 (s, 2H, Py-CH_2-N_{Amide}), 4.71 (broad, 2H, C_{Amide}-CH_2-N_{NHC}). ^{13}C NMR (75 MHz, DMSO-d_6) δ = 214.87, 168.08, 163.85, 154.40, 153.52, 149.09, 147.32, 140.51, 139.53, 125.64, 123.37, 122.38, 122.08, 121.19, 58.04, 52.27, 51.92. Anal. Calcd for $C_{17}H_{16}ClN_5NiO{\cdot}1.5H_2O$: C 47.76, H 4.48, N 16.38; found C 47.58, H 4.78, N 16.25. ESI-MS found (calc): $[M–Cl]^+$ *m/z* 364.1 (364.07).

[Ni(**L2**)]PF_6:
A Schlenk flask was charged with [Ni(dme)Cl_2] (0.5 mmol, 0.11 g), H_2**L2**Cl (0.5 mmol, 0.195 g), NH_4PF_6 (0.5 mmol, 0.10 g), K_2CO_3 (1.9 mmol, 0.26 g) and dry DMF (10 mL) under an argon atmosphere. The brown solution was stirred at room temperature for 2 days. The reaction mixture was filtered and the filtrate was left standing for a few days, during which time yellow crystals formed. The crystalline solid was collected by filtration, washed with diethyl ether and dried under vacuum. Yield: 22% (60 mg). Yellow needle crystals suitable for X -ray crystallography crystals were obtained directly from filtrate after the reaction. The compound is poorly soluble in DMSO. ^{1}H NMR (400 MHz, acetonitrile-d_3) δ 8.93 (d, *J* = 5.6 Hz, 2H, Py-H), 8.12 (t, *J* = 7.7 Hz, 1H, Py-H), 8.01 (t, *J* = 7.7 Hz, 1H, Py-

H), 7.80 (dd, J = 16.2, 7.9 Hz, 2H, NCH), 7.62 (m, 3H, Py-H), 7.48 (m, 3H, Py-H, Ar-H), 7.34 (t, J = 6.6 Hz, 1H, Ar-H), 5.79 (s, 2H, Py-CH_2-N_{NHC}), 4.89 (s, 2H, Py-CH_2-N_{Amide}), 4.82 (broad, 2H, C_{Amide}-CH_2-N_{NHC}). ^{13}C NMR (101 MHz, acetonitrile-d_3) δ = 154.40, 148.69, 141.76, 140.89, 127.05, 126.88, 125.33, 125.26, 124.41, 122.32, 112.35, 111.93, 59.50, 50.85, 50.52. The six quaternary carbons could not be detected due to the low concentration caused by the limited solubility of the compound. Anal. Calcd for $C_{21}H_{18}F_6N_5NiOP$: C 45.03, H 3.24, N 12.50; found C 44.26, H 3.42, N 12.07. ESI-MS found (calc): $[M–PF_6]^+$ *m/z* 414.1 (414.09).

5.5 Acknowledgements

S. Luo gratefully acknowledges a grant from the Chinese Scholarship Council (no. 201306410011). We thank Mr. J.M.M. van Brussel for ESI-MS measurements.

5.6 References

[1] B. Rausch, M.D. Symes, G. Chisholm, L. Cronin, *Science* 2014, 345, 1326-1330.
[2] T.R. Simmons, G. Berggren, M. Bacchi, M. Fontecave, V. Artero, *Coord. Chem. Rev.* 2014, 270, 127-150.
[3] N. Kaeffer, A. Morozan, J. Fize, E. Martinez, L. Guetaz, V. Artero, *ACS Catalysis* 2016, 6, 3727-3737.
[4] E.S. Rountree, D.J. Martin, B.D. McCarthy, J.L. Dempsey, *ACS Catalysis* 2016, 3326-3335.
[5] D.L. DuBois, R.M. Bullock, *Eur. J. Inorg. Chem.* 2011, 1017-1027.
[6] J.P. Porcher, T. Fogeron, M. Gomez-Mingot, E. Derat, L.M. Chamoreau, Y. Li, M. Fontecave, *Angew. Chem. Int. Ed.* 2015, 54, 14090-14093.
[7] X.W. Song, X.J. Gao, H.X. Liu, H. Chen, C.N. Chen, *Inorg. Chem. Commun.* 2016, 70, 1-3.
[8] K. Hou, H.T. Poh, W.Y. Fan, *Chem. Commun.* 2014, 50, 6630-6632.
[9] P. Zhang, M. Wang, Y. Yang, T. Yao, L. Sun, *Angew. Chem. Int. Ed.* 2014, 53, 13803-13807.
[10] J. Berding, M. Lutz, A.L. Spek, E. Bouwman, *Organometallics* 2009, 28, 1845-1854.
[11] J. Berding, T.F. van Dijkman, M. Lutz, A.L. Spek, E. Bouwman, *Dalton Trans.* 2009, 6948-6955.
[12] Z. Xi, B. Liu, W. Chen, *J. Org. Chem.* 2008, 73, 3954-3957.
[13] M.C. Jahnke, T. Pape, F.E. Hahn, *Eur. J. Inorg. Chem.* 2009, 1960-1969.
[14] K. Kawano, K. Yamauchi, K. Sakai, *Chem. Commun.* 2014, 50, 9872-9875.
[15] M. van der Meer, E. Glais, I. Siewert, B. Sarkar, *Angew. Chem. Int. Ed.* 2015, 54, 13792-13795.
[16] M.H. Reineke, M.D. Sampson, A.L. Rheingold, C.P. Kubiak, *Inorg. Chem.* 2015, 54, 3211-3217.
[17] P. Comba, W. Goll, B. Nuber, K. Várnagy, *Eur. J. Inorg. Chem.* 1998, 2041-2049.
[18] N.W. Alcock, G. Clarkson, P.B. Glover, G.A. Lawrance, P. Moore, M. Napitupulu, *Dalton Trans.* 2005, 518-527.
[19] F.A. Chavez, M.M. Olmstead, P.K. Mascharak, *Inorg. Chem.* 1996, 35, 1410-1412.

[20] V. Fourmond, S. Canaguier, B. Golly, M.J. Field, M. Fontecave, V. Artero, *Energy Environ Sci.* 2011, 4, 2417-2427.
[21] R.S. Nicholson, I. Shain, *Anal. Chem.* 1964, 36, 706-723.
[22] M.P. Stewart, M.-H. Ho, S. Wiese, M.L. Lindstrom, C.E. Thogerson, S. Raugei, R.M. Bullock, M.L. Helm, *J. Am. Chem. Soc.* 2013, 135, 6033-6046.
[23] E.S. Rountree, B.D. McCarthy, T.T. Eisenhart, J.L. Dempsey, *Inorg. Chem.* 2014, 53, 9983-10002.
[24] L. Gan, T.L. Groy, P. Tarakeshwar, S.K.S. Mazinani, J. Shearer, V. Mujica, A.K. Jones, *J. Am. Chem. Soc.* 2015, 137, 1109-1115.
[25] R. Tatematsu, T. Inomata, T. Ozawa, H. Masuda, *Angew. Chem. Int. Ed.* 2016, 55, 5247-5250.
[26] E.I. Musina, V.V. Khrizanforova, I.D. Strelnik, M.I. Valitov, Y.S. Spiridonova, D.B. Krivolapov, I.A. Litvinov, M.K. Kadirov, P. Lonnecke, E. Hey-Hawkins, Y.H. Budnikova, A.A. Karasik, O.G. Sinyashin, *Chem. -Eur. J.* 2014, 20, 3169-3182.
[27] R.M. Stolley, J.M. Darmon, M.L. Helm, *Chem. Commun.* 2014, 50, 3681-3684.
[28] V. Fourmond, P.-A. Jacques, M. Fontecave, V. Artero, *Inorg. Chem.* 2010, 49, 10338-10347.
[29] P.F. Huo, C. Uyeda, J.D. Goodpaster, J.C. Peters, T.F. Miller, *ACS Catalysis* 2016, 6, 6114-6123.
[30] A. Kermagoret, P. Braunstein, *Organometallics* 2008, 27, 88-99.
[31] M. Woods, A.D. Sherry, *Inorg. Chem.* 2003, 42, 4401-4408.
[32] J. Dinda, S.D. Adhikary, S.K. Seth, A. Mahapatra, *New J. Chem.* 2013, 37, 431-438.
[33] G.M. Sheldrick, *Acta Cryst. C* 2015, 71, 3-8.

CHAPTER 6

Cobalt Complexes of Pyridine-Amide Functionalized Carbene Ligands as Electrocatalysts for HER

*Two pyridyl-amide substituted imidazolium salts H_2**L1**Cl and H_2**L2**Cl were synthesized and successfully employed as ligand precursors for the syntheses of novel cobalt(III) complexes [Co(**L1**)$_2$]Cl and [Co(**L2**)$_2$]Cl bearing chelating N-heterocyclic carbene (NHC) ligands. The crystal structure determination of [Co(**L1**)$_2$]PF_6 and [Co(**L2**)$_2$]Cl revealed that the central cobalt ions in both complexes are bound by two ligands binding in a meridional tridentate mode, with two dangling benzyl groups in the first compound and pyridine groups in the latter. The reversible redox properties of the two compounds were investigated using cyclic voltammetry. In dimethylformamide in presence of acetic acid the two compounds show electrocatalytic activity in proton reduction as confirmed by cyclic voltammetry and quantified with gas chromatography. Compound [Co(**L2**)$_2$]Cl equipped with two uncoordinated pyridine groups that can act as proton relay, shows higher electrocatalytic activity in HER compared with [Co(**L1**)$_2$]Cl, though a total turnover of 1.5 in 2h is barely to be announced as efficient catalyst for HER. Nevertheless, the neat compound synthesis method and good stability of the compounds in acid might be a merit.*

This chapter will be published: S. Luo, M.A. Siegler, and E. Bouwman, manuscript in preparation

6.1 Introduction

The design of molecular electrocatalysts for the hydrogen evolution reaction (HER) is one of the important research topics of the last decade. In 2007, DuBois's research group reported a class of nickel complexes comprising chelating phosphane ligands with pendant nitrogen bases showing excellent electrocatalytic activity for the hydrogen evolving reaction (HER).[1] Since then, the development of functional models for the active site of hydrogenases to be applied as electrocatalysts for the HER has been receiving increasing attention. Apart from the aforementioned Ni-diphosphane catalysts, a number of other new classes of electrocatalysts with outstanding activity in the HER have been reported, i.e. the cobaloxime catalysts,[2, 3] and polypyridyl-based catalyst with first row transition metals, e.g. Co, Cu, Ni and Fe.[4-7] Cobalt as one of the inexpensive transition metals, receives considerable attention in the design molecular catalyst.[2-5] N-heterocyclic carbene (NHC) ligands have been extensively studied in transition metal coordination chemistry with applications in homogeneous catalysis,[8, 9] but so far this kind of strong σ donor ligands has not been widely used to design electrocatalysts for the HER. In recent years only a few Co-NHC complexes have been reported as electrocatalysts for the HER.[10, 11]

In this chapter, the synthesis and characterization is reported of two new cobalt(III)-NHC complexes, which show electrocatalytic activity in the HER in dimethylformamide using acetic acid as the proton source. Their catalytic activity is compared with the related Ni-NHC complexes that are discussed in Chapter 5, with the aim to study the influence of different transition metal ions on the redox potentials and catalytic activity in the HER.

6.2 Results and Discussion

6.2.1 Synthesis of the complexes

The new Co-NHC compounds $[Co(\mathbf{L1})_2]Cl$ and $[Co(\mathbf{L2})_2]Cl$ were prepared by reacting the ligand precursors[12] with anhydrous cobalt(II) acetate in acetonitrile or DMF in the presence of K_2CO_3. The following workup procedure was done in an air atmosphere, and the compounds were obtained as brown solids in a yield of 25% and 30%, respectively (Figure 6.1). Attempts were undertaken to synthesize complexes with a 1:1 metal-to-ligand ratio by varying the ratios of the starting materials. However, only the $[Co(\mathbf{Lx})_2]Cl$ type complexes were obtained, which were characterized with X-ray diffraction and mass spectrometry. Although a cobalt(II) salt was used in the complex synthesis, the formation of cobalt(III) complexes was apparent by the diamagnetic ^1H NMR spectra of the obtained compounds (Figure AVI.1). The ESI-MS spectra of both cobalt complexes exhibit base peaks corresponding to the $[M - Cl]^+$ cations (Figure AVI.2).

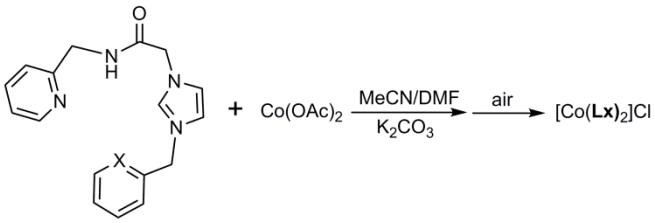

*Figure 6.1. Synthetic route of the complexes [Co(**L1**)$_2$]Cl and [Co(**L2**)$_2$]Cl.*

6.2.2 Structural characterization of the complexes

It appeared to be difficult to obtain single crystals suitable for X-ray structure determination. Needle-shaped single crystals of [Co(**L2**)$_2$]Cl were obtained from DCM; however, the counter ion appeared to be extremely disordered, making the crystallographic refinement unsatisfactory. Block-shaped crystals were obtained from a mixture of MeCN/H_2O, but the crystal that was mounted on the diffractometer appeared not to be a single crystal, but rather a composite of two crystals related by a rotation. Fortunately the diffraction data obtained with this crystal are satisfactory for crystallographic refinement. The crystallographic and refinement data are provided in Table AVI.1. For complex [Co(**L1**)$_2$]Cl it also appeared difficult to obtain single crystals. Thus, anion exchange was performed by adding a solution of the complex [Co(**L1**)$_2$]Cl in acetonitrile to a boiling acetonitrile solution of NH_4PF_6. Orange-colored, block-shaped crystals were obtained within one week; unfortunately, again part of the PF_6^- anion as well as co-crystallized solvent molecules appeared to be severely disordered. It is assumed that the flexible benzyl arm in [Co(**L1**)$_2$]Cl hampers crystallization of this compound. Similar problems have been reported for the structures of a number of Co^{III}-NHC complexes because of the disorder of counter ions.[10, 13] The general structure of the cationic complex in [Co(**L1**)$_2$]Cl could be reliably determined from the difference Fourier maps. Projections of the [Co(**L1**)$_2$]$^+$ and [Co(**L2**)$_2$]$^+$ cations are shown in Figure AVI.3 and Figure 6.2, respectively. Selected bond distances and angles are provided in Table AVI.2.

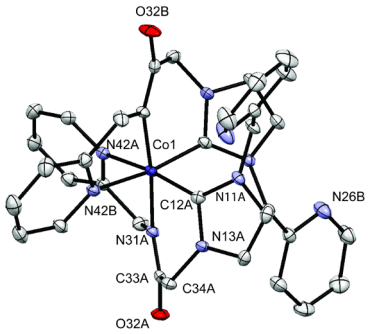

*Figure 6.2. Displacement ellipsoid plots of the cationic complex in [Co(**L2**)$_2$]Cl, drawn at 50% probability level with selected atom numbering. For clarity the hydrogen atoms, chloride ion and the lattice water molecules are omitted.*

The projection of $[Co(\mathbf{L1})_2]PF_6$ reveals that the central cobalt ion is coordinated by two ligands bound in a tridentate fashion. The meridional binding of the ligand is largely dictated by the sp^2 hybridization of the amide nitrogen atom. The Co–C and Co–N bond lengths are slightly longer than the related distances found in the nickel compounds described in Chapter 5. The Co–C bond lengths are similar to those in reported Co-carbene complexes.[13-18] $[Co(\mathbf{L2})_2]Cl$ presents a similar coordination sphere for the central cobalt ion as in $[Co(\mathbf{L1})_2]PF_6$, with two uncoordinated methylpyridine groups instead of benzyl groups.

6.2.3 Electrochemical properties of the complexes

The electrochemical properties of the two complexes have been investigated using cyclic voltammetry (CV) in DMF solutions. For the complex $[Co(\mathbf{L1})_2]Cl$, two reversible redox couples appeared with $E_{1/2}$ at −1.19 V and −1.84 V vs. Ag/AgCl. Similarly, for complex $[Co(\mathbf{L2})_2]Cl$ two redox waves were found at approximately the same potentials (Figure 6.3, Table 6.1). In addition, in the voltammogram of $[Co(\mathbf{L2})_2]Cl$ two small irreversible reductive waves were found at −1.66 V and −2.00 V. As the CVs of the ligand precursors do not show redox activity at these potentials (see Appendix VI, Figure AVI.5), it is assumed that the two reversible or quasi-reversible events are metal-centered. Thus, these two processes are tentatively assigned to the Co^{III}/Co^{II}, and Co^{II}/Co^{I} redox couples. Depending on the coordinating ligands and coordination geometry, the Co^{III}/Co^{II} and Co^{II}/Co^{I} redox potentials can be largely different, ranging from 1.40 V to −0.83 V for Co^{III}/Co^{II} and −0.23 V to −1.38 for Co^{II}/Co^{I} vs. Ag/AgCl.[10, 11, 14] The redox potentials of the cobalt(III) compounds reported in this Chapter appear to be more negative by nearly 0.5 V comparing to the potentials in literatures,[10, 11, 14] most likely because of the highly electron-donating nature of the carbene ligands.

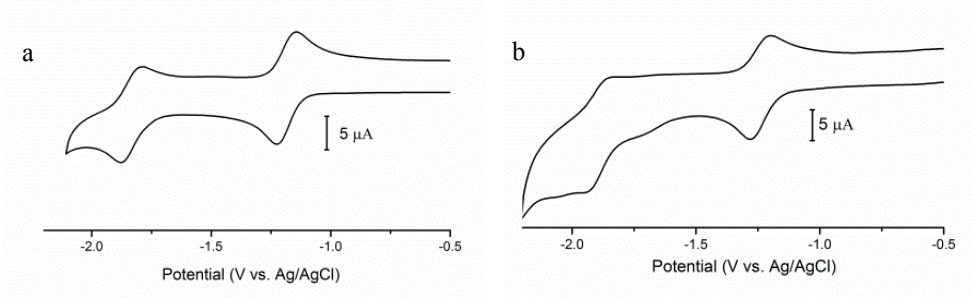

Figure 6.3. CVs of 1 mM (a) complex $[Co(\mathbf{L1})_2]Cl$ and (b) $[Co(\mathbf{L2})_2]Cl$ in DMF containing 0.1 M TBAP as electrolyte at scan rate 0.1 V/s, using glassy carbon working electrode.

Table 6.1. Electrochemical data of the cobalt compounds.[a]

	E_{pc1} [V]	E_{pa1} [V]	$E_{1/2}$ [V] (ΔE_p [mV])	E_{pc2} [V]	E_{pa2} [V]	$E_{1/2}$ [V] (ΔE_p [mV])
$[Co(\mathbf{L1})_2]Cl$	−1.23	−1.14	−1.19 (90)	−1.88	−1.79	−1.84 (90)
$[Co(\mathbf{L2})_2]Cl$	−1.24	−1.16	−1.20 (80)	−1.89	−1.81	−1.85 (80)

[a] All voltammograms were recorded in DMF; the potentials are referenced to the Ag/AgCl couple. Conditions: scan rate = 0.1 V/s, compound (1 mM), TBAP (0.1 M), glassy carbon working electrode.

6.2.4 Proton reduction activity of the complexes

For both compounds the electrocatalytic activity was determined for the HER in DMF, using acetic acid as the proton source. In the presence of low acid concentrations (10 eq acid) using complex [Co(**L1**)$_2$]Cl, two irreversible reductive peaks were found at −1.17 and −1.32 V, followed by an obvious catalytic wave at −1.81 V vs Ag/AgCl. The voltammogram of complex [Co(**L2**)$_2$]Cl showed a similar result, showing two irreversible reduction peaks at −1.16 and −1.45 V, followed by a catalytic wave at −1.78 V (Figure 6.4). The first reductive event occurred at slightly more positive potentials than the Co^{III}/Co^{II} reductive event in the absence of acid. A new reduction process seems to be present at a potential that is much more positive than the reductive wave ascribed to the Co^{II}/Co^{I} couple that in the absence of acid is located around −1.8 V.

The CV of a solution of the acid in DMF in the absence of catalyst, the CV of the ligand precursor H_2**L2**Cl in the presence of acid, and the CV of the complex [Co(**L2**)$_2$]Cl are compared in Figure 6.5. The CV of pure acid does not show a significant catalytic current and the CV of the ligand precursor H_2**L2**Cl shows a small reductive wave (discussed in detail in appendix VI). Thus the catalytic current found in the presence of the coordination compound must be related to the cobalt redox couple.

The voltammograms that were obtained for complex [Co(**L2**)$_2$]Cl in varying concentrations of acid are shown in Figure 6.6. The catalytic current increased with increasing concentrations of the acid, and the onset potential of the catalytic peak gradually shifts to more positive potentials. This shift in onset potential indicates that a proton-coupled electron transfer (PCET) process is operative.[7, 19]

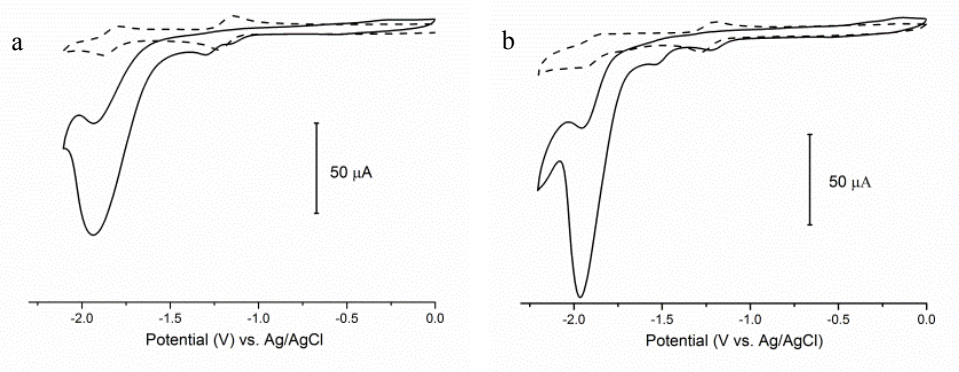

*Figure 6.4. CVs of 1 mM complex [Co(**L1**)$_2$]Cl (a) and [Co(**L2**)$_2$]Cl (b) in absence (dashed line) and in presence (solid line) of 10 mM acetic acid in DMF containing 0.1 M TBAP as electrolyte at scan rate 0.1 V/s, using glassy carbon working electrode.*

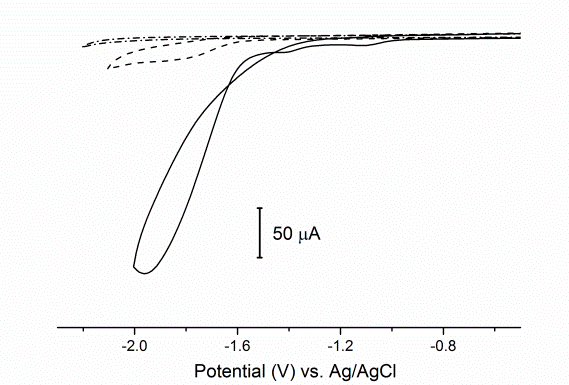

*Figure 6.5. CVs of 30 mM acetic acid (dash-dotted line), 1 mM H_2**L2**Cl in presence of 30 mM acetic acid (dashed line) and 1 mM [Co(**L2**)$_2$]Cl in presence of 30 mM acetic acid (solid line) in DMF containing 0.1 M TBAP as electrolyte at scan rate 0.1 V/s, using glassy-carbon working electrode.*

Plots of i_c/i_p as a function of the square root of the acid concentration are shown in Figure 6.7. A large catalytic current (i_c/i_p = 28 for [Co(**L1**)$_2$]Cl and i_c/i_p = 62 for [Co(**L2**)$_2$]Cl) was observed at 70 eq acid concentration at a scan rate of 0.1 V/s with an overpotential of 940 mV for [Co(**L1**)$_2$]Cl and 830 mV for [Co(**L2**)$_2$]Cl. The complex [Co(**L2**)$_2$]Cl shows asmaller overpotential largely due to the PCET process. For both [Co(**L1**)$_2$]Cl and [Co(**L2**)$_2$]Cl the plot of i_c/i_p show a linear relationship with the square root of acid concentration (Figure 6.7). It indicates the reaction is first-order with respect to acid concentration. Thus, for [Co(**L1**)$_2$]Cl we can use the equation (5) and (6) which show in Chapter 5 to calculate a rate constant k_{obs} of 160 s^{-1} in presence of 70 mM acid at a scan rate of 0.1 V/s. From the plots of k_{obs} versus $[H]^+$, the second-order rate constant was determined to be 2400 M^{-1} s^{-1} (Figure 6.8). Using the same method, for [Co(**L2**)$_2$]Cl we obtained higher rate constant 10500 M^{-1} s^{-1}.

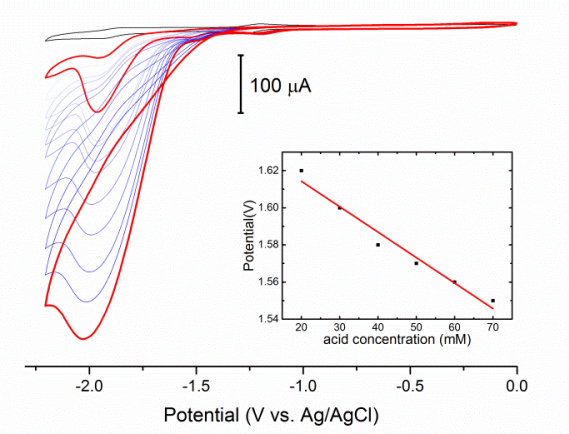

*Figure 6.6. CVs of 1 mM complex [Co(**L2**)$_2$]Cl in presence of various acid concentrations (0 − 70 mM). in DMF containing 0.1 M TBAP as electrolyte. Inset: plot of onset potentials as a function of acid concentration (R^2 = 0.96). Conditions: Scan rate = 0.1 V/s, TBAP (0.1 M), glassy-carbon working electrode.*

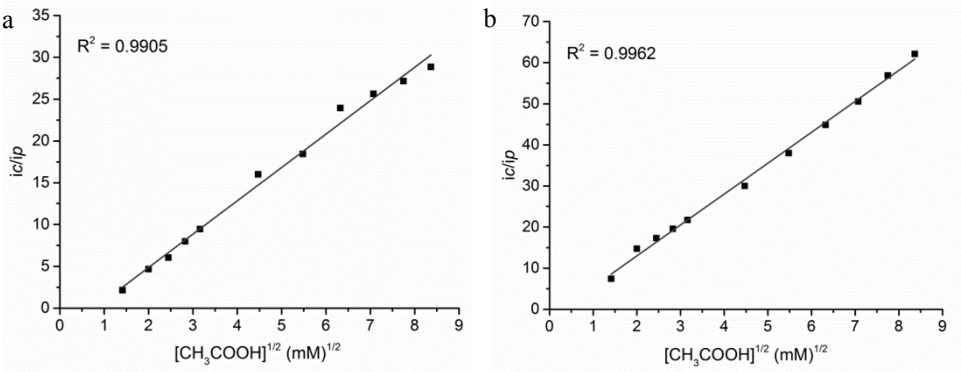

Figure 6.7. Plots of i_c/i_p vs. $[CH_3COOH]^{1/2}$ $(mM)^{1/2}$ for 1 mM $[Co(\mathbf{L1})_2]Cl$ (a) and 1 mM $[Co(\mathbf{L2})_2]Cl$ (b) in presence of various acid concentration in DMF containing 0.1 M TBAP as supporting electrode at 0.1 V/s, using glassy carbon working electrode.

The controlled potential electrolysis (CPE) experiments were carried out to determine which of the two complexes is more active as a electrocatalyst for HER. Hydrogen production was confirmed and quantified using gas chromatography (GC) following CPE at −1.8 V. The faradaic efficiencies were determined to be 77% for $[Co(\mathbf{L1})_2]Cl$ and 82% for $[Co(\mathbf{L2})_2]Cl$. After subtracting the blank (volume of H_2 produced in absence of catalyst, for data treatment see Appendix I) it was deduced that 75 µL and 145 µL H_2 were generated in presence of 1 mM $[Co(\mathbf{L1})_2]Cl$ and $[Co(\mathbf{L2})_2]Cl$, respectively, over 2 h electrolysis, corresponding to 0.6 and 1.2 mol H_2 per mol of catalyst. Although the activity still is rather low, the compound $[Co(\mathbf{L2})_2]Cl$, equipped with free pyridine arms, gave a twice higher catalytic activity in the HER in the same conditions.

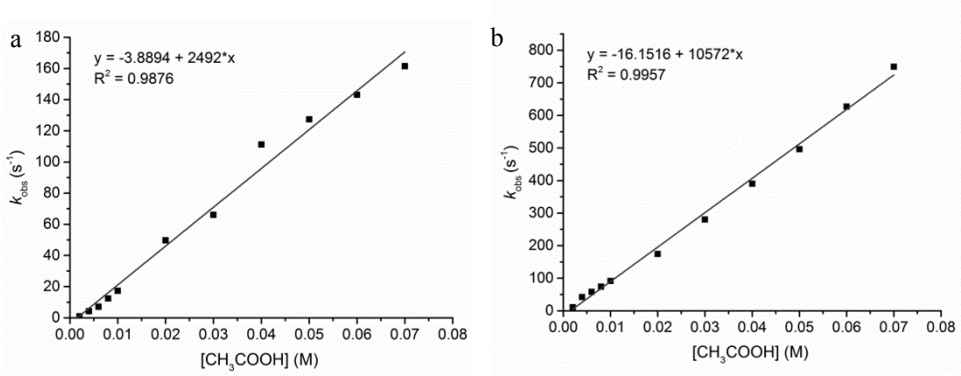

Figure 6.8. Plot of k_{obs} vs. $[CH_3COOH]$ (M) for (a) 1mM $[Co(\mathbf{L1})_2]Cl$ and (b) 1mM $[Co(\mathbf{L1})_2]Cl$ in presence of various acid concentration in DMF containing 0.1 M TBAP as supporting electrode at 0.1 V/s, using glassy carbon working electrode.

6.2.5 Stability of the compounds in acid

In order to investigate how the complexes might interact with protons in electrocatalysis, excess acetic acid-d_4 was added to the complex $[Co(\mathbf{L1})_2]Cl$ or $[Co(\mathbf{L2})_2]Cl$ in acetonitrile-

d_3 (Figure 6.9 and Figure AVI.7). The NMR spectra of [Co(**L1**)$_2$]Cl showed the resonances of the alkyl protons to shift downfield in presence of acid, especially the protons adjacent to the amide (Figure 6.9). The shifts of these alkyl protons are tentatively ascribed to the formation of hydrogen bonds between the amide oxygen and the acid. For complex [Co(**L2**)$_2$]Cl, which equips two free pyridine group, the resonances of alkyl protons were also largely shift down field in presence of acid (Figure AVI.7). It is not only due to the hydrogen bond formation but also due to the protonation of the free pyridine group. The protonation can be confirmed by the EI-MS spectrum of the NMR sample (Figure AVI.8). We found peaks at m/z = 337.5 and 674.7, which assign to [Co(**L2**D)$_2$]$^{2+}$ and [Co(**L2**)(**L2**D)]$^+$ fragments. Meanwhile, no extra peaks appeared upon addition of an excess of acid, indicating both complexes are stable in acidic organic solutions.

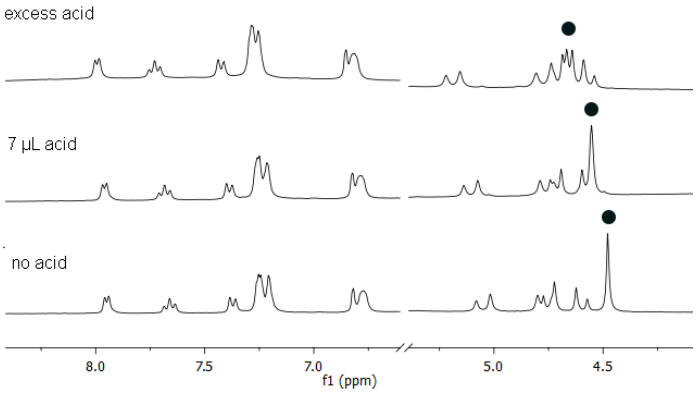

*Figure 6.9. ^{1}H NMR spectra of [Co(**L1**)$_2$]Cl in acetonitrile-d_3 in absence or presence of acetic acid. The black dots refer to the chemical shift of the CH2 between carbene and amide.*

6.3 Conclusion

In this Chapter, the two new cobalt-NHC complexes [Co(**L1**)$_2$]Cl and [Co(**L2**)$_2$]Cl were synthesized. In both octahedral Co^{III} compounds the ligands are coordinated in a meridional tridentate fashion. Although the ligand H$_2$**L2**Cl in combination with Ni^{II} ions forms square-planar coordination compounds with the binding of only one ligand in Chapter 5, we were unable to obtain cobalt compounds with only one ligand coordinated. The strong ligand-field splitting caused by the carbene and amide donor atoms apparently stabilizes a low-spin cobalt(III) compound in an octahedral geometry. More sterically hindering groups should be employed as pendant groups to be able to generate a cobalt(II) compound in a square-planar or 5-coordinate geometry.

Cyclic voltammetry of the two Co-NHC complexes revealed that indeed it is difficult to reduce the Co^{III} center (quite negative Co^{III}/Co^{II} and Co^{II}/Co^{I} redox potentials), which is in agreement with the large ligand-field splitting. The saturated coordination sphere of the cobalt(III) ion in principle makes it difficult to form the cobalt hydride intermediate that is essential in the catalytic proton reduction reaction. However, still both complexes show

electrocatalytic activity in HER using acetic acid as the proton source in dimethylformamide. Large catalytic currents (i_c/i_p = 28 for [Co(**L1**)$_2$]Cl and i_c/i_p = 62 for [Co(**L2**)$_2$]Cl) are observed in the presence of 70 eq acid and at a scan rate of 0.1 V/s with an overpotential of 910 mV for [Co(**L1**)$_2$]Cl and 790 mV for [Co(**L2**)$_2$]Cl. The complex [Co(**L2**)$_2$]Cl shows a smaller overpotential and higher catalytic activity largely due to the PCET process that most likely is facilitated by the presence of free pyridine groups.

6.4 Experimental

6.4.1 Materials

Commercial chemicals were used without further purification. Acetonitrile, tetrahydrofuran, dichloromethane and diethyl ether were obtained from a PureSolv MD5 solvent dispenser. Dry ethanol and dimethylformamide were prepared by adding molecular sieves into commercial anhydrous solvent. The rest commercial solvents were used without further purification. The ligand H_2**L1**Cl was synthesized following a literature method,[12] and the synthesis of the ligand H_2**L2**Cl is described in Chapter 5.

6.4.2 Analytical methods

^{1}H and ^{13}C NMR spectra were recorded on a Bruker 300DPX spectrometer. Mass spectra were obtained using a Finnigan Aqueous Mass Spectrometer (MS) with electro spray ionization (ESI). Cyclic voltammetry was recorded with an Autolab PGstat10 potentiostat controlled by GPES4 software under argon. A 3 mm diameter glassy carbon electrode was used as working electrode and plantium as the counter electrode. The experimental reference electrode was a commercially available Ag/AgCl (E^o = 0.210 V vs. NHE) electrode. Ferrocene was added at the end of each measurement as an internal standard when experiments were carried out in organic solvents; using our conditions the $E_{1/2}$ for the Fc/Fc^+ couple was located at 0.52 V vs. Ag/AgCl, with a ΔE of 90 ~ 110 mV.

Controlled-potential electrolysis (CPE) experiments were carried out in an H-shaped double-compartment cell. A glassy carbon electrode plate with a surface area of 0.07 cm^2 was used as the working electrode for electrolysis. The auxiliary electrode was a platinum gauze electrode. The reference electrode was a commercially available aqueous Ag/AgCl electrode. The sample was bubbled with helium gas for 10 min before measurements and the electrolysis was carried out under helium atmosphere. The solutions in both compartments were constantly stirred during electrolysis experiments. Evolved H_2 gas during electrolysis experiments was quantified by gas chromatography, which was performed on a Shimadzu GC2010 at 35 ºC fitted with a Supelco Carboxen 1010 molecular sieve column. Two parallel experiments were done and the results of two experiments were averaged.

6.4.3 Single crystal X-ray crystallography

For [Co(**L2**)$_2$]Cl, all reflection intensities were measured at 110(2) K using a SuperNova diffractometer (equipped with Atlas detector) with Mo Kα radiation (λ = 0.71073 Å) under the program CrysAlisPro (Version CrysAlisPro 1.171.39.29c, Rigaku OD, 2017). The same program was used to refine the cell dimensions and for data reduction. The structure was solved with the program SHELXS-2014/7 (Sheldrick, 2015) and was refined on F^2 with SHELXL-2014/7 (Sheldrick, 2015).[20] Numerical absorption correction based on gaussian integration over a multifaceted crystal model was applied using CrysAlisPro. The temperature of the data collection was controlled using the system Cryojet (manufactured by Oxford Instruments). The H atoms were placed at calculated positions (unless otherwise specified) using the instructions AFIX 23 or AFIX 43 with isotropic displacement parameters having values 1.2 Ueq of the attached C atoms. The H atoms attached to O1W/O2W/O3W were found from difference Fourier maps (the locations of the H atoms attached to O2W are probably not very accurate as the H atoms might be disordered), and their coordinates were refined freely (the O─H and H…H bond distances were restrained to be 0.84(3) and 1.33(3) Å using the DFIX instruction). The structure is partly disordered.

The fragment N31B-C33B-O32B-C34B-N13B is disordered over two orientations. The occupancy factors of the major component of the disorder refines to 0.519(9). The lattice water molecule O3W has an occupancy factor of 0.5 as it is found on an inversion center.

The crystal that was mounted on the diffractometer was not a single crystal, but rather a composite of two crystals related by a rotation of ca. 1.9° around the reciprocal direction [−0.02 1.00 0.07]. The BASF scale factor refines for 0.0366(18).

For [Co(**L1**)$_2$]PF_6, only the structure of the cations complex could be determined. The counter ions are severely disordered hampering full refinement of the structure.

6.4.4 Complex synthesis

[Co(**L1**)$_2$]Cl:
A Schlenk flask was charged with commercially available anhydrous cobalt(II) acetate (0.35 mmol, 0.06 g), H_2**L1**Cl (0.7 mmol, 0.17 g), K_2CO_3 (2.68 mmol, 0.37 g) and dry DMF (10 mL) under an N_2 atmosphere. The dark brown solution was stirred at room temperature for 2 days. The reaction mixture was filtered to remove the insoluble products and the filtrate was added dropwise into 100 ml diethyl ether. The formed yellow-brown solid was collected by filtration and redissolved in anhydrous acetonitrile. This solution was passed through a short celite column. The solution was concentrated to around 2 mL, and then was added dropwise into diethylether to result in a light brown solid. Single crystals of [Co(**L1**)$_2$]PF_6 for X-ray determination were obtained from anion exchange. The anion exchange was performed by adding a solution of the complex [Co(**L1**)$_2$]Cl in acetonitrile to a boiling acetonitrile solution of NH_4PF_6. Yield: 25% (60 mg). ^{1}H NMR (400 MHz, acetonitrile-d_3) δ 7.95 (d, J = 5.5 Hz, 2H, Py-*H*), 7.66 (td, J = 7.7, 1.4 Hz, 2H, Py-*H*), 7.38 (d, J = 7.8 Hz, 2H, Py-*H*), 7.29 – 7.24 (m, 6H, Ar-*H*), 7.22 (d, J = 7.22 Hz, 2H, Py-*H*), 7.20

(d, J = 5.5 Hz, 2H, $C_{imidazole}$-*H*), 6.82 (d, J = 2.0 Hz, 2H, $C_{imidazole}$-*H*), 6.78 (dd, J = 5.5, 3.7 Hz, 4H, Ar-*H)*, 5.05 (d, J = 19.1 Hz, 2H, Ar-CH*H*-$N_{imidazole}$), 4.77 (d, J = 19.6 Hz, 2H, Ar-CH*H*-$N_{imidazole}$), 4.75 (d, J = 15.2 Hz, 2H, Py-CH*H*-N_{Amide}), 4.60 (d, J = 15.2 Hz, 2H, Py-CH*H*-N_{Amide}), 4.48 (s, 4H, C(O)-CH_2-$N_{imidazole}$). ^{13}C NMR (101 MHz, acetonitrile-d_3) δ = 212.58, 208.75, 208.63, 208.65, 149.67, 139.95, 129.86, 129.16, 128.48, 125.76, 125.51, 125.15, 122.85, 56.02, 55.99, 52.41. ESI-MS found (calculated): $[M–Cl]^+$ *m/z* 669.3 (669.21).

$[Co(\mathbf{L2})_2]Cl$:
A Schlenk flask was charged with anhydrous cobalt(II) acetate (0.85 mmol, 0.15 g), H_2**L2**Cl (0.85 mmol, 0.29 g), K_2CO_3 (3.4 mmol, 0.47 g) and dry CH_3CN (10 mL) under an N_2 atmosphere. To this mixture 2 mL DMF was added. The dark brown suspension was stirred at room temperature for 2 days. The reaction mixture was filtered to remove the insoluble products, and the filtrate was added dropwise into 100 ml diethyl ether. The yellow-brown solid was collected by filtration, redissolved in anhydrous acetonitrile and passed through a short celite column. The solution was concentrated to around 2 mL, and added dropwise into diethyl ether to result in a light brown solid. Single crystals of $[Co(\mathbf{L2})_2]Cl$ for X-ray determination were obtained from a DCM solution of complex in 3 days. Yield: 30% (90 mg). ^{1}H NMR (300 MHz, acetonitrile-d_3) δ 8.42 (dd, J = 17.9, 4.8 Hz, 2H, Py-*H*), 7.90 (d, J = 5.7 Hz, 2H, Py-*H*), 7.76 – 7.62 (m, 4H, Py-*H*), 7.43 (d, J = 7.8 Hz, 2H, Py-*H*), 7.20 (q, J = 7.0 Hz, 4H, Py-*H*), 7.12 (d, J = 1.8 Hz, 2H, $C_{imidazole}$-*H*), 7.02 (d, J = 7.8 Hz, 2H, Py-*H*), 6.87 (d, J = 2.0 Hz, 2H, $C_{imidazole}$-*H*), 5.30 (d, J = 18.8 Hz, 2H, Py-CH*H*-N_{NHC}), 4.98 (d, J = 15.8 Hz, 2H, Py-CH*H*-N_{Amide}), 4.79 (d, J = 15.8 Hz, 2H, Py-C*H*H-N_{Amide}), 4.65 – 4.46 (m, 4H, C(O)-C*H*H-N_{NHC}, Py-C*H*H-$N_{imidazole}$), 4.37 (d, J = 17.0 Hz, 2H, C(O)-CH*H*-$N_{imidazole}$). ^{13}C NMR (75 MHz, acetonitrile-d_3) δ = 170.07, 164.36, 155.26, 150.38, 149.18, 139.87, 138.05, 126.39, 125.26, 124.82, 124.00, 123.26, 122.70, 55.92, 55.78, 53.28. ESI-MS found (calculated): $[M–Cl]^+$ *m/z* 671.1 (671.2).

6.5 Acknowledgements

S. Luo gratefully acknowledges a grant from the Chinese Scholarship Council (no. 201306410011). We thank Mr. J.M.M van Brussel for ESI-MS measurements.

6.6 References

[1] A.D. Wilson, R.K. Shoemaker, A. Miedaner, J.T. Muckerman, D.L. DuBois, M.R. DuBois, *Proc. Natl. Acad. Sci. U. S. A.* 2007, 104, 6951-6956.

[2] J.L. Dempsey, B.S. Brunschwig, J.R. Winkler, H.B. Gray, *Acc. Chem. Res.* 2009, 42, 1995-2004.

[3] P.A. Jacques, V. Artero, J. Pecaut, M. Fontecave, *Proc. Natl. Acad. Sci. U. S. A.* 2009, 106, 20627-20632.

[4] W.K.C. Lo, C.E. Castillo, R. Gueret, J. Fortage, M. Rebarz, M. Sliwa, F. Thomas, C.J. McAdam, G.B. Jameson, D.A. McMorran, J.D. Crowley, M.-N. Collomb, A.G. Blackman, *Inorg. Chem.* 2016, 55, 4564-4581.

[5] P. Zhang, M. Wang, Y. Yang, T. Yao, L. Sun, *Angew. Chem. Int. Ed*. 2014, 53, 13803-13807.
[6] J.W. Jurss, R.S. Khnayzer, J.A. Panetier, K.A. El Roz, E.M. Nichols, M. Head-Gordon, J.R. Long, F.N. Castellano, C.J. Chang, *Chemical Science* 2015, 6, 4954-4972.
[7] P. Zhang, M. Wang, Y. Yang, D. Zheng, K. Han, L. Sun, *Chem. Commun.* 2014, 50, 14153-14156.
[8] M.C. Jahnke, T. Pape, F.E. Hahn, *Eur. J. Inorg. Chem.* 2009, 1960-1969.
[9] C. Fliedel, P. Braunstein, *J. Organomet. Chem.* 2014, 751, 286-300.
[10] K. Kawano, K. Yamauchi, K. Sakai, *Chem. Commun.* 2014, 50, 9872-9875.
[11] M. van der Meer, E. Glais, I. Siewert, B. Sarkar, *Angew. Chem. Int. Ed.* 2015, 54, 13792-13795.
[12] J.-Y. Lee, J.-Y. Lee, Y.-Y. Chang, C.-H. Hu, N.M. Wang, H.M. Lee, *Organometallics* 2015, 34, 4359-4368.
[13] Z. Xi, B. Liu, C. Lu, W. Chen, *Dalton Trans.* 2009, 7008-7014.
[14] Z. Mo, Y. Li, H.K. Lee, L. Deng, *Organometallics* 2011, 30, 4687-4694.
[15] F. Hering, J.H.J. Berthel, K. Lubitz, U.S.D. Paul, H. Schneider, M. Härterich, U. Radius, *Organometallics* 2016, 35, 2806-2821.
[16] A. Massard, P. Braunstein, A.A. Danopoulos, S. Choua, P. Rabu, *Organometallics* 2015, 34, 2429-2438.
[17] S. Dürr, D. Ertler, U. Radius, *Inorg. Chem.* 2012, 51, 3904-3909.
[18] S. Saha, M. Kaur, K. Singh, J.K. Bera, *J. Organomet. Chem.* 2016, 812, 87-94.
[19] R.M. Bullock, A.M. Appel, M.L. Helm, *Chem. Commun.* 2014, 50, 3125-3143.
[20] G.M. Sheldrick, *Acta Cryst. C* 2015, 71, 3-8.

CHAPTER 7

Summary, Conclusions &Outlook

7.1 Summary

7.1.1 Introduction

Dihydrogen gas is considered as one of the most attractive clean fuels, which produces only water when it is combusted in pure dioxygen.[1] The hydrogen evolution reaction (HER), the reaction in which protons are reduced into dihydrogen, is one of the most intensively studied reactions. The typical heterogeneous catalyst for HER is platinum; using platinum-based materials as working electrode in electrolytic cells H_2 can be produced efficiently.[2] However the downside is evident: platinum is a noble metal with limited reserves and consequently a relatively high price. In nature, hydrogenases can efficiently catalyze the transformation between protons and dihydrogen.[3] Inspired by the natural enzymes, many structural and functional models of the hydrogenases have been designed by chemists and some of these models have been found to be good electrocatalysts for HER.

N-Heterocyclic carbenes (NHCs) form a class of ligands that generally are regarded as useful ligands comparable with phosphanes for their use in homogeneous catalysts,[4, 5] but the electrocatalytic behavior of transition metal complexes bearing NHC ligands so far have been largely ignored. Nickel compounds with diphosphane ligands have been found to be effective catalysts for HER.[6] The aim of the research described in this thesis is to investigate the electrocatalytic properties of transition metal NHC compounds, in order to make a preliminary estimation on whether this class of complexes has the potential to generate a promising electrocatalyst based on inexpensive transition metals for efficient proton reduction in the near future.

In Chapter 1, the active sites of hydrogenases are briefly discussed, followed by a concise overview of well-studied structural models and functional models of hydrogenases as electrocatalysts for the hydrogen evolution reaction. Furthermore, a brief introduction is provided on transition metal NHC complexes and the electrochemical research reported for these compounds. Subsequently a general mechanism of metal-centered homogenous electrocatalysis for HER is discussed.

7.1.2 Electrocatalytic behavior of nickel complexes bearing thiolate-functionalized NHC ligands

In the design of structural and functional mimics for hydrogenases, a thiolate-bridged dinuclear structure seems to be essential. Therefore thiolate-functionalized carbene ligands were among the first candidates in our study. In Chapter 2, four sulfur-functionalized carbene ligands and their dinuclear nickel-NHC complexes are described. The four ligands differ by the alkyl chain length between the NHC and the thiolate group (two or three carbon atoms) and the second functionality at the NHC being a benzyl or a pyridylmethyl group. The nickel(II) ions are coordinated to the NHC carbon atom and bridged by the pendant thiolate groups. The benzyl-functionalized nickel-carbene compounds [**1**] and [**2**], revealed weak electrocatalytic activity for HER. However, it was found that the pyridyl-

functionalized compounds [**3**]Br_2 and [**4**]Br_2 show higher catalytic activity in HER than their benzyl-containing analogues. Unfortunately, the limited stability of solutions of the complexes [**3**]Br_2 and [**4**]Br_2 in presence of air and the rather low electrocatalytic efficiency of the compounds limit their potential application as proton reduction catalysts. Meanwhile, to generate understanding of the role of the thiolate and pyridine groups in the electrocatalytic cycle still requires further research.

7.1.3 Electrocatalytic behavior of nickel complexes bearing pyridine-functionalized NHC ligands

Based on the conclusion of the research described in Chapter 2, the research focus switched from thiolate-functionalized carbene ligands to pyridine-functionalized carbene ligands. (Chapter 3 to Chapter 5).

In Chapter 3, the synthesis is described of two bis-(benz)imidazolium salts alkylated with pyridyl side arms thus forming potentially tetradentate ligands, which were used as precursors in the synthesis of novel nickel compounds of N-heterocyclic carbenes (Ni-NHC). Four Ni-NHC complexes with different (imidazole-based or benzimidazole-based) carbene ligands and different counter ions (Br^- or PF_6^-) were isolated and characterized by various methods. The nickel ions in these mononuclear complexes are either in square-pyramidal or square-planar geometries. It was found that the use of imidazole-based carbenes results in more negative Ni^{II}/Ni^{I} and Ni^{I}/Ni^{0} redox couples. However, the nickel compounds with imidazole-based ligands revealed much higher activity in the electrocatalytic reduction of protons, as well as better acid tolerance. Furthermore, it was shown that the presence of halide ions results in more negative potentials for the Ni^{II}/Ni^{I} and Ni^{I}/Ni^{0} redox couples, and also leads to larger overpotentials for proton reduction. The imidazole-based complex with PF_6^- counter ions shows the highest catalytic efficiency (i_c/i_p = 50, k_{obs} = 490 s^{-1} at 0.1 V/s) of all complexes investigated for the catalytic proton reduction, using acetic acid in DMF, although the overpotential at which dihydrogen is produced is sizeable.

In Chapter 5, the synthesis is described of two pyridyl- and amide-functionalized substituted (benz)imidazolium salts, which were successfully employed as ligand precursors for the syntheses of novel nickel(II) complexes bearing tetradentate NHC ligands. Single crystal X-ray crystallography revealed that the nickel ions in both compounds are in slightly distorted square-planar geometries. Cyclic voltammetry of the two compounds showed irreversible reduction events, indicating that electron transfer is immediately followed by a fast chemical reaction or structural rearrangement. The nickel compounds were shown to be potential electrocatalysts for HER using cyclic voltammetry. The production of dihydrogen gas was confirmed using gas chromatography (GC) monitoring the controlled-potential electrolysis at −1.8 V vs. Ag/AgCl; the faradaic efficiency was determined to be around 85% for both complexes. In the presence of the imidazole-based and benzimidazole-based complexes 185 µL and 105 µL H_2 was generated, respectively, over 2 h electrolysis, corresponding to a mere 1.5 and 0.9 mol H_2 per mol of

catalyst. The imidazole-based compound not only shows higher activity in catalyzing HER, but is also active at a lower overpotential. This indicates that proton delivery between the ligand and the metal center is operative, which breaks the correlation between energy costs and kinetic barriers.

In Chapter 4, the synthesis and characterization is reported of two new nickel complexes of benzimidazole-based carbene ligands containing either one or two pyridyl groups per NHC and the study of their electrocatalytic activity in H_2 evolution. Single crystal X-ray crystallography revealed that the nickel ions in both compounds are in a square-planar geometry with like donor atoms of the two bidentate ligands in *cis* positions. The binding of two potentially tridentate ligands in this configuration in one of the nickel compounds results in the presence of two free pyridyl groups. The redox properties of the two complexes were determined using cyclic voltammetry. Electrocatalytic proton reduction experiments using these complexes were performed in DMF with acetic acid as the proton source. The compound containing two additional free pyridyl groups not only exhibits higher electrocatalytic activity, but also has a smaller overpotential for the reduction of protons. The comparison of these two similar structures provides convincing experimental evidence that the pyridyl group acts as proton relay during the proton reduction process.

7.1.4 Electrocatalytic behavior of cobalt compounds of pyridine-amide-functionalized carbene ligands

Whereas in Chapter 2 – 5 the research was focused on the synthesis and study of the electrocatalytic properties of nickel-NHC complexes, in the research described in Chapter 6, the attention was turned to cobalt-NHC complexes, as cobalt is also known to form active catalysts for HER. The imidazole-based tetradentate ligand described in Chapter 5 and a related tridentate ligand in which one of the pyridyl groups is replaced with a benzyl group were used to synthesise two cobalt-NHC compounds. In contrast to the square-planar geometry observed for the Ni-NHC compound of the tetradentate ligand, the cobalt ions in the Co-NHC complexes are in octahedral geometries by the coordination with two ligands binding in tridentate modes. Both Co(III) complexes display reversible redox couples in organic solution. The electrocatalytic behavior of the two cobalt compounds were investigated in DMF solutions, using acetic acid as proton source. Unfortunately, the Co^{III}/Co^{II} redox potential occurs at very negative potentials compared to that of reported compounds of pyridyl-functionalized carbene ligands.[7] The complex of the tetradentate ligand equipped with an additional pyridyl arm shows a smaller overpotential and higher catalytic activity for proton reduction (the slope of a plot of the k_{obs} vs $[H^+]$ giving an estimated rate constant of 10500 $M^{-1}s^{-1}$). Hydrogen production was confirmed and quantified using gas chromatography (GC) following CPE at −1.8 V vs. Ag/AgCl; in the presence of 1 mM of the benzyl-substituted or pyridine-substituted compound 75 μL and 145 μL H_2 was generated, respectively, over 2 h electrolysis, corresponding to 0.6 and 1.2 mol H_2 per mol of catalyst.

7.2 Conclusions & Outlook

Research related to the electrochemical and electrocatalytic properties of metal-NHC complexes has been largely neglected for several decades, despite the redox-innocent nature of the N-heterocyclic carbene ligands and their successful application in homogeneous catalysis. With the design and development of functionalized carbene ligands, the ligand can take part in the catalytic reaction. In this thesis, our investigations are described of the possibility to use metal-NHC complexes as electrocatalysts for the proton reduction reaction. Criteria for potential electrocatalysts are the ease of preparation, the stability of the compounds in (aqueous) solutions, the overpotential at which proton reduction is catalyzed, the activity of the compounds in terms of dihydrogen production and lifetime.

A number of different nickel(II) complexes and two cobalt(III) compounds of functionalized NHC ligands are reported in this thesis. The mononuclear nickel(II) and cobalt(III) complexes are quite stable in air as well as moist atmospheres, and thus are easy to store and handle. The dimeric thiolate-pyridyl-containing complexes described in Chapter 2 are stable as solids, but are not stable in solutions containing dioxygen. All compounds show activity as potential electrocatalyst for HER, although their performance is far from comparable with the well-studied systems such as the nickel compound with diphosphane ligands[6] and cobaloxime systems.[8] Based on the results described in this thesis a number of conclusions and assumptions can be given.

It was found that generally the nickel compounds of imidazole-based NHC ligands show better catalytic activity for HER than the compounds with benzimidazole-based carbene ligands (Chapter 3 and 5). Thus, in future work, a search for NHC ligands with higher electron density may be recommended for the development of new efficient candidate electrocatalysts for HER. Nevertheless, as the carbene ligand is a strong electron donor, on one hand the use of more electron-donating carbene ligands will aid in the formation of the necessary metal-hydride intermediate, but on the other hand the presence of the electron-donating ligand will make it more difficult to reduce the metal center, resulting in larger overpotentials. Thus the search for a suitable NHC framework may be the first priority for future research.

Additionally, it has been shown that the presence of free pendant pyridine groups can greatly improve catalytic activity of the compounds (Chapter 4 and 6). These pyridine groups may act as proton relay in the catalytic cycle and accelerate proton delivery to the reduced metal center. However, in the synthesis of complexes with pyridine-functionalized carbene ligands, it is challenging to prevent coordination of the pyridine functionality to the metal center. In general, it is relatively difficult to form the metal-carbene bond, which requires relatively harsh experimental conditions. In contrast, the formation of metal-nitrogen bonds is much easier. Thus, if we want to obtain coordination compounds in which a free, non-coordinating pyridine is available as a proton relay, the preference of the metal

center for a certain geometry and the design of the ligands are important. In ligands described in this thesis, the carbene ligands are substituted with the 2-methylpyridyl group. Due to the chelating nature of the resulting ligands, the pyridine functionality readily coordinates with metal center (Chapter 2, 3 and 5). Only in the case that more donor atoms are available than the metal center is willing to accept, the additional pyridine may be left uncoordinated and available for protonation (Chapter 4, 6). Future modifications of this type of electrocatalysts may focus on the use of pyridyl substituents that are connected to the ligand via the 3 or 4 position; by doing so the chelating nature of the ligand is lost, effectively preventing the formation of a metal-nitrogen bond. During the course of the studies described in this thesis attempts have been undertaken to synthesize ligands functionalized with pyridine groups attached via the 3-position, but this appeared to be rather challenging, resulting in alkylation of the pyridine nitrogen atom. New synthesis routes need to be developed in order to create these novel ligands.

In Chapters 2 and 5, the relationship between acid concentration and the magnitude of the catalytic current (i_c/i_p) has been studied. Surprisingly, a linear relationship was observed, indicating that two protons are involved in the rate-determining step of the catalytic reaction using the catalysts described in these chapters. As the nickel compounds described in Chapters 2 and 5 do not have a free pyridine group to accept a proton, it may be postulated that in these catalyst the coordinating pyridyl group dissociates during catalytic turnover. Additional studies are necessary for a better understanding of the catalytic mechanism of these compounds.

Transition metal complexes of N-heterocyclic carbenes have been well studied in the last decades, and a vast amount of creative applications of such complexes as catalysts in various kinds of reactions have been explored. However, research on the electrocatalytic activity of metal-NHC complexes is limited and the results described in this thesis form just a start of a potentially emerging field. Using transition metal compounds of NHC ligands in electrocatalysis of a number of reactions can be attempted in the future, for example CO_2 reduction.[9, 10] The work described in this thesis has provided insight in electrochemistry of transition metal carbene complexes to take upon such new lines of potential application.

7.3 Reference

[1] P.D. Tran, J. Barber, *Phys. Chem. Chem. Phys.* 2012, 14, 13772-13784.
[2] A. Dey, *Inorg. Chem.* 2016, 55, 10831-10834.
[3] T.R. Simmons, G. Berggren, M. Bacchi, M. Fontecave, V. Artero, *Coord. Chem. Rev.* 2014, 270, 127-150.
[4] R.H. Crabtree, *J. Organomet. Chem.* 2005, 690, 5451-5457.
[5] J.-N. Luy, S.A. Hauser, A.B. Chaplin, R. Tonner, *Organometallics* 2015, 34, 5099-5112.
[6] D.L. DuBois, *Inorg. Chem.* 2014, 53, 3935-3960.
[7] K. Kawano, K. Yamauchi, K. Sakai, *Chem. Commun.* 2014, 50, 9872-9875.
[8] J.L. Dempsey, B.S. Brunschwig, J.R. Winkler, H.B. Gray, *Acc. Chem. Res.* 2009, 42, 1995-2004.

[9] V.S. Thoi, C.J. Chang, *Chem. Commun.* 2011, 47, 6578-6580.
[10] V.S. Thoi, N. Kornienko, C.G. Margarit, P. Yang, C.J. Chang, *J. Am. Chem. Soc.* 2013, 135, 14413-14424.

.

APPENDIX I

Setup used for the quantification of dihydrogen evolution
and equations for the determination of overpotentials

I.1. CPE-GC setup for the quantification of dihydrogen evolution

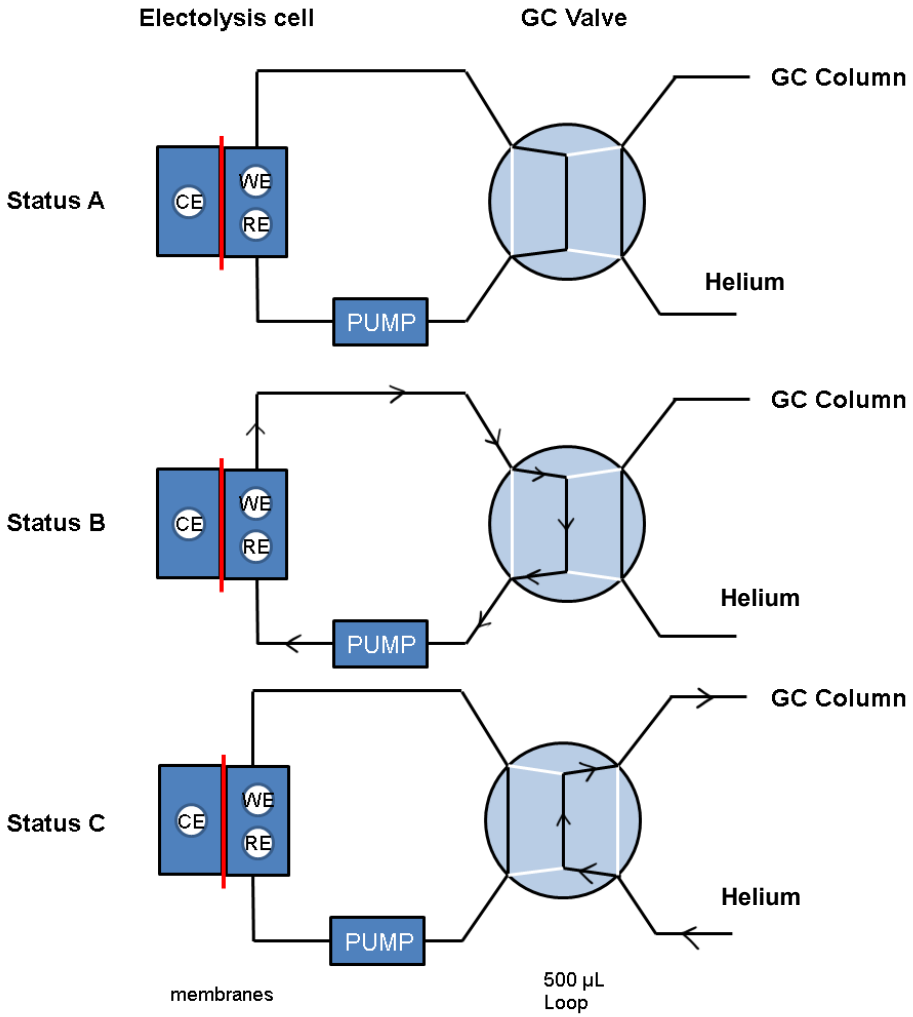

Figure AI.1. Schematic drawing of the CPE-GC setup for H_2 quantification. CE = counter electrode, WE = working electrode, RE = reference electrode; for explanation see text.

Dihydrogen evolution was measured using the setup schematically depicted in Figure AI.1. The whole setup mainly consists of three parts: the electrolysis cell, a GC valve and a GC column. The electrolysis cell is a two chamber cell separated by Nafion membranes. The counter electrode is placed in one chamber; the working electrode and reference electrode are placed in the other chamber. The chamber containing the working electrode is connected to the GC valve and contains a stir bar and 5 mL of the sample to be investigated. A pump is set between the electrochemical cell and the GC valve to circulate the helium

carrier gas. To ensure minimal leakage of air and gases, polyether ether ketone (PEEK) tubing was used for all connections between the cell, pump and GC valve.

I.2. Dihydrogen evolution measurements

Before starting the measurement, the headspace in the electrochemical cell was deaerated by pumping it around for 10 min under a constant flux of helium gas. The process of H_2 quantification can be divided into three steps: the electrolysis step, the loading step and the injection into the GC column. Firstly, the electrolysis cell is switched on and Controlled Potential Coulometry (CPC) is carried out at the selected potential (Figure AI.1 Status A). After the electrolysis experiment the potentiostat was switched off. Then the pump was turned on and the produced H_2 was delivered from the cell to a 500 μL loop (Figure AI.1 Status B). After that, the pump was switched off and the gas in the loop was delivered to a Shimadzu GC2010 fitted with a Supelco Carboxen 1010 molecular sieve column at 35 ºC using the GC valve (Figure AI.1 Status C). Helium is used as the carrier gas and the H_2 is detected using a TCD detector operated at 80 mA.

I.3. Determination of H_2 calibration line and example of dihydrogen quantification using the calibration line.

For the H_2 quantification experiments, a H_2 calibration line was made. The GC setup discussed in Section I.2 was used to make the H_2 calibration line. The electrochemical cell was fitted with the electrodes, stir bar and filled with 5 mL of the solvent. The use of an entirely identical cell setup ensures that the volume of the system is constant. Hamilton GASTIGHT® Syringes were used to take a certain volume (ranging from 40 to 800 μL) of pure H_2 which is then injected into the electrolysis cell. The gas in the cell is then measured in the GC setup following the procedure described in Section I.2. The H_2 calibration line used for the generation of the data described in this dissertation is shown in Figure AI.2. The function of the fit of the H_2 calibration line is:

$$V(H_2) = 0.01649 \times \text{Area} - 2.9941;$$

Taking compound [Ni(**L1**)]Cl in Chapter 5 as an example for the calculation: Compound [Ni(**L1**)]Cl (2 mg) and acetic acid (24 μL) were added into 5 mL DMF containing TBAP in a concentration of 0.1 M as supporting electrolyte to make a solution that contains 1 mM catalyst and 80 mM acid. The CPC potential was set to −1.8 V vs. Ag/AgCl. After 2 hours of electrolysis GC analysis resulted in a peak for H_2 with Area = 17230. Under the same conditions, for a solution containing the acid but in the absence of catalyst, the GC shows the Area(acid) = 6000. Thus, the volume of dihydrogen produced by the catalyst is:

$$V(H_2) = 0.01649 \times (17230 - 6000) - 2.9941 = 184.9\ \mu L$$

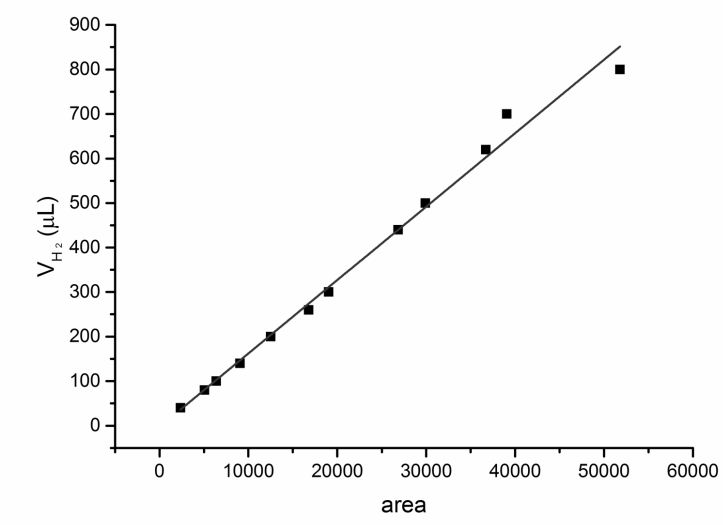

Figure AI.2. Calibration line for the quantification of H_2 using the GC setup.

I.4. Determination of the overpotential

The overpotential of a molecular electrocatalyst for H_2 production is the difference between the thermodynamic potential for the reduction of acid and the actual potential of the observed catalytic wave.[1] In this this dissertation, the half-wave potential is taken as a reference because it is both easier to obtain from the experiment and easier to compute theoretically:

$$\eta = E_{1/2}^{T} - E_{1/2}^{E} \quad (1)$$

In equation (1), $E_{1/2}^{E}$ is the experimental half-wave potential, which can be obtained from the potential of the maximum of the first derivative of the forward scan of stationary cyclic voltammograms and subtracting 15 mV.[2] $E_{1/2}^{T}$ is the thermodynamic standard potential computed in the case of an electrochemically reversible process taking into account the homoconjugation effect given by equation (2).[2]

$$E_{1/2}^{T} = E_{\mathrm{H^+/H_2}}^{\circ} - \frac{2.303 \times RT}{F} \mathrm{p}K_a + \varepsilon_D - \frac{RT}{2F} \ln \frac{C_0}{C_{\mathrm{H_2}}^{\circ}} \qquad (2)$$

In equation 2, F is Faraday's constant, T is 295 K, R is the universal gas constant, C_0 is the total concentration of acid. $C_{\mathrm{H_2}}^{\circ}$ is the concentration of dissolved dihydrogen corresponding to a partial pressure of 10^5 Pa. ε_D is a measure of the diffusion rate of the products with respect to that of reactant. The values of the physical-chemical constants ($E_{\mathrm{H^+/H_2}}^{\circ}$, $C_{\mathrm{H_2}}^{\circ}$ and ε_D) were taken from the literature.[2]

Taking compound [Ni(**L1**)]Cl in Chapter 5 as an example for the calculation: In DMF solution, $E^{\circ}_{\mathrm{H^+/H_2}} = -0.62\ V$ vs. $Fc^{+/0}$, $C^{\circ}_{\mathrm{H_2}} = 1.9\ mM$, $\varepsilon_D = 0.04\ V$, and p*K*a of acetic acid in DMF solution is 13.5, the acid concentration C_0 = 80 mM, which gives the value of $E^T_{1/2}$:

$$E^T_{1/2} = -0.62 - \frac{2.303 \times 8.314 \times 295}{96500} \times 13.5 + 0.04 - \frac{8.314 \times 295}{2 \times 96500} \ln \frac{80}{1.9} = -1.419\ \mathrm{V}$$

From the cyclic voltammetry of [Ni(**L1**)]Cl in presence of 80 mM acetic acid, the experimental half wave potential is obtained: $E^E_{1/2} = -2.345\ V$ vs. $Fc^{+/0}$.

Thus the overpotential is obtained: $\eta = E^T_{1/2} - E^E_{1/2} = 0.93\ \mathrm{V}$

I.5. Other equations used in this thesis

$$n(H_2)(\mathrm{mol}) = \frac{V(H_2)}{V_m}$$

$$N = \frac{Q\ (\mathrm{C})}{1.6 \times 10^{-19}(\mathrm{C})}$$

$$n(H_2)(\mathrm{mol}) = \frac{N}{N_A} \times \frac{1}{2}$$

Avogadro constant $N_A = 6.02 \times 10^{23}$, molar volume V_m = 24.465 L/mol.

References:

[1] R.M. Bullock, A.M. Appel, M.L. Helm, *Chem. Commun.* 2014, 50, 3125-3143.

[2] V. Fourmond, P.-A. Jacques, M. Fontecave, V. Artero, *Inorg. Chem.* 2010, 49, 10338-10347.

APPENDIX II

Supplementary information on Chapter 2

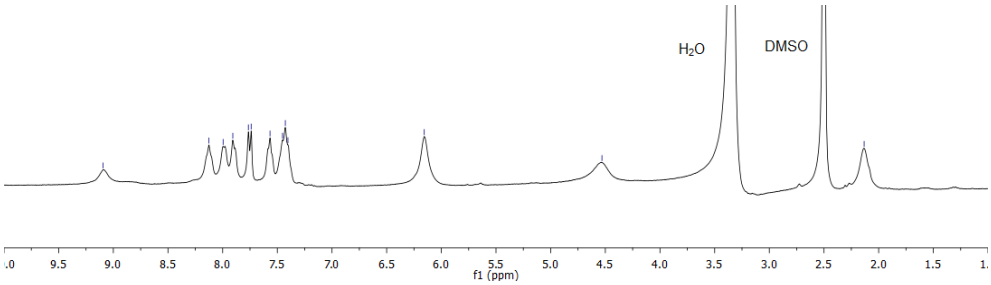

*Figure AII.1. ^{1}H NMR spectrum of complex$[Ni_2(PyC_2S)_2]Br_2$ [**3**]Br_2 in DMSO-d_6.*

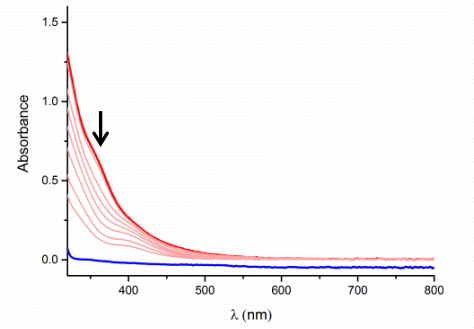

*Figure AII.2. UV-vis spectroscopic changes of a 1 mM solution of compound [**3**] in DMF in air, after addition of 210 equivalents of acetic acid in 4 h (red lines) and overnight (blue line). Spectra were recorded with a transmission dip probe set at a path length of 2.2 mm.*

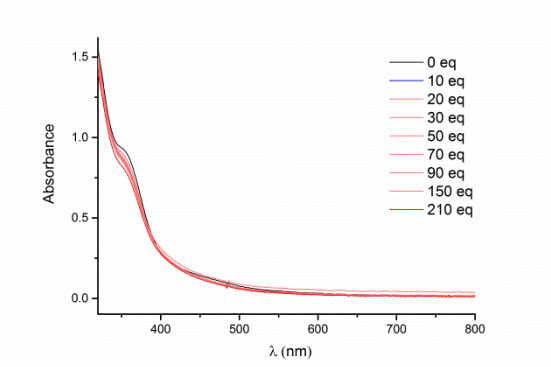

*Figure AII.3. UV-vis spectroscopic changes after sequentially adding acid (0 to 210 equivalents) into 1 mM solution of compound [**3**]Br_2 in DMF under an N_2 atmosphere. Spectra were recorded with a transmission dip probe set at a path length of 2.2 mm.*

Table AII.1. Selected crystallographic and structure refinement data for complex [1], [2], [3]Br_2 and [4]Br_2

	[1]	**[2]**	**[3]**Br_2	**[4]**Br_2
Empirical formula	$C_{32}H_{30}N_4Ni_2S_2Cl_2$	$C_{34}H_{34}N_4Ni_2S_2Cl_2$, $2(CH_2Cl_2)$	$4(C_{30}H_{28}N_6Ni_2S_2Br_2)$, CH_3OH	$C_{32}H_{32}N_6Ni_2S_2Br_2$, H_2O
Formula weight	723.04	920.94	3287.81	860.01
Temperature (K)	110(2)	110(2)	110(2)	110(2)
Crystal system	triclinic	monoclinic	monoclinic	monoclinic
Space group	*P −1*	*C 2/c*	*P 21/c*	*C 2/c*
a (Å)	8.9583(6)	31.5940(7)	27.8967(7)	30.7978(18)
b (Å)	12.2922(6)	8.77402(14)	19.0838(3)	12.2424(4)
c (Å)	13.9276(5)	31.5044(7)	29.1772(8)	21.0829(11)
α (°)	89.367(3)	90	90	90
β (°)	84.431(4)	116.465(3)	118.293(3)	121.879(7)
γ (°)	79.089(5)	90	90	90
V (Å^3)	1498.79(14)	7818.0(3)	13677.5(6)	6750(7)
Z	2	8	4	8
D_{calc} (g/cm^3)	1.602	1.565	1.597	1.693
μ (mm^{-1})	4.741	6.277	5.488	5.606
F (000)	744	3776	6600	3472
Crystal size (mm)	0.28× 0.11 × 0.05	0.40 × 0.08 × 0.05	0.24 × 0.13 × 0.02	0.11 × 0.07 × 0.06
Unique Reflections	15862	7687	26679	10502
R-factor, $I > 2\sigma(I)$	$R_1 = 0.0561$, $wR_2 = 0.1524$	$R_1 = 0.0333$, $wR_2 = 0.0814$	$R_1 = 0.0571$, $wR_2 = 0.1526$	$R_1 = 0.0484$, $wR_2 = 0.1111$
R-factor (all data)	$R_1 = 0.0619$, $wR_2 = 0.1588$	$R_1 = 0.0413$, $wR_2 = 0.0867$	$R_1 = 0.0733$, $wR_2 = 0.1662$	$R_1 = 0.0748$, $wR_2 = 0.1188$
$\Delta\rho_{max}$, $\Delta\rho_{min}$ (e Å^{-3})	0.95,−0.84	0.87, −0.61	1.93, −1.15	0.82, −0.88

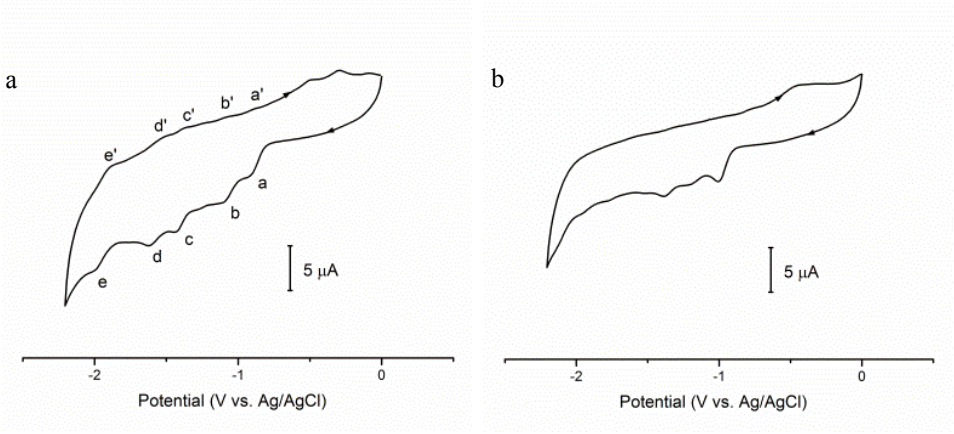

*Figure AII.4. The CV of complex [**3**]Br_2 (a) and [**4**]Br_2 (b) recorded in DMF containing 0.1 M TBAP as supporting electrolyte at scan rate 0.1 V/s, using a glassy carbon working electrode.*

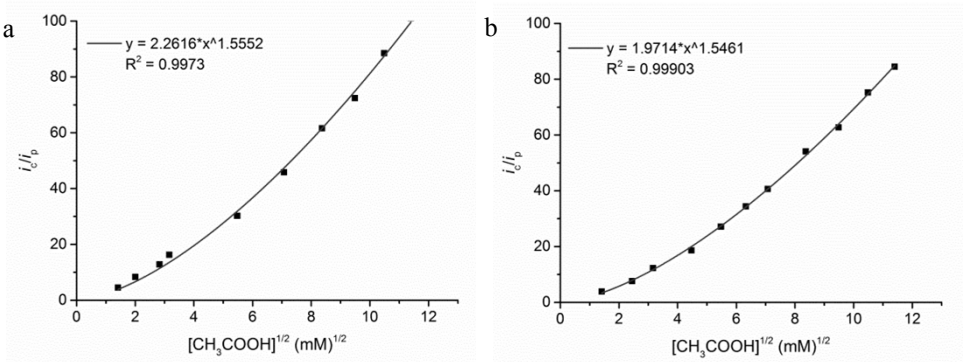

*Figure AII.5. Plot of i_c/i_p vs. $[CH_3COOH]^{1/2}$ ($mM^{1/2}$) for [**3**]Br_2 (a) and [**4**]Br_2 (b) in presence of various acid concentrations in DMF containing 0.1 M TBAP as supporting electrode at 0.1 V/s, using a glassy carbon working electrode.*

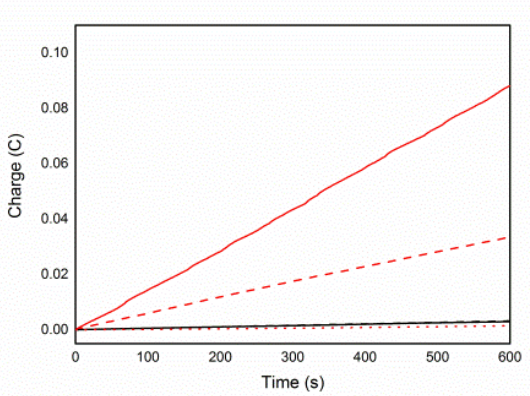

*Figure AII.6. Charge vs. time plot over 600 s during CPC at potential of −1.8 V. Black line: compounds in absence of acid; Red line: compounds in presence of 50 mM acetic acid (dashed = 1 mM $[Ni_2Cl_2(BnC_2S)_2]$ **[1]**, solid = 1mM $[Ni_2(PyC_2S)_2]Br_2$ **[3]**Br_2); Dotted red line: 50 mM acetic acid only. Using glass carbon as working electrode.*

Table AII.2. Raw data for Figure 2.10 and Figure AII.5.

***[3]**Br_2*

$[CH_3COOH]$ (mM)	$[CH_3COOH]^{1/2}$ $(mM)^{1/2}$	i_p (µA)	i_c (µA)	i_c/i_p
2	1.41	8	36	4.5
4	2	8	67	8.38
8	2.83	8	103	12.88
10	3.16	8	130	16.25
30	5.48	8	242	30.25
50	7.07	8	367	45.88
70	8.37	8	493	61.63
90	9.49	8	579	72.38
110	10.49	8	708	88.5
130	11.40	8	808	101

***[4]**Br_2*

$[CH_3COOH]$ (mM)	$[CH_3COOH]^{1/2}$ $(mM)^{1/2}$	i_p (µA)	i_c (µA)	i_c/i_p
2	1.41	8	31	3.88
6	2.45	8	61	7.63
10	3.16	8	98	12.25
20	4.47	8	149	18.63
30	5.48	8	217	27.13
40	6.32	8	275	34.38
50	7.07	8	325	40.63
70	8.37	8	433	54.13
90	9.49	8	502	62.75
110	10.49	8	602	75.25
130	11.40	8	676	84.5

APPENDIX III

Supplementary information on Chapter 3

*Table AIII.1. Selected crystallographic and structure refinement data for complexes **1a, 2a** and **2b***

	1a	**2a**	**2b**
Empirical formula	$C_{34}H_{28}BrN_6Ni$, (Br), 1.5(H_2O)	$C_{26}H_{24}N_6Ni$, 2(Br), 2.361(H_2O), 0.431(O)	$C_{26}H_{24}N_6Ni$, 2(PF_6)
Formula weight	766.18	688.50	769.16
Temperature (K)	110(2)	110(2)	110(2)
Crystal system	monoclinic	monoclinic	monoclinic
Space group	*C 2/c*	*C* 2/*c*	*P* 2_1/*c*
a (Å)	36.2037(12)	32.8374 (6),	23.0500(14)
b (Å)	11.2404(2)	8.89992 (13)	9.5940(3)
c (Å)	16.7135(6)	20.2657 (4)	14.7070(7)
β (°)	109.865(4)	109.610(2)	105.683(6)
V (Å^3)	6396.7(4)	5579.13 (18)	3131.3(3)
Z	8	8	4
D_{calc} (g/cm^3)	1.591	1.639	1.632
μ (mm^{-1})	3.145	4.65	2.796
F (000)	3096	2777	1552
Crystal size (mm)	0.27 × 0.17 × 0.10	0.26 × 0.09 × 0.02	0.25 × 0.14 × 0.01
Reflections collected, unique, $I > 2\sigma(I)$	25476, 7345, 6196	23382, 5423, 4625	18755, 6111, 5006
R-factor, $I > 2\sigma(I)$	$R_1 = 0.0290$, $wR_2 = 0.0635$	$R_1 = 0.0298$, $wR_2 = 0.0761$	$R_1 = 0.0698$, $wR_2 = 0.1823$
R-factor (all data)	$R_1 = 0.0400$, $wR_2 = 0.0674$	$R_1 = 0.0372$, $wR_2 = 0.0810$	$R_1 = 0.0832$, $wR_2 = 0.1933$
$\Delta\rho_{max}$, $\Delta\rho_{min}$ (e Å^{-3})	0.43, –0.49	0.61, –0.56	0.92, –0.71

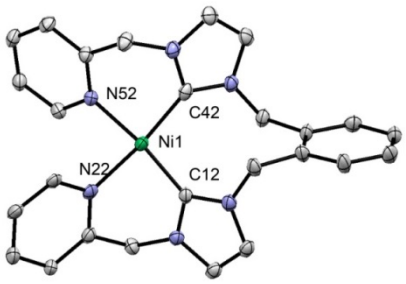

*Figure AIII.1. Displacement ellipsoid plot (50% probability level) of the cationic part [Ni(**L2**)]$^{+}$ in **2a** at 110(2) K. Selected atom numbering has been added for the first coordination sphere. Hydrogen atoms, the lattice water molecules and the two bromide anions are omitted for clarity.*

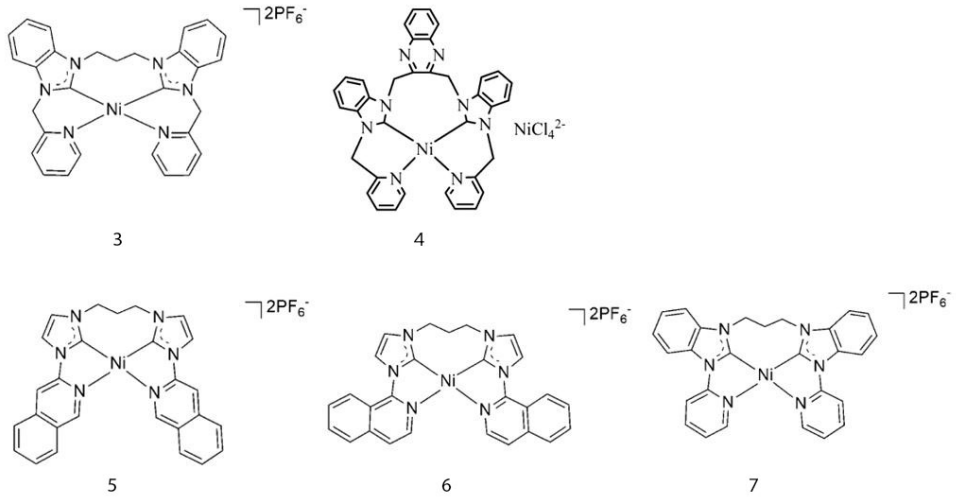

Figure AIII.2. Reported pyridinemethyl/pyridinyl/isoquinolinyl substituted Ni-NHC compounds.[1, 2]

Table AIII.2. Selected bond distances (Å) of reported Ni-NHC compounds in Figure AIII.2.

	3[a]	**4**[b]	**5**[a]	**6**[a]	**7**[a]
Ni1─N22	1.944(3)	1.945(9)	1.956(4)	1.944(1)	1.937
Ni1─N52	1.931(3)	1.945(9)	1.931(4)	1.948(1)	1.937
Ni1─C12	1.899(4)	1.883(1)	1.856(4)	1.847(1)	1.847
Ni1─C42	1.904(4)	1.883(1)	1.851(4)	1.848(2)	1.847
τ_4	0.092	0.033	0.120	0.116	0.137

[a]These complexes published by Thoi[1]. [b]These complexes published by Liu[2].

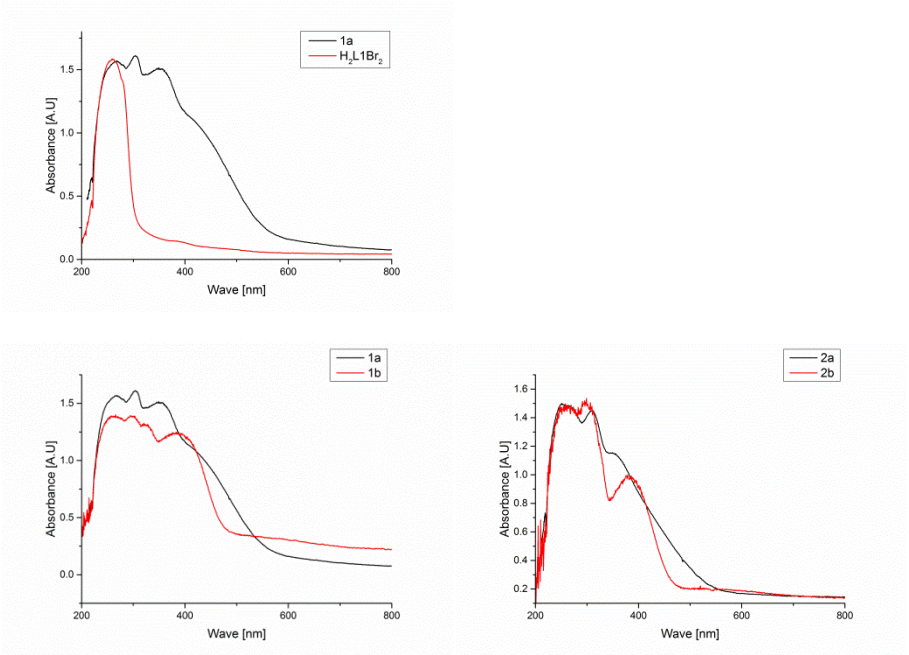

*Figure AIII.3. Solid state absorption spectra of H_2**L1**Br_2, **1a**, **1b**, **2a** and **2b**.*

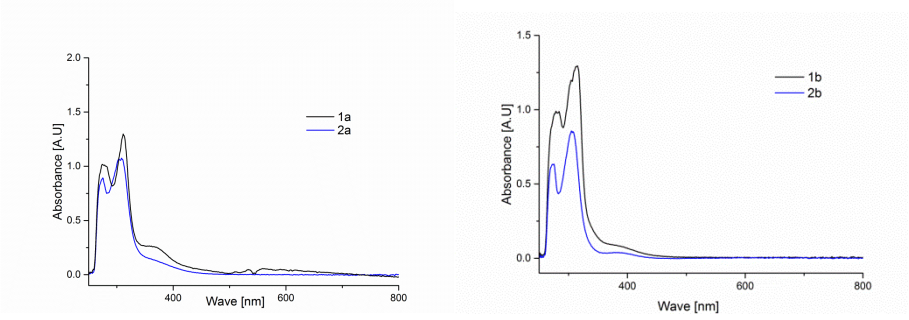

*Figure AIII.4. UV-vis spectra of **1a** (1 mM), **2a** (1 mM), **1b** (1 mM) and **2b** (1 mM) in DMF solution.*

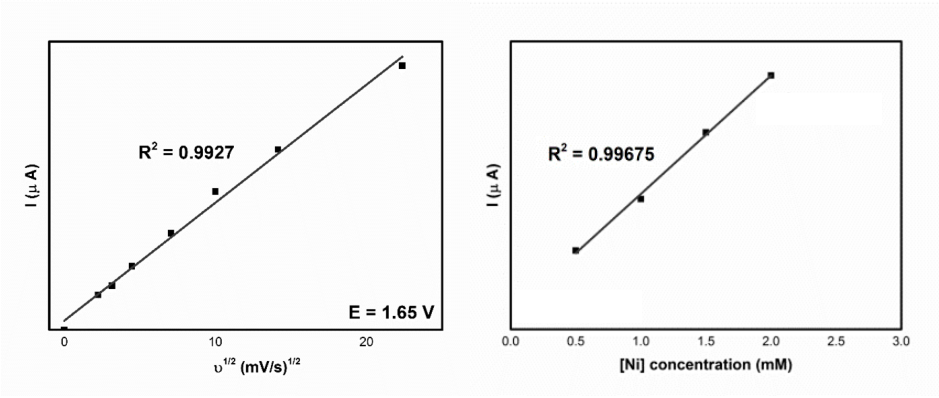

*Figure AIII.5. Plots of reductive current vs. the square root of the scan rate (right) and Plots of reductive current vs. the concentration (left) of **1a** in DMF at E = −1.65 V vs. $Fc^{+/0}$.*

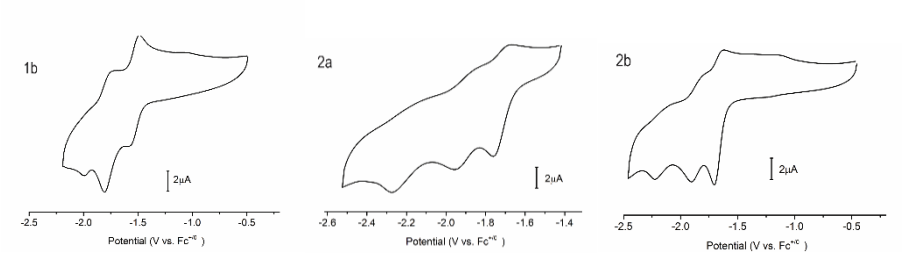

*Figure AIII.6. CV of 1 mM **1b**, **2a** and **2b** recorded in DMF. Conditions: scan rate = 0.1 V/s, TBAP (0.1 M), glassy-carbon working electrode.*

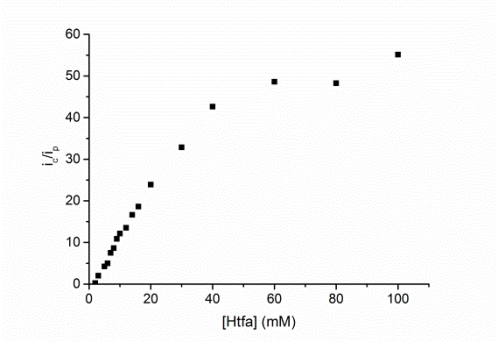

*Figure AIII.7. Plot of i_c/i_p as a function of Htfa concentration (1-100 mM) in DMF in presence of **1a** (1 mM). Conditions: scan rate = 0.1 V/s, TBAP (0.1 M), glassy-carbon working electrode.*

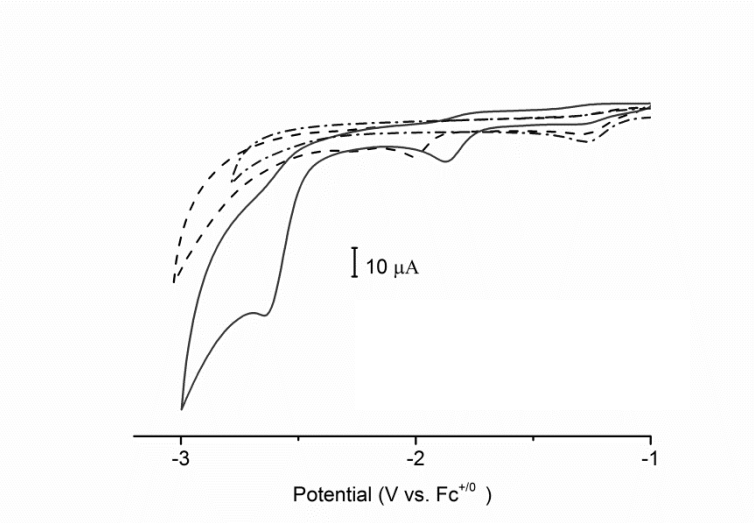

*Figure AIII.8. Cyclic voltammograms of solutions of **1a** (1 mM) (solid line) or H_2**L1**Br_2 (1 mM) (dashed line) in DMF in the presence of 10 mM acetic acid (dot-dashed line). Conditions: scan rate = 0.1V/s, TBAP (0.1 M), glassy-carbon working electrode.*

Table AIII.3. Raw data for Figure 3.4 and Figure AIII.7.

[Htfa] (mM)	$[Htfa]^{1/2}$ $(mM)^{1/2}$	i_p (µA)	i_c (µA)	i_c/i_p
2	1.41	8	2	0.25
3	1.73	8	16	2
5	2.23	8	34	4.25
6	2.45	8	40	5
7	2.66	8	60	7.5
8	2.83	8	69	8.63
9	3	8	87	10.88
10	3.16	8	97	12.13
12	3.46	8	108	13.5
14	3.74	8	133	16.63
16	4	8	149	18.63
20	4.47	8	191	23.88
30	5.48	8	263	32.88
40	6.32	8	341	42.63
60	7.75	8	389	48.63
80	8.94	8	386	48.25
100	10	8	441	55.13

Table AIII.4. Raw data for Figure 3.6 and Figure 3.7.

1a

$[CH_3COOH]$ (mM)	$[CH_3COOH]^{1/2}$ $(mM)^{1/2}$	i_p (µA)	i_c (µA)	i_c/i_p
1	1	7	40	5.71
2	1.41	7	47	6.71
4	2	7	55	7.85

6	2.45	7	61	8.71
8	2.83	7	66	9.42
10	3.17	7	70	10
12	3.46	7	70	10
16	4	7	77	11

1b

$[CH_3COOH]$ (mM)	$[CH_3COOH]^{1/2}$ $(mM)^{1/2}$	i_p (μA)	i_c (μA)	i_c/i_p
1	1	6	24	4
2	1.41	6	36	6
3	1.73	6	40	6.67
4	2	6	45	7.50
6	2.45	6	49	8.17
8	2.83	6	53	8.83
10	3.16	6	54	9
12	3.46	6	56	9.33
16	4	6	56	9.33
20	4.47	6	59	9.83

2a

$[CH_3COOH]$ (mM)	$[CH_3COOH]^{1/2}$ $(mM)^{1/2}$	i_p (μA)	i_c (μA)	i_c/i_p
1	1	10	22	2.2
2	1.41	10	49	4.9
3	1.73	10	61	6.1
5	2.23	10	70	7
8	2.82	10	96	9.6
10	3.16	10	110	11
12	3.46	10	126	12.6
16	4	10	149	14.9
20	4.47	10	156	15.6
30	5.48	10	225	22.5
40	6.32	10	273	27.3
50	7.07	10	331	33.1
60	7.74	10	378	37.8
70	8.37	10	423	42.3
80	8.94	10	423	42.3

2b

$[CH_3COOH]$ (mM)	$[CH_3COOH]^{1/2}$ $(mM)^{1/2}$	i_p (μA)	i_c (μA)	i_c/i_p
1	1	9	38	4.22
2	1.41	9	46	5.11
4	2	9	59	6.56
6	2.45	9	70	7.78
8	2.83	9	84	9.33
10	3.16	9	99	11
20	4.47	9	149	16.56
30	5.48	9	203	22.56

40	6.32	9	249	27.67
60	7.75	9	356	39.56
80	8.94	9	451	50.11
120	10.95	9	625	69.44

References

[1] V.S. Thoi, N. Kornienko, C.G. Margarit, P. Yang, C.J. Chang, J. *Am. Chem. Soc.* 2013, 135, 14413-14424.

[2] Q.-X. Liu, Z.-Q. Yao, X.-J. Zhao, Z.-X. Zhao, X.-G. Wang, *Organometallics* 2013, 32, 3493-3501.

APPENDIX IV

Supplementary information on Chapter 4

*Table AIV.1. Crystallographic and structure refinement data for the complexes [Ni(**L1**)$_2$]Br$_2$ and [Ni(**L2**)$_2$]Br$_2$.*

	[Ni(**L1**)$_2$]Br$_2$	[Ni(**L2**)$_2$]Br$_2$
Empirical formula	$C_{40}H_{34}N_6Ni\cdot 2(Br)\cdot 0.904(H_2O)\cdot 0.416(O)$	$2(C_{38}H_{32}N_8Ni)\cdot 4(Br)\ CH_2Cl_2\cdot 4.184(O)\cdot 3(H_2O)$
Formula weight	840.16	1844.38
Temperature (K)	110(2)	110(2)
Crystal system	Triclinic	Monoclinic
Space group	*P*−*1*	*Cc*
a (Å)	11.5677 (3)	33.1815 (6)
b (Å)	16.6345 (4)	10.5397 (2)
c (Å)	19.7170 (6)	22.6091 (5)
α (°)	108.593 (2),	90
β (°)	93.914 (2)	95.2398 (18)
γ (°)	100.426 (2)	90
V (Å^3)	3504.17 (17)	7873.9 (3)
Z	4	4
D_{calc} (g/cm^3)	1.593	1.556
μ (mm^{-1})	2.88	2.64
F (000)	1705	3734
Crystal size (mm)	0.22 × 0.08 × 0.05	0.60 × 0.50 × 0.31
No. of measured, independent and observed [$I > 2\sigma(I)$] reflections	47791, 16092, 12186	51937, 17652, 16325
R-factor, $I > 2\sigma(I)$	$R_1 = 0.0387$, $wR_2 = 0.0830$	$R_1 = 0.0345$, $wR_2 = 0.0794$
R-factor (all data)	$R_1 = 0.0611$, $wR_2 = 0.0915$	$R_1 = 0.0394$, $wR_2 = 0.0818$
$\Delta\rho_{max}$, $\Delta\rho_{min}$ (e Å^{-3})	1.03, −0.57	1.16, −0.55

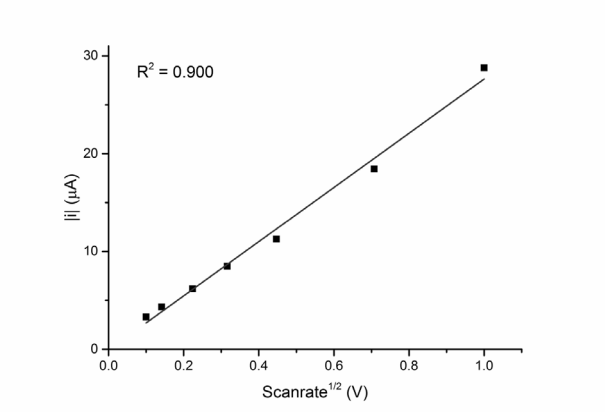

Figure AIV.1. Plots of reductive current i_{pc} vs. the square root of the scan rate for [Ni(**L1**)$_2$]Br$_2$ in DMF containing 0.1 M TBAP as supporting electrolyte at different at E_{pc} = −1.04 V, using a glassy carbon working electrode.

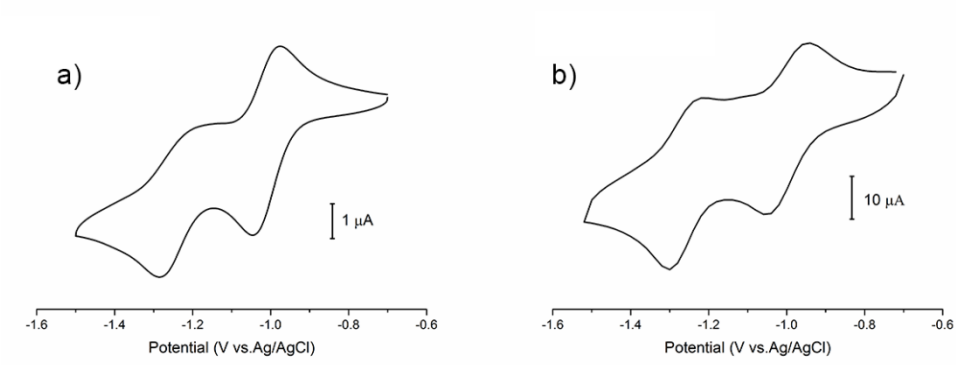

*Figure AIV.2. CVs of [Ni(**L1**)$_2$]Br$_2$ 1 mM in DMF containing 0.1 M TBAP as supporting electrolyte at different scan rate: (a) 10 mV/s; (b) 500 mV/s, using a glassy carbon working electrode.*

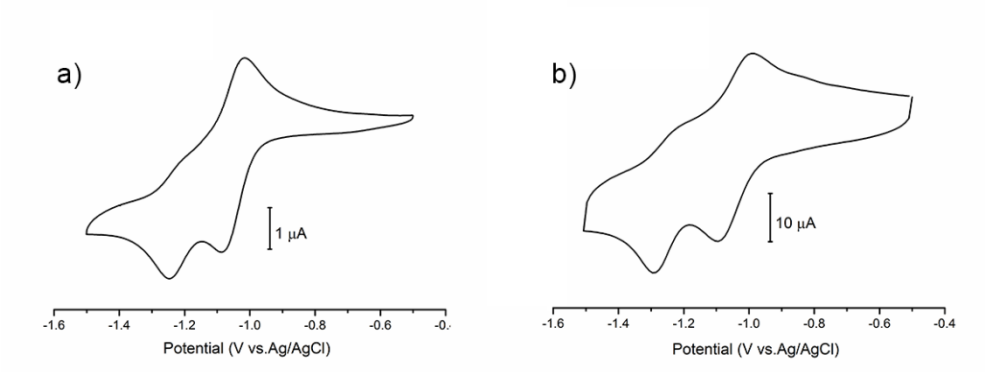

*Figure AIV.3. CV of [Ni(**L2**)$_2$]Br$_2$ in DMF containing 0.1 M TBAP as supporting electrolyte at different scan rate: (a) 10 mV/s; (b) 500 mV/s, using glassy carbon working electrode.*

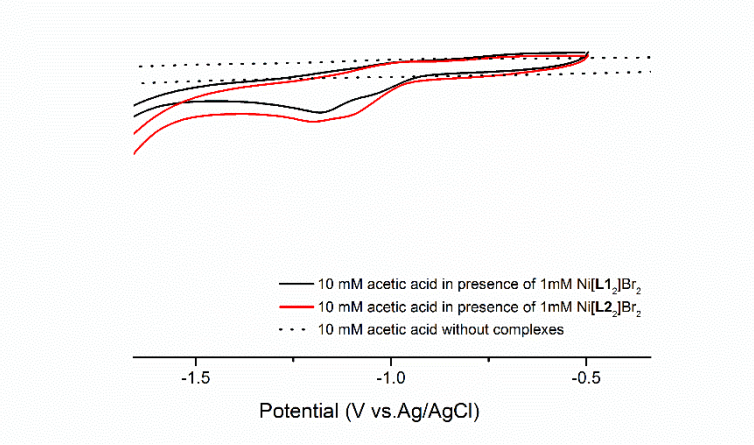

*Figure AIV.4. Zoom of CVs of complexes [Ni(**L1**)$_2$]Br$_2$ and [Ni(**L2**)$_2$]Br$_2$ in presence of 10 mM acetic acid in DMF containing 0.1 M TBAP as supporting electrolyte at scan rate 0.1 V/s, using a glassy carbon working electrode.*

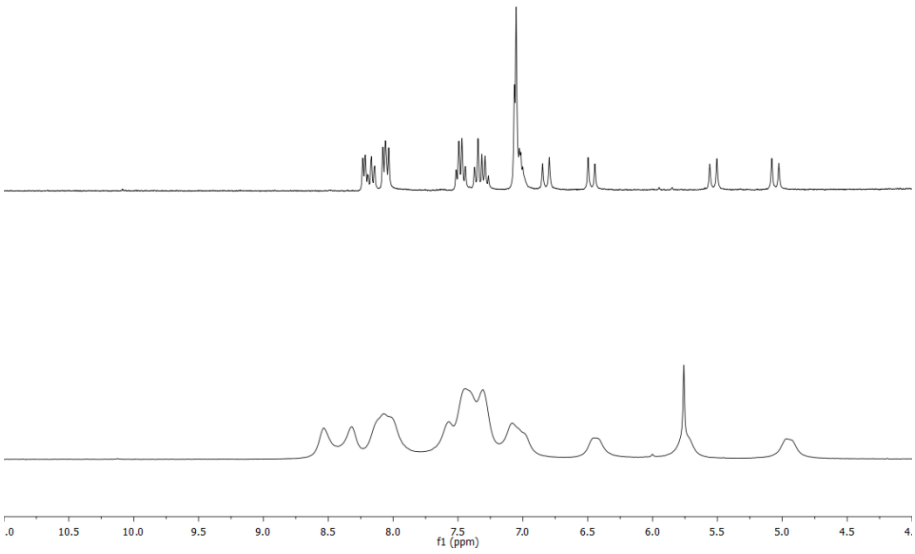

*Figure AIV.5. ^{1}H NMR spectra of complex [Ni(**L1**)$_2$]Br$_2$ (top) and [Ni(**L2**)$_2$]Br$_2$ (bottom) in DMSO-d$_6$.*

APPENDIX V

Supplementary information on Chapter 5

*Table AV.1. Selected crystallographic and structure refinement data for complexes [Ni(**L1**)]Cl and [Ni(**L2**)]PF_6.*

	[Ni(**L1**)]Cl	[Ni(**L2**)]PF_6
Empirical formula	$C_{17}H_{16}N_5NiO$,(Cl), 2.858(H_2O), 0.142(O)	$C_{21}H_{18}N_5NiO$, PF_6
Formula weight	454.27	560.08
Temperature (K)	110(2)	110(2)
Crystal system	monoclinic	triclinic
Space group	P $2_1/c$	P-1
a (Å)	9.4516(3)	7.1151(3)
b (Å)	14.7691(3)	11.9382(5)
c (Å)	13.4335(3)	12.9537(5)
α (°)	90	94.498(3)
β (°)	100.847(3)	97.028(3)
γ (°)	90	106.050(4)
V ($Å^3$)	1841.70(8)	1042.18(8)
Z	4	2
D_{calc} (g/cm^3)	1.638	1.785
μ (mm^{-1})	3.176	2.82
F (000)	943	568
Crystal size (mm)	0.17 × 0.11 × 0.01	0.24 × 0.13 × 0.05
No. of measured, independent and observed [$I > 2\sigma(I)$] reflections	10101, 3295, 2629	13223, 4059, 3515
R-factor, I > 2σ(I)	$R_1 = 0.0414$, $wR_2 = 0.1130$	$R_1 = 0.0320$, $wR_2 = 0.0777$
R-factor (all data)	$R_1 = 0.0572$, $wR_2 = 0.1030$	$R_1 = 0.0393$, $wR_2 = 0.0817$
$\Delta\rho_{max}$, $\Delta\rho_{min}$ (e $Å^{-3}$)	0.52, −0.70	0.57, −0.35

*Table AV.2. Selected bond distances (Å) and angles (°) of compounds [Ni(**L1**)]Cl and [Ni(**L2**)]PF_6.*

bond distances (Å)	[Ni(**L1**)]Cl	[Ni(**L2**)]PF_6	angles (°)	[Ni(**L1**)]Cl	[Ni(**L2**)]PF_6
Ni1–C12	1.832(3)	1.835(2)	C12-Ni1-N31	90.8(1)	89.95(8)
Ni1–N31	1.873(3)	1.856(2)	C12-Ni1-N22	89.3(1)	89.87(8)
Ni1–N42	1.936(2)	1.940(2)	C12-Ni1-N42	164.9(1)	162.96(8)
Ni1–N22	1.918(2)	1.918(2)	N31-Ni1-N22	169.3(1)	170.82(7)
C12–N13	1.336(4)	1.343(3)	N31-Ni1-N42	85.8(1)	85.62(7)
C12–N11	1.351(4)	1.349(2)	N22-Ni1-N42	96.8(1)	97.09(7)
C33–N31	1.313(4)	1.339(3)			
C33–O32	1.259(4)	1.247(3)			

*Table AV.3. Hydrogen bond list for compound [Ni(**L1**)]Cl.*

	D-H (Å)	H...A (Å)	D...A (Å)	<(DHA) (°)
O1W-H1W1...O32	0.82(2)	2.03(3)	2.847(3)	169(4)
O1W-H1W2...O32	0.84(2)	1.99(3)	2.822(3)	171(4)
O2W_a-H2W1_a...Cl1	0.89(3)	2.24(3)	3.123(4)	171(6)
O2W_a-H2W2_a...O3W_a	0.86(3)	2.28(8)	2.781(6)	117(7)
O2W'_b-H2W3_b...Cl1	0.84(3)	2.60(10)	3.353(11)	149(17)
O2W'_b-H2W4_b...Cl1	0.84(3)	2.66(5)	3.489(11)	167(16)
O3W_a-H3W1_a...O32	0.95(3)	1.90(3)	2.841(4)	170(6)
O3W_a-H3W2_a...Cl1	0.95(3)	2.05(3)	3.004(4)	175(5)

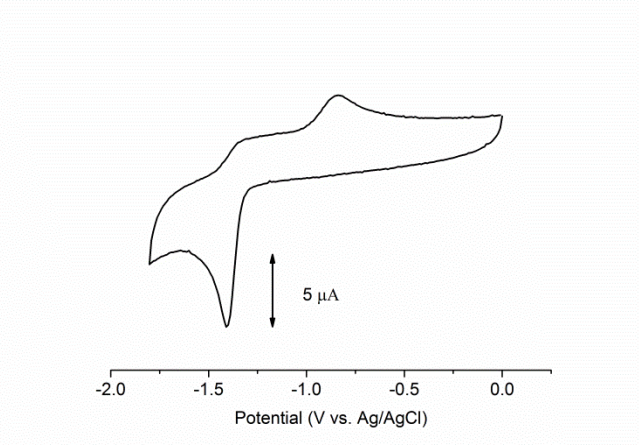

*Figure AV.1. Cyclic voltammogram of [Ni(**L1**)]Cl (1mM) recorded in DMF containing 0.1 M TBAP at scan rate 0.1 V/s, using a glassy carbon working electrode.*

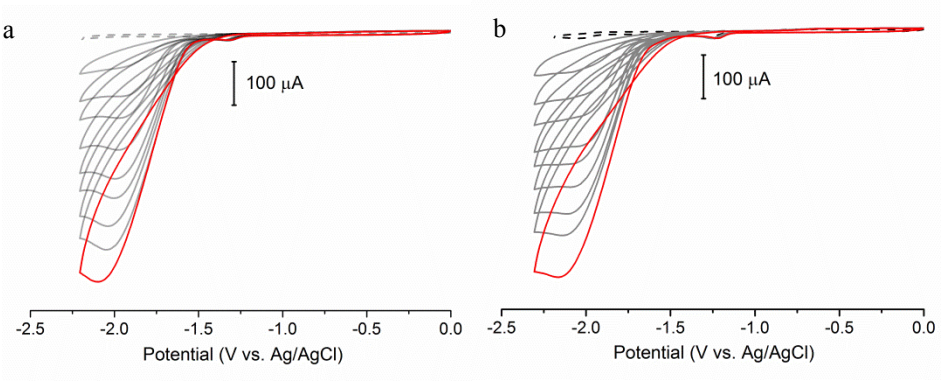

*Figure AV.2. CVs of 1 mM complex [Ni(**L1**)]Cl (a) and [Ni(**L2**)]PF_6 (b) in presence of various acid concentrations (0 − 100 mM) in. DMF containing 0.1 M TBAP as supporting electrode at a scan rate of 0.1 V/s, using a glassy carbon working electrode.*

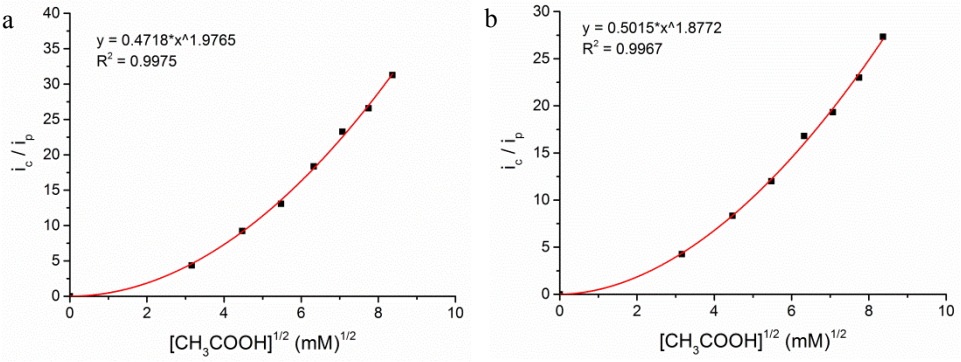

Figure AV.3. Plot of i_c/i_p vs. $[CH_3COOH]^{1/2}$ $(mM)^{1/2}$ for [Ni(**L1**)]Cl (a) and [Ni(**L2**)]PF_6 (b) in presence of various acid concentration in DMF containing 0.1 M TBAP as supporting electrode at 0.1 V/s, using a glassy carbon working electrode.

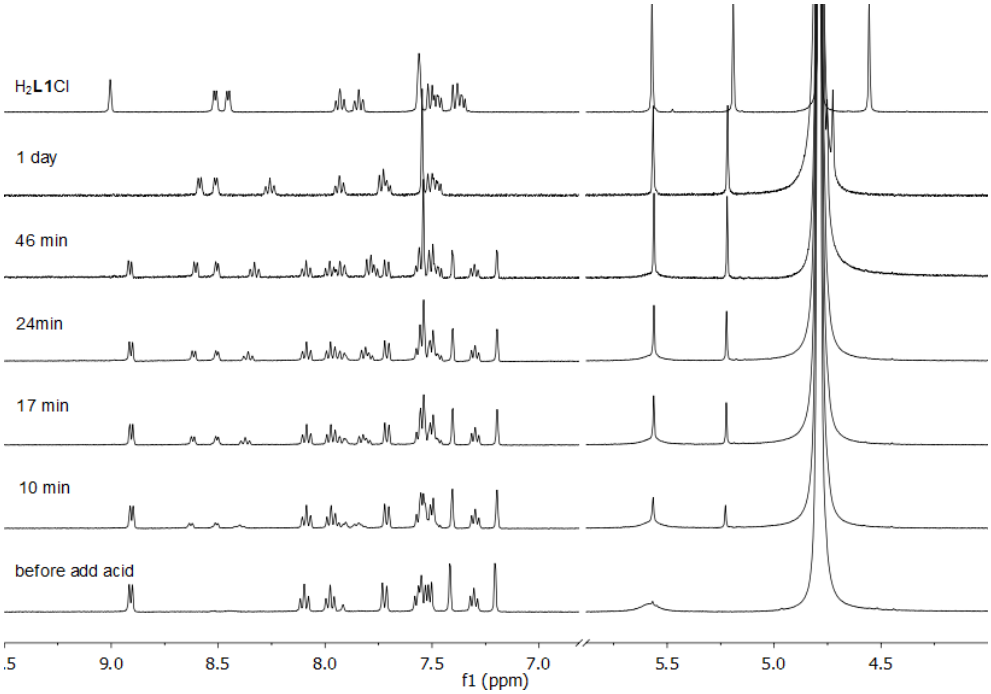

*Figure AV.4. ^{1}H NMR spectra of [Ni(**L1**)]Cl in D_2O in absence and in presence of acetic acid-d_4; ^{1}H NMR spectrum of ligand precursor H_2**L1**Cl is given at the top as comparison. Solvent residual signal set at 4.79 ppm for D_2O. After 1 day the chemical shift of decomposed complex shows slightly difference with the chemical shift of ligand precursor, probably due to the protonation of pyridine and amide group in acid environment.*

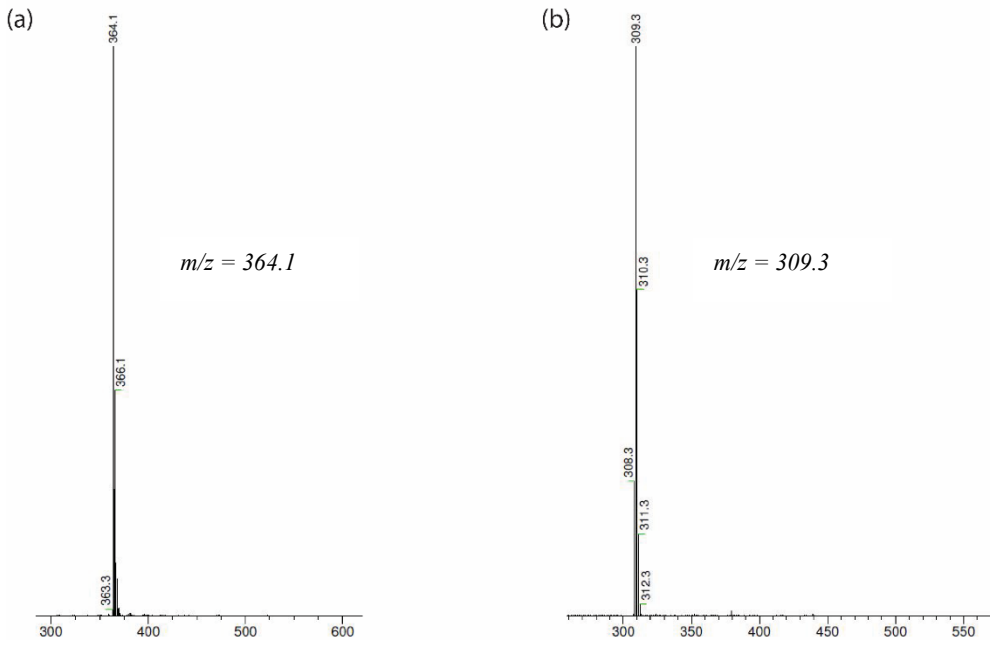

*Figure AV.5. Mass spectra of compound [Ni**L1**]Cl in D_2O before (a) and after (b) addition of acetic acid-d_4. Calculated for $[Ni\mathbf{L1}]^+$ m/z 364.07;calculated for $[HD\mathbf{L1}]^+$ m/z 309.16.*

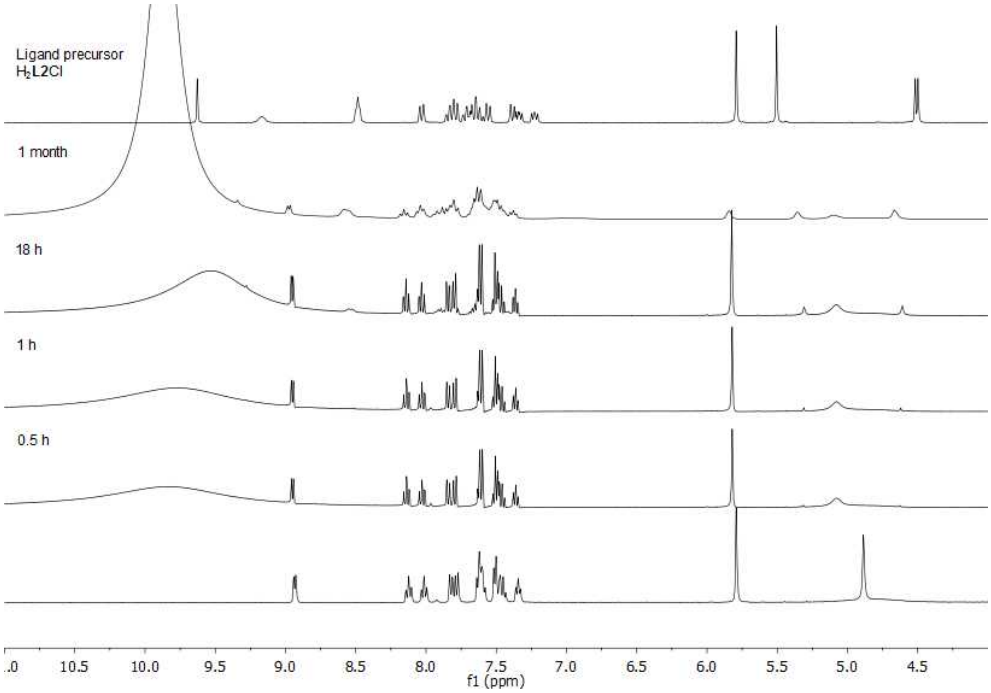

*Figure AV.6. ^1H NMR spectra of [Ni(**L2**)]PF_6 in acetonitrile-d_3 in absence (bottom) and presence of acetic acid-d_4; ^1H NMR spectrum of ligand precursor is given at the top as comparison.*

Table AV.4. Raw data for Figure 5.6 and Figure AV.3.

*[Ni(**L1**)]Cl*

$[CH_3COOH]$ (mM)	$[CH_3COOH]^{1/2}$ $(mM)^{1/2}$	i_p (μA)	i_c (μA)	i_c/i_p
10	3.16	14	61	4.36
20	4.47	14	129	9.21
30	5.48	14	183	13.07
40	6.32	14	257	18.36
50	7.07	14	326	23.29
60	7.76	14	372	26.57
70	8.37	14	438	31.29
80	8.94	14	493	35.21

*[Ni(**L2**)]PF_6*

$[CH_3COOH]$ (mM)	$[CH_3COOH]^{1/2}$ $(mM)^{1/2}$	i_p (μA)	i_c (μA)	i_c/i_p
10	3.16	15	64	4.27
20	4.47	15	125	8.33
30	5.48	15	180	12
40	6.32	15	252	16.8
50	7.07	15	290	19.33

60	7.75	15	347	23.13
70	8.37	15	410	27.33
80	8.94	15	461	30.73

Table AV.5. Raw data for Figure 5.7.

Scan rate (V/s)	i_c (μA)
0.05	630
0.1	751
0.2	1058
0.3	1354
0.5	1560
1	1987
2	2356

APPENDIX VI

Supplementary information on Chapter 6

*Table AVI.1. Selected crystallographic and structure refinement data for complexes [Co(**L2**)$_2$]Cl.*

	[Co(**L2**)$_2$]Cl
Empirical formula	$2(C_{34}H_{32}CoN_{10}O_2)\cdot 5(H_2O)\cdot 2(Cl)$
Formula weight	1504.23
Temperature (K)	110(2)
Crystal system	monoclinic
Space group	P $2_1/n$
a (Å)	13.5141(3)
b (Å)	16.3049(4)
c (Å)	15.5444(4)
α (°)	90
β (°)	105.250 (2)
γ (°)	90
V (Å^3)	3304.54 (14)
Z	2
D_{calc} (g/cm^3)	1.638
μ (mm^{-1})	0.66
F (000)	943
Crystal size (mm)	0.27 × 0.24 × 0.13
No. of measured, independent and observed [$I > 2\sigma(I)$] reflections	25481, 10320, 7559
R-factor, I > 2σ(I)	$R_1 = 0.0396$, $wR_2 = 0.1003$
R-factor (all data)	$R_1 = 0.0544$, $wR_2 = 0.0915$
$\Delta\rho_{max}$, $\Delta\rho_{min}$ (e Å^{-3})	0.63, −0.53

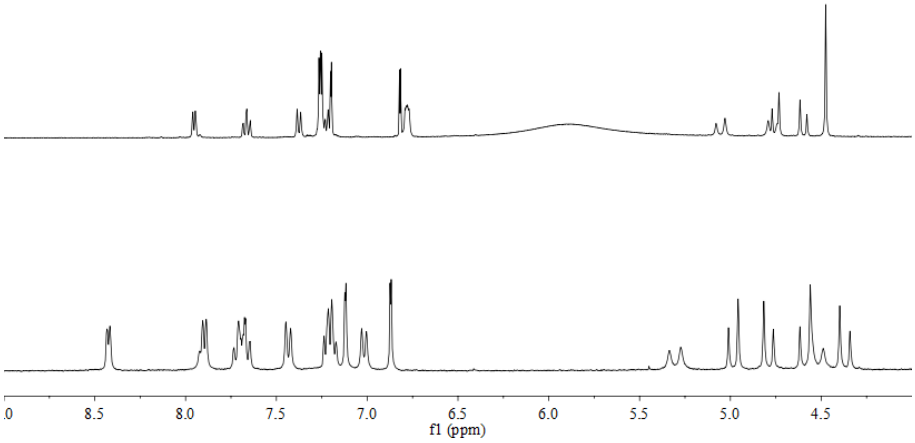

*Figure AVI.1. ^{1}H NMR spectra of complex [Co(**L1**)$_2$]Cl (top) and [Co(**L2**)$_2$]Cl (bottom) in acetonitrile-d_3.*

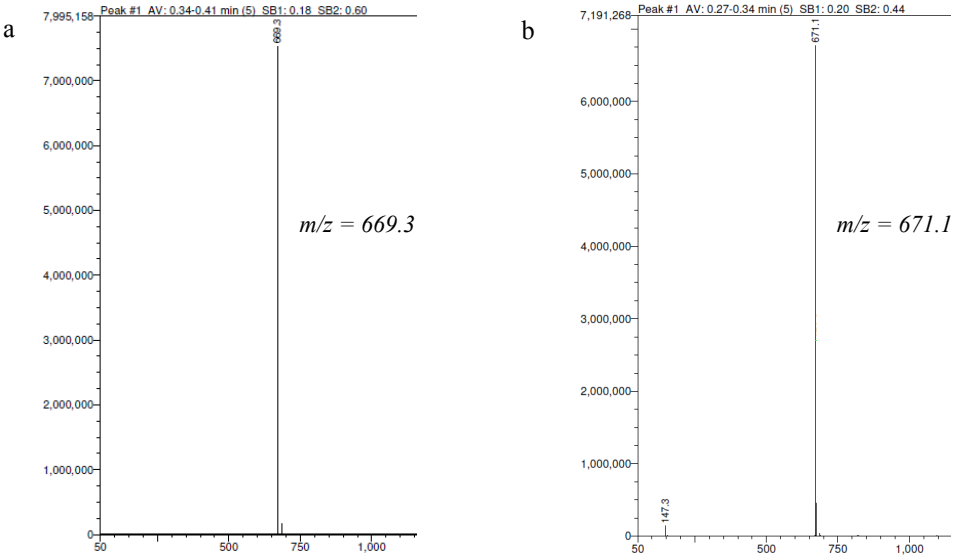

*Figure AVI.2. ESI-MS spectra of complex (a) [Co(**L1**)$_2$]Cl (calculated $[M–Cl]^+$ m/z 669.21) and (b) [Co(**L2**)$_2$]Cl (calculated $[M–Cl]^+$ m/z 671.2).*

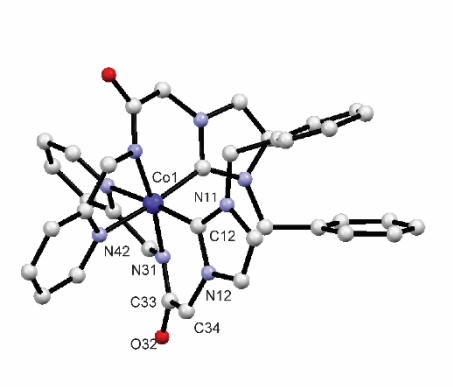

*Figure AVI.3. Ball and stick projection of the cationic complex in [Co(**L1**)$_2$]PF$_6$ with selected labeling. The counter ions could not be located due to disorder.*

*Table AVI.2. Selected bond distances (Å) and angles (°) of compounds [Co(**L1**)$_2$]PF$_6$ and [Co(**L2**)$_2$]Cl.*

	[Co(**L1**)$_2$]PF$_6$	[Co(**L2**)$_2$]Cl
Co1–C12A	1.9067	1.917(2)
Co1–N31A	1.9023	1.9236(17)
Co1–N42A	2.0087	1.9867(18)
C12B-Co1-N31A	93.25	93.66(8)
C12A-Co1-N31A	91.97	89.84(8)
N31B-Co1-N42A	92.79	96.8(12)
N31A-Co1-N42A	81.99	81.53(7)
C12B-Co1-C12A	88.29	88.01(9)
N42B-Co1-N42A	88.68	86.56(7)
C12B-Co1-N42A	91.83	92.54(8)
C12A-Co1-N42A	173.95	171.37(8)
C12B-Co1-N42B	173.95	171.53(8)
N31A-Co1-N31B	172.72	174.10

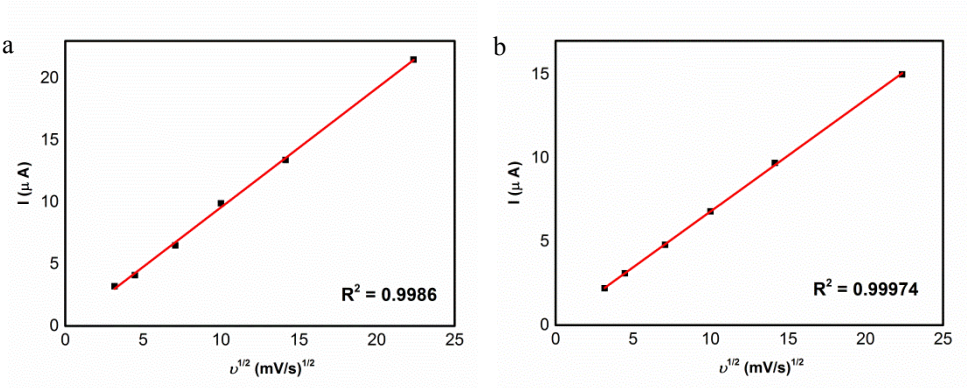

*Figure AVI.4. Plots of reductive current vs. the square root of the scan rate of [Co(**L1**)$_2$]Cl (a) and [Co(**L2**)$_2$]Cl **(b)** in DMF both at E = −1.22 V vs. Ag/AgCl, respectively.*

*Redox properties of H$_2$**L1**Cl and H$_2$**L2**Cl*

The redox properties of the ligand precursors were also investigated. Both the precursors H$_2$**L1**Cl and H$_2$**L2**Cl show an irreversible reduction at around −2 V (for H$_2$**L1**Cl at −2.03 V and H$_2$**L2**Cl at −2.15 V) (Figure AVI.5). In addition, CVs of two ligand precursors were recorded in the presence of various concentrations of acetic acid (from 10 mM to 40 mM). For both ligand precursors a new irreversible reductive current response is observed at around −1.84 V. This catalytic current response was observed before the reduction of ligand (Figure AVI.5). The catalytic current remained steady and stopped to increase at a certain concentration of acid (10 mM for H$_2$**L1**Cl and 20 mM for H$_2$**L2**Cl). In presence of 40 mM acetic acid, compared to H$_2$**L1**Cl, the catalytic current of H$_2$**L2**Cl is doubled. Although without metal center, both ligand precursors show weak catalytic activity on HER. But the catalytic activity of H$_2$**L2**Cl is faster than its partner. Considering the structure difference between two ligand precursors (H$_2$**L2**Cl contains two pyridine group but H$_2$**L1**Cl only contains one), we assume that the pyridine group takes part into the electrocatalytic cycle.

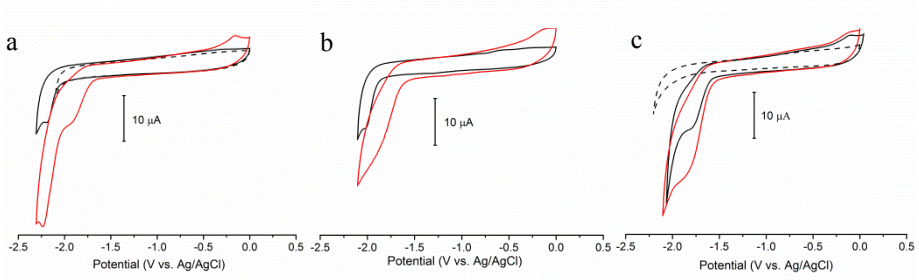

*Figure AVI.5. CVs of ligand precursors H$_2$**L1**Cl (1 mM) and H$_2$**L2**Cl (1 mM) in absence and in presence of acid: (a) CVs of H$_2$**L1**Cl in absence of acid (solid black line in the range 0 to −2.3 V; black dashed line in the range 0 to −2.1 V) and in presence of 10 mM acetic acid (solid red line); (b) CVs of H$_2$**L2**Cl in absence of acid (solid black line) and in presence of 10 mM acetic acid (solid red line); (c) CVs of H$_2$**L1**Cl (1 mM) (solid black line) and H$_2$**L2**Cl (1 mM) (solid red line) in presence of 40 mM acetic acid (black dashed line).*

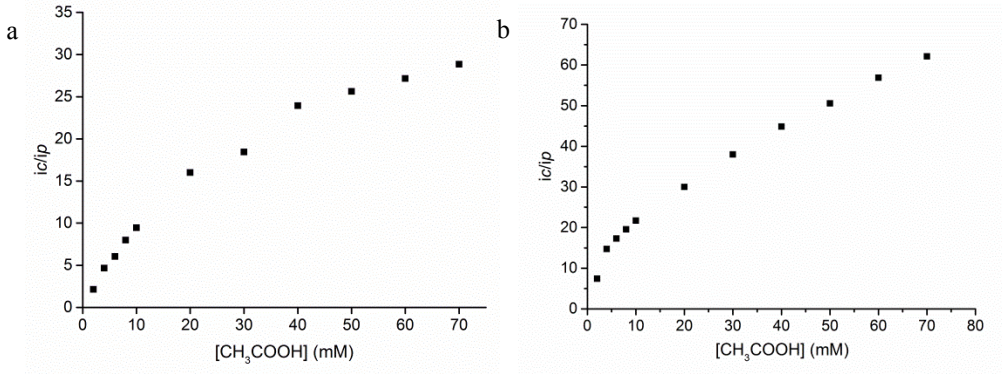

*Figure AVI.6. Plot of i_c/i_p vs. [CH_3COOH] (mM) for [Co(**L1**)$_2$]Cl (a) and [Co(**L2**)$_2$]Cl (b), measured in presence of various acid concentration in DMF containing 0.1 M TBAP as supporting electrode at 0.1 V/s, using glassy carbon working electrode.*

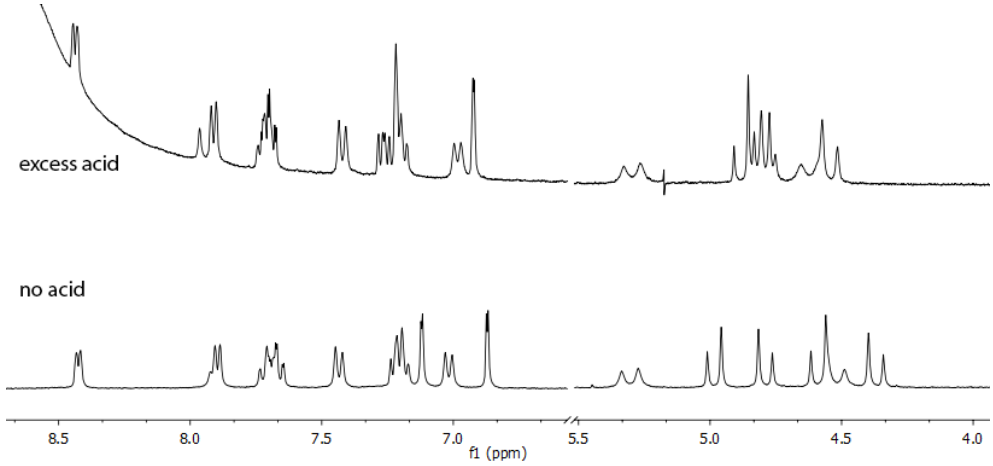

*Figure AVI.7. ^1H NMR spectra of [Co(**L2**)$_2$]Cl in acetonitrile-d_3 in absence or presence of acetic acid-d_4. The peaks shifted downfield in presence of acid probably due to the protonation of the free pyridine group. The protonation can be confirmed by the EI-MS spectrum of the sample after NMR measurement (Figure AVI.8).*

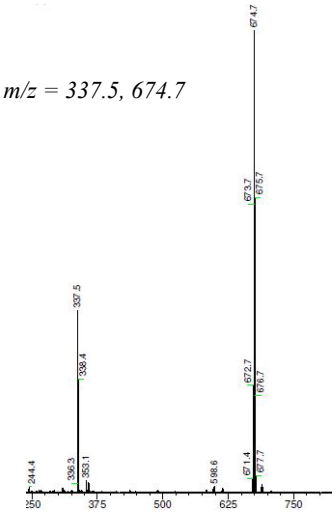

*Figure AVI.8. Mass spectra of compound [Co(**L2**)$_2$]Cl in acetonitrile-d$_3$ in prence of acetic acid-d$_4$. Calculated for [Co(**L2**D)$_2$]$^{2+}$ m/z 337.6;calculated for [Co(**L2**)(**L2**D)]$^+$ m/z 673.22.*

Table AVI.2. Raw data for Figure 6.7, Figure 6.8 and Figure AVI.6.

*[Co(**L1**)$_2$]Cl*

[CH_3COOH] (mM)	[CH_3COOH]$^{1/2}$ (mM)$^{1/2}$	i_p (μA)	i_c (μA)	i_c/i_p	k_{obs} (s^{-1})
2	1.41	11	26	2.36	0.90
4	2	11	54	4.91	4.23
6	2.45	11	67	6.09	7.07
8	2.83	11	87	7.91	12.39
10	3.16	11	102	9.27	17.30
20	4.47	11	177	16.09	49.72
30	5.48	11	203	18.45	66.06
40	6.32	11	261	23.73	111.22
50	7.07	11	279	25.36	127.36
60	7.75	11	294	26.73	143.11
70	8.37	11	313	28.45	161.46

*[Co(**L2**)$_2$]Cl*

[CH_3COOH] (mM)	[CH_3COOH]$^{1/2}$ (mM)$^{1/2}$	i_p (μA)	i_c (μA)	i_c/i_p	k_{obs} (s^{-1})
2	1.41	7	52	7.43	10.71
4	2	7	103	14.71	42.00
6	2.45	7	121	17.29	57.97
8	2.83	7	137	19.57	74.31
10	3.16	7	152	21.71	91.47
20	4.47	7	210	30	174.6
30	5.48	7	266	38	280.17
40	6.32	7	314	44.86	390.36
50	7.07	7	354	50.57	496.15
60	7.75	7	398	56.86	627.15
70	8.37	7	435	62.14	749.18

Samenvatting

Inleiding

Waterstofgas wordt beschouwd als een van de meest aantrekkelijke duurzame brandstoffen, omdat bij de verbranding van waterstofgas alleen water ontstaat. De reductie van protonen tot moleculair waterstof, de waterstof-evolutiereactie (HER), is een van de meest bestudeerde reacties.[1] Conventionele heterogene elektrokatalysatoren voor de reductie van protonen tot waterstofgas bestaan veelal uit platina, waarbij op platina-gebaseerde materialen als werkelektrode wordt gebruikt.[2] Het nadeel van het gebruik van platina is evident, gezien het een schaars en kostbaar edelmetaal is. Het hydrogenase enzym is in staat de transformatie van protonen tot moleculair waterstof met hoge efficiëntie te katalyseren.[3] Geïnspireerd door deze natuurlijke enzymen zijn door chemici vele structurele en functionele modellen ontworpen en gesynthetiseerd, waarvan sommige naar voren zijn gekomen als goede elektrokatalysatoren voor de reductie van protonen.

N-heterocyclische carbenen (NHCs) worden gezien als liganden die nuttig zijn voor toepassing in homogene katalysatoren, en vergelijkbaar zijn met fosfaanliganden.[4, 5] Tot nu toe is echter de bestudering van de elektrokatalytische eigenschappen van overgangsmetaalcomplexen met NHC-liganden grotendeels onderbelicht gebleven. Nikkelverbindingen met difosfaanliganden zijn uitgebreid bestudeerd op hun elektrokatalytische activiteit in de HER.[6] Hierdoor is het van bijzonder belang dat de elektrokatalytische eigenschappen van metaal-NHC complexen bestudeerd worden, door middels een verkennende studie te inventariseren of deze klasse van verbindingen de potentie hebben om efficiënte HER elektrokatalysatoren te leveren.

In Hoofdstuk 1 wordt de structuur van de actieve plaats van hydrogenases kort besproken, gevolgd door een beknopt overzicht van structurele en functionele modellen voor hydrogenase. Vervolgens wordt een korte overzicht gegeven van metaal-NHC-verbindingen in de context van elektrochemisch onderzoek. Tenslotte wordt een algemeen mechanisme besproken van de HER gekatalyseerd door moleculaire elektrokatalysatoren.

Elektrokatalytische activiteit van nikkelverbindingen met thiolaat-gefunctionaliseerde NHC-liganden

Naar mate het onderzoek naar modellen voor de actieve plaats van hydrogenase vorderde en er meer structurele en functionele modellen verschenen, is consensus bereikt dat de aanwezigheid van thiolaatbruggen in de structuur van de elektrokatalysatoren essentieel is. Op basis van deze kennis leken metaalverbindingen met zwavel-gefunctionaliseerde carbeenliganden de meest geschikte kandidaten voor een verkennende studie. In Hoofdstuk 2 worden vier zwavel-gefunctionaliseerde carbeenliganden beschreven alsook de dinucleaire nikkel-NHC-complexen die hiermee verkregen zijn. De vier liganden verschillen in de lengte van de alkylketen tussen de thiolaatgroep en de NHC-ring (twee of drie koolstofatomen) en in de tweede functionaliteit op de NHC-ring dat ofwel een benzylgroep of een pyridylmethyl groep is. Het nikkel(II)-ion coördineert met het NHC-

koolstofatoom en de thiolaatgroep, welke een brug vormt naar het tweede nikkelion. De thiolaat- en benzyl-gefunctionaliseerde carbeencomplexen [**1**] en [**2**] lieten een lage katalytische activiteit zien voor de HER. Echter, de complexen [**3**]Br_2 en [**4**]Br_2, waarin het carbeenligand gesubstitueerd is met pyridylgroepen, vertoonden een hogere katalytische activiteit voor HER dan de benzylbevattende verbindingen. Helaas limiteert het gebrek aan stabiliteit van complexen [**3**]Br_2 en [**4**]Br_2 in oplossing en zuurstof en de relatief lage elektrokatalytische activiteit van de verbindingen praktische toepassing ervan. Het verkrijgen van inzicht in de rol van de thiolaat- en pyridinegroep in de katalytische cyclus vergt meer onderzoek en kan bijdragen aan het ontwerp van een efficiënte, biologisch-geïnspireerde elektrokatalysator.

Elektrokatalytische activiteit van nikkelcomplexen met pyridine-gefunctionaliseerde NHC-liganden

Gebaseerd op de bevindingen die beschreven zijn in Hoofdstuk 2, is de focus van het onderzoek verschoven van thiolaat-gefunctionaliseerde naar pyridine-gefunctionaliseerde carbeenliganden. Om een goede vergelijking te kunnen maken is wederom uitgegaan van het overgangsmetaal nikkel (Hoofdstuk 3 – 5).

In Hoofdstuk 3 wordt de synthese en karakterisering beschreven van twee bis-(benz)imidazolium zouten gealkyleerd met pyridylgroepen, die gebruikt zijn als voorlopers voor de synthese van nieuwe nikkel-NHC-complexen. De vier Ni-NHC-verbindingen met verschillende carbeenliganden (gebaseerd op imidazool of benzimidazool) en verschillende tegenionen (Br^- of PF_6^-) zijn geïsoleerd en gekarakteriseerd met verschillende methoden. Het nikkelion in de verbindingen wordt door de liganden omringd in een vierkant-piramidale of een vlakvierkante geometrie. Er is gevonden dat de Ni^{II}/Ni^{I} en Ni^{I}/Ni^{0} redoxkoppels van de nikkelverbindingen met imidazool-gebaseerde carbeenliganden bij meer negatieve potentialen liggen. Daartegenover staat dat deze verbindingen een veel hogere activiteit vertonen in elektrokatalytische protonreductie. Verder vertonen de nikkelverbindingen met deze carbeenliganden een hogere tolerantie ten opzichte van zuur. Van alle onderzochte complexen in een medium met azijnzuur, heeft de nikkelverbinding met het imidazool-gebaseerde ligand en met PF_6^- als tegenion de hoogste katalytische activiteit voor protonreductie (i_c/i_p = 50, k_{obs} = 490 s^{-1} bij 0.1 V/s), alhoewel de overpotentiaal voor protonreductie significant is. Verder is naar voren gekomen dat de aanwezigheid van halide-ionen resulteert in een negatievere potentiaal voor de Ni^{II}/Ni^{I} en Ni^{I}/Ni^{0} redoxkoppels en ook leidt tot hogere overpotentialen voor protonreductie.

In Hoofdstuk 5 wordt de synthese van twee (benz)imidazolium zouten beschreven die gesubstitueerd zijn met een pyridyl-amidegroep. Deze zouten zijn succesvol toegepast als ligandvoorlopers voor de synthese van nieuwe nikkel(II)-complexen met tetradentate liganden, waaronder een NHC-functionaliteit. Röntgendiffractie aan éénkristallen heeft aangetoond dat de nikkel(II)-ionen in beide verbindingen een licht verstoorde vlakvierkante geometrie hebben. Cyclische voltammetriemetingen van de twee nikkelcomplexen laten irreversibele reducties zien, wat erop duidt dat elektronoverdracht direct gevolgd wordt

door een snelle chemische reactie of een structurele verandering. De vorming van moleculair waterstof in elektrokatalyse-experimenten is bevestigd met gaschromatografie (GC) tijdens gecontroleerde elektrolyse bij −1.8 V. De faradaische efficiëntie was voor beide complexen rond de 85%. Gedurende 2 uur elektrolyse is in de aanwezigheid van de imidazool- en de benzimidazool-gebaseerde NHC-complexen 185 μL en 105 μL waterstofgas gegenereerd, corresponderend met 1.5 en 0.9 mol H_2 per mol katalysator. Het imidazool-gebaseerde complex liet niet alleen een hogere activiteit zien in de katalyse van de HER, maar deze bleek ook werkzaam bij een lagere overpotentiaal. Deze geeft aan dat protonoverdracht tussen het ligand en het metaalion plaatsvindt, waardoor de correlatie tussen energiekosten en kinetische barrières niet meer op gaat.

Naast de pogingen de elektronendichtheid van het metaalcentrum te regelen door middel van het gebruik van verschillende NHC-liganden is ook gekeken of de aanwezigheid van een vrije, niet gecoördineerde, pyridinegroep bijdraagt aan het verhogen van de katalytische activiteit van de verbindingen in de HER. In Hoofdstuk 4 wordt de synthese en karakterisering beschreven van twee nieuwe nikkelverbindingen met pyridyl-gefunctionaliseerde carbeenliganden gebaseerd op benzimidazool. Röntgendiffractie aan éénkristallen heeft aangetoond dat de nikkelionen in beide verbindingen een vlakvierkante geometrie hebben met soortgelijke donoratomen van twee bidentate liganden in *cis*-posities. De binding van twee potentiële tridentate liganden in deze configuratie in een van de complexen zorgt voor de aanwezigheid van twee niet-gecoördineerde pyridylgroepen, die beschikbaar zijn voor binding van protonen. De redoxeigenschappen van de twee complexen is bepaald met cyclische voltammetrie en elektrokatalytische experimenten voor protonreductie zijn uitgevoerd in DMF met azijnzuur als bron van protonen. De verbinding met de vrije pyridylgroepen vertoonde niet alleen een hogere elektrokatalytische activiteit, maar ook een lagere overpotentiaal voor protonreductie. De vergelijking tussen deze twee verbindingen laat overtuigend zien dat de pyridylgroep kan bijdragen aan de efficiëntie van de katalyse door protonen te binden en over te dragen gedurende het reductieproces.

Elektrokatalytische activiteit van kobaltcomplexen met pyridine-amide-gefunctionaliseerde carbeenliganden

In Hoofdstuk 2 tot Hoofdstuk 5 wordt gefocust op de synthese en elektrokatalytische eigenschappen van nikkel-NHC-complexen. In Hoofdstuk 6 wordt het onderzoek naar kobalt-NHC-complexen beschreven, omdat bekend is dat kobaltverbindingen ook actieve katalysatoren kunnen opleveren voor HER. Een van de liganden uit Hoofdstuk 5 en een vergelijkbare tridentaat ligand waarin een van de pyridinegroepen is vervangen door een benzylgroep zijn gebruikt om twee kobalt-NHC-verbindingen te maken. In tegenstelling tot de vlakvierkante geometrie van de nikkel(II)-verbindingen, zijn de kobalt(III)-ionen in de Co-NHC-verbindingen in een octaëdrische geometrie, die gevormd wordt door de binding van twee tridentate liganden. Beide kobalt-complexen vertonen een reversibele redoxkoppel in een organische oplosmiddel. De elektrokatalytische activiteit is bestudeerd van de twee kobalt-NHC-verbindingen in DMF, waarbij azijnzuur als protonenbron werd gebruikt. Helaas bleek de Co^{III}/Co^{II} redoxpotentiaal veel negatiever te zijn dan wat in de

literatuur is gerapporteerd voor soortgelijke complexen met pyridyl-gefunctionaliseerde carbeenliganden.[7] De kobaltverbinding met twee extra pyridylgroepen laat een kleinere overpotentiaal zien en hogere katalytische activiteit (10500 M^{-1} s^{-1}). De productie van moleculair waterstof is gekwantificeerd met behulp van gaschromatografie; gedurende 2 uur elektrolyse bij een potentiaal van –1.8 V werd in aanwezigheid van 1 mM van het benzyl-gefunctionaliseerde of het pyridine-gefunctionaliseerde complex respectievelijk 75 µL en 145 µL waterstofgas gegenereerd, hetgeen overeenkomt met 0.6 en 1.2 mol H_2 per mol katalysator.

Referenties

[1] P.D. Tran, J. Barber, *Phys. Chem. Chem. Phys.* 2012, 14, 13772-13784.
[2] A. Dey, *Inorg. Chem.* 2016, *55*, 10831-10834.
[3] T.R. Simmons, G. Berggren, M. Bacchi, M. Fontecave, V. Artero, *Coord. Chem. Rev.* 2014, 270, 127-150.
[4] R.H. Crabtree, *J. Organomet. Chem.* 2005, 690, 5451-5457.
[5] J.-N. Luy, S.A. Hauser, A.B. Chaplin, R. Tonner, *Organometallics* 2015, 34, 5099-5112.
[6] D.L. DuBois, *Inorg. Chem.* 2014, 53, 3935-3960.
[7] K. Kawano, K. Yamauchi, K. Sakai, *Chem. Commun.* 2014, 50, 9872-9875.

List of publications

‘Composition and Structure about Several Tourmaline Minerals’
S. Luo, X. Wu, Q. Hu, J. Wang, C. Liu, Y. Sun, *China Ceramics*, 2010, 3-7.

‘Structural characterization of a new decavanadate compound with organic molecules and inorganic ions’
S. Luo, X. Wu, Q. Hu, J. Wang, C. Liu, Y. Sun. *J. Struct. Chem.* 2012, 53, 915-920.

‘Synthesis, structure, and luminescent properties of 2 novel 5-chlorhydroxybenzoate-imidazole metal-organic complexes’
H. Chen, S. Luo, X. Wu, Y. Wang, B. Hu, C.Hu. G. Huang, Q. Du, *Turk. J. Chem.* 2014, 38, 79-87.

‘Nickel Complexes of Pyridine-Functionalized N-Heterocyclic Carbenes: Syntheses, Structures, and Activity in Electrocatalytic Hydrogen Production’
S. Luo, M.A. Siegler, E. Bouwman, *Eur. J. Inorg. Chem.* 2016, 4693-4700.

‘Dinuclear nickel complexes of thiolate-functionalized carbene ligands and their electrochemical properties’
S. Luo, M.A. Siegler, E. Bouwman, submitted.

‘Pyridyl pendant arms of Ni-NHC complexes as proton shuttles in HER reaction’
S. Luo, D.F. Bruggeman, M.A. Siegler, and E. Bouwman, submitted.

‘Nickel complexes with pyridine-amide functionalized carbene ligands: synthesis, structure and electrocatalytic activity on HER’
S. Luo, M.A. Siegler, E. Bouwman, manuscript in preparation.

‘Cobalt(III) complexes with tridentate/tetradentate carbene ligands: synthesis, structure and electrocatalytic properites’
S. Luo, M.A. Siegler, E. Bouwman, manuscript in preparation.

Curriculum Vitae

Siyuan Luo was born in Wuhan, Hubei Province, China on August 21st, 1989. In 2007, she graduated from Wuhan No.3 high school in Wuhan, China. After the university entrance exam in 2007, she was admitted to the China University of Geosciences (Wuhan), where she studied with a major of materials chemistry from 2007 to 2011. In 2011, she obtained her BSc degree on the thesis entitled "Synthesis and Structural Characterization of a New Decavanadate Compound with Organic Molecules and Inorganic Ions" under the supervision of Prof. X. Wu. In 2011, she was admitted to the successive postgraduate and doctoral program in the major of rock and mineral materials under the supervision of Prof. X. Wu in the China University of Geosciences (Wuhan).

In September 2013, she started her PhD research in the group Metals in Catalysis, Biomimetics & Inorganic Materials at Leiden University under the supervision of Prof. dr. E. Bouwman, with a scholarship from the Chinese Scholarship Counsel. During her PhD studies, she supervised one MSc and two BSc students, and she participated in the Leiden University PhD courses "Time management", "Effective communication", "On being a scientist", "Communication in Science", as well as the HRSMC summer school on "Advanced Metal-Organic Chemistry and Catalysis" in Deurne, the Netherlands in 2014. She successfully applied for a travel grant with the Leiden University Fund / Kroese-Duijsters Fonds (2016) for attending the ICCC conference.

Parts of the results reported in this thesis were presented at meetings and conferences:

- Advanced Metal-Organic Chemistry and Catalysis (AMOCC) summer school in Deurne, 2014, poster presentation.
- Netherlands' Chemistry and Catalysis Conference (NCCC) XVI in Noordwijkerhout, 2015, poster presentation.
- 42nd International Conference on Coordination Chemistry (ICCC) in Brest, France, 2016, poster presentation. (6110/07-06-20161L, Kroese - Duijsters)
- Reedijk (LIC) symposium in Leiden, 2016, poster presentation.
- HRSMC symposium in Leiden, 2016, poster presentation.
- NWO Chains conference in Veldhoven, 2016, oral presentation.